

Probing the Linker Design of a Conjugate Peptide Vaccine

By

Jasmine Marama Seifert-Simpson

A thesis submitted to Victoria University of Wellington in fulfilment of the
requirements for the degree of Master of Science

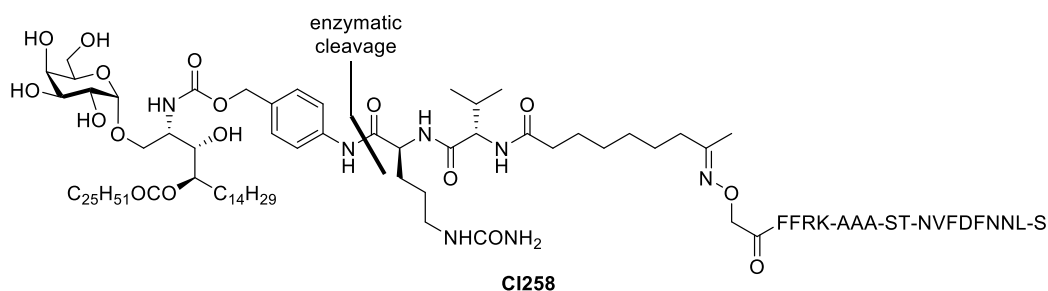
Ferrier Research Institute

Victoria University of Wellington

2020

Abstract

This thesis investigates different chemical approaches to facilitate the exploration of structure-activity relationships related to lipopeptide vaccine **CI258**, with the overall aim of improving vaccine efficacy and synthetic tractability. The vaccine design comprises a lipid antigen, which functions as a vaccine adjuvant, connected to a peptide antigen via a cleavable and self-immolative linker. In vivo processing of **CI258** releases the active vaccine components, with the first step in this processing the enzymatic cleavage at the indicated site. This thesis aims to synthesise compounds that give insight into how the enzymatic cleavage rate affects activity. Topics include the synthesis of advanced diastereomeric intermediates to probe the effect of the dipeptide linker stereochemistry. Consideration will also be given to the necessity of the immolative *para*-amino benzyl carbamate linker. Research towards altering the biodistribution of the vaccine design is also reported.



Acknowledgements

First and foremost, my heartfelt thanks go to my supervisors Professor Gavin Painter and Professor David Larsen. Both have provided invaluable contributions to my research and development as a chemist.

I'd like to thank all of the Painter team, especially the other students and my office mates, for their help and never-ending support both in and out of the lab.

I gratefully acknowledge the support provided by the Ferrier Research Institute throughout my studies. Everyone at the Institute has been extremely welcoming and helpful.

Thanks also go to my friends and family outside of chemistry for their wonderful support during this challenging postgraduate experience. A special mention to Lachie, who got me through the tough bits.

Contents

Abstract	i
Acknowledgements	ii
Contents	iii
Abbreviations	v
Chapter 1 Introduction	1
1.1 History of Vaccines	1
1.2 Vaccine Types	2
1.3 Immunologic Adjuvants	4
1.4 Conjugate Vaccines	6
1.5 Cleavable Linkers	8
1.6 Self-Immolative Spacers	11
1.7 Lead Vaccine Conjugate CI258	13
1.8 Proposed Work	16
Chapter 2 Investigating the Effect of P1 Stereochemistry	17
2.1 Target Compounds L- and D-12	17
2.2 Stereospecific Synthesis of Linkers	18
2.3 Synthesis of Ketone Epimers L- and D-12	20
2.4 Summary and Future Work	27
Chapter 3 Removing the Immolative Linker	29
3.1 Synthesis of Model Linker 13	30
3.2 Cathepsin B Assay of Model Linker 13	32
3.3 Summary and Future Work	33
Chapter 4 Efforts Towards Altering Biodistribution	34
4.1 LogP Analysis	35
4.2 Discrete PEG Linkers	36

4.3	Iterative Synthesis of Discrete PEG Chains	37
4.4	HPLC Analysis of Intermediates.....	43
4.5	Derivatisations of Discrete PEG Linkers	43
4.6	Summary and Future Work	54
Chapter 5	Concluding Remarks	56
5.1	Investigating the Effect of Stereochemistry at P1	56
5.2	Removing the Immolative Linker	57
5.3	Efforts Towards Altering Biodistribution	57
Chapter 6	Experimental	59
6.1	General Experimental.....	59
6.2	Synthetic Protocols.....	62
References	87

Abbreviations

ADC	antibody-drug conjugate	MHC	major histocompatibility complex
APC	antigen presenting cell		
aq	aqueous	NHS	<i>N</i> -hydroxysuccinimide
ax	axial	NKT	natural killer T
CAD	charged aerosol detector	o/n	overnight (15 – 21 hours)
calcd	calculated	PABA	<i>para</i> -aminobenzyl alcohol
Cbz	carboxybenzyl	PABC	<i>para</i> -aminobenzyl carbamate
CuAAC	copper-catalysed azide–alkyne cycloadditions	PBS	phosphate-buffered saline
DCC	<i>N,N</i> -dicyclohexylcarbodiimide	PE	petroleum ether
DIPEA	<i>N,N</i> -diisopropylethylamine	PEG	polyethylene glycol
DMF	dimethylformamide	PG	protecting group
DMP	Dess–Martin periodinane	<i>p</i> NP	<i>para</i> -nitro phenyl
DMSO	dimethyl sulfoxide	PRR	pattern recognition receptor
DNPH	2,4-dinitrophenylhydrazine	rt	room temperature (18 – 20 °C)
DOX	doxorubicin	R _t	retention time
EDTA	ethylenediaminetetraacetic acid	SPAAC	strain-promoted alkyne-azide cycloadditions
EEDQ	<i>N</i> -ethoxycarbonyl-2-ethoxy-1,2-dihydroquinoline	TEMPO	(2,2,6,6-tetramethylpiperidin-1-yl)oxyl
eq	equatorial	THF	tetrahydrofuran
equiv	equivalents	TIC	total ion chromatogram
ESI	electrospray ionisation	TLR	Toll-like receptor
Fmoc	fluorenylmethyloxycarbonyl	Trt	trityl
HBTU	2-(1 <i>H</i> -benzotriazol-1-yl)-1,1,3,3-tetramethyluronium hexafluorophosphate	Ts	tosyl
Hib	<i>Haemophilus influenzae</i> type B		
HPLC	high performance liquid chromatography		
IFA	incomplete Freund's adjuvant		

Chapter 1 Introduction

This introductory chapter first discusses the general field of vaccines, their history and the different types thereof before a brief introduction to the area of vaccine adjuvants, including the synthetic glycolipid α -galactosylceramide (α -GalCer). Conjugate vaccines and the various methods of conjugation are considered next, leading into an overview of cleavable linkers, specifically enzymatically labile linkers. Following this is a discussion of self-immolative spacers and their role in drug conjugates. This chapter concludes with details of our current lead conjugate vaccine and potential areas for optimisation.

1.1 History of Vaccines

Saving an estimated 2.5 million lives globally each year, vaccines are one of medicine's greatest successes.¹⁻³ Among other remarkable achievements, vaccination programs have accomplished the complete eradication of smallpox and lowered the incidence of polio by 99%.^{1, 4, 5} For many other diseases they have substantially decreased the infection-associated morbidity and mortality in vaccinated populations.^{6, 7}

Histories of vaccination usually begin with the 18th century English physician Edward Jenner, and his work towards a smallpox vaccine.⁸⁻¹⁰ Smallpox was a particularly virulent virus with a 30% fatality rate.¹¹⁻¹³ Although Jenner is generally reported as the first to investigate smallpox immunisation, evidence suggests that the Chinese and other cultures made use of smallpox variolation as early as the 15th century.^{14, 15} Variolation is the process of immunising individuals with pox material taken from a smallpox patient. But it has limited efficacy and can lead to full smallpox infections with substantial contagiousity.¹⁶

In 18th century Britain, it was a common observation that milkmaids were often immune to smallpox. From this, Jenner postulated that infection with the milder cowpox virus prevented future infection with the deadly smallpox virus. Jenner tested this hypothesis by inoculating patients with pus taken from a milkmaid's cowpox blisters. The patients did not develop any

serious infections. A few months later Jenner tested the success of the inoculation by injecting the patients with smallpox scab material. No smallpox infection followed, the inoculation had been effective. Jenner reported his findings to the Royal Society, who after some debate, accepted his results.¹⁷ Smallpox vaccination soon became widespread, and by the mid-1800's the British Government had made the vaccination compulsory.¹⁸ Thus Jenner had developed the first vaccine, and smallpox went on to be the first human disease to be completely eliminated, with the World Health Organisation certifying global eradication of the disease in 1980.¹⁹

1.2 Vaccine Types

Early vaccines contained a weakened form of the pathogen, known as live-attenuated, which is produced by growing the bacteria or virus in cell culture until it is no longer virulent but can still elicit a protective immune response.²⁰ Live attenuated vaccines can generate strong, long-lasting immunity, but they do suffer from safety concerns, namely the possibility for the microorganisms to regain pathogenicity, which is of particular concern in immunocompromised patients.^{4, 21-26} Examples of live attenuated vaccines currently in use in New Zealand include measles, mumps and rubella; oral rotavirus; varicella (chicken pox); and herpes zoster (shingles).²⁷

Other main classes of vaccines include inactivated, toxoid and subunit/conjugate vaccines.²⁸ Inactivated vaccines contain whole microbes that have been “killed” with heat, radiation or chemicals so they are no longer virulent but will still be recognised by the immune system. While inactivated vaccines are substantially safer than live attenuated vaccines, they do not confer as long-lasting immunity.²² Examples of inactivated vaccines on the New Zealand schedule include hepatitis A, influenza and polio.²⁷ In a similar manner to inactivated vaccines made from whole organisms, toxoid vaccines are produced by inactivating bacterial toxins. Examples of toxoid vaccines include tetanus, diphtheria and pertussis.²⁷ However, like inactivated vaccines, toxoid vaccines can also suffer from poor immunogenicity, often requiring multiple doses to achieve immunity.

Traditional vaccines made with attenuated or killed whole microorganisms are extremely effective at disease prevention. However, safety issues associated with these complex mixtures prevent their use in all situations.²⁶ Vaccines can be simplified through identification and

isolation of the active components responsible for the generation of protective immunity. For example, antibodies recognize certain chemical structures on the surface of the microbe such as proteins or their glycosylated derivatives. Minimal antigenic components, or epitopes, are the smallest segments able to be recognized by the immune system. These are commonly much smaller than whole proteins. For example, protein sections (i.e. peptides) or polysaccharides displayed on microbial surface proteins can serve as epitopes. In some vaccines, fragments from the microbe such as cell wall components or nucleic acid sequences are used to optimise responses to the antigen components.

With better chemical definition and characterisation vaccines can be tailored to have improved safety and efficacy profiles. Subunit vaccines can therefore exhibit reproducibility and safety advantages over the live-attenuated or inactivated alternatives. However, they can struggle to evoke sufficient immune responses. This can be overcome by the inclusion and co-delivery of an immune stimulant (adjuvant) or a carrier protein to produce conjugate vaccines, examples of which include Hepatitis B, human papilloma virus and *Haemophilus influenzae* type b (Hib).²⁷

Peptide vaccines utilise protein fragments as the antigenic component. With a very well-defined structure, peptide vaccines are some of the simplest, and as such, perhaps the safest vaccines.²⁹ The development of automated solid phase peptide synthesis allows these vaccines to offer substantial manufacturing advantages over many of the above types. As peptide vaccines are often fully synthetic, they are amenable to redesign and optimisation for varying applications. Furthermore, the vaccine target can be changed by varying the epitopes incorporated in the peptide sequence. However, as for other subunit vaccines, the major disadvantage of peptide vaccines is their low immunogenicity. To overcome this limitation, peptide vaccines are formulated to enhance the retention and delivery of the peptide antigens or combined with immune stimulants (adjuvants), which assist in the development of immune responses against the peptide antigens.

1.3 Immunologic Adjuvants

The word “adjuvant” comes from the Latin *adjuvare* meaning “to help”.³⁰ Vaccine adjuvants are defined as compounds that enhance immune responses to antigens.³⁰⁻³² They are commonly used in combination with poorly immunogenic antigens such as the inactivated toxins in toxoid vaccines or the protein fragments in peptide vaccines.²¹ Adjuvants are highly variable in chemical composition and have many different modes of action, some of which include enhancing the delivery of the antigenic cargo to the correct tissue and cell types whereas others activate specific receptors on immune cells.

Vaccine adjuvants were first discovered in the early 20th century, when French scientist Gaston Ramon noticed that horses generated higher levels of antibodies when they developed abscesses at the vaccine injection site.³¹⁻³³ He probed this by the co-injection of starch, breadcrumbs or tapioca with the inactivated bacterial toxoid vaccines. The results confirmed his hypothesis that substances that increased local inflammation could increase the immune response to the toxoid. At a similar time, scientists in London discovered the capability of aluminium salts to enhance immune responses.³³⁻³⁵ Unlike the breadcrumbs of Ramon, aluminium salts (alum) were later approved for use in vaccines. For approximately 70 years they were the only vaccine adjuvants licensed for use in humans.² Initially it was believed that the salts’ ability to slow the release of antigen from the site of injection prolonged the contact between the antigen and the immune system.^{28, 31, 36} However, it has been shown that this “depot effect” is not responsible for its adjuvant activity. Instead, it appears alum may cause the release of uric acid, which in turn activates components of the immune system.^{35, 37} Alum has also been shown to reduce antigen degradation.³⁸

In 1930 Jules Freund developed a strong adjuvant consisting of a water-in-mineral oil emulsion and heat-killed mycobacteria.³⁹ Complete Freund’s adjuvant (CFA) is highly effective in stimulating the immune system, but is also very reactogenic (causes adverse reactions), which prevents its use in humans. Incomplete Freund’s adjuvant (IFA) lacks the mycobacterium component present in CFA, in other words it is simply a water-in-oil emulsion. IFA is less reactogenic than CFA and has been used extensively in vaccine research.^{40, 41}

In addition to adjuvants like alum and IFA that aid in antigen delivery and stability, compounds that stimulate pattern recognition receptors (PRRs) can also be effective adjuvants.⁴² PRRs are a class of receptors expressed on cells of the innate immune system that allow detection of

broad classes of pathogens through binding to pathogen-associated molecular patterns.³⁶ PRR binding stimulates an immune response to eliminate the pathogen in part through the production of large numbers of immunomodulatory cytokines and chemokines. This process can be harnessed in vaccines by the development of adjuvants that bind to and activate PRRs, thus promoting an immune response to the co-administered vaccine antigen. Membrane bound PRRs include Toll-like receptors (TLRs) and C-type lectins. Examples of TLR ligands used as vaccine adjuvants include unmethylated CpG structures found in prokaryotic DNA and bacterial lipopeptide structures.⁴³ Mycobacterial cell wall glycolipid trehalose dimycolate is an example of a C-type lectin ligand, which can act as a strong immunostimulant.^{44, 45}

The binding of ligands to PRRs causes the activation of innate immune cells, including antigen presenting cells (APCs), which can ultimately enhance adaptive responses.^{46, 47} The activation of APCs is vital for the development of a strong immune response. An alternative route to APC activation is through auxiliary cells such as the subset of innate-like T cells known as natural killer T (NKT) cells.⁶ Presentation of lipid antigens on MHC-class I like molecule CD1d by an APC stimulates the NKT cell, which can then provide positive feedback signals to the APC that include the release of soluble factors and the provision of CD40L for CD40 ligation (Figure 1.1).⁴⁸ The activated APC can then trigger various immune responses, including the activation of CD8⁺ T cells.^{48, 49} When included in vaccines, the recognition of the lipid NKT cell antigen leads to enhanced antigen-specific immune responses, thus these lipid antigens can also be classed as vaccine adjuvants.⁵⁰

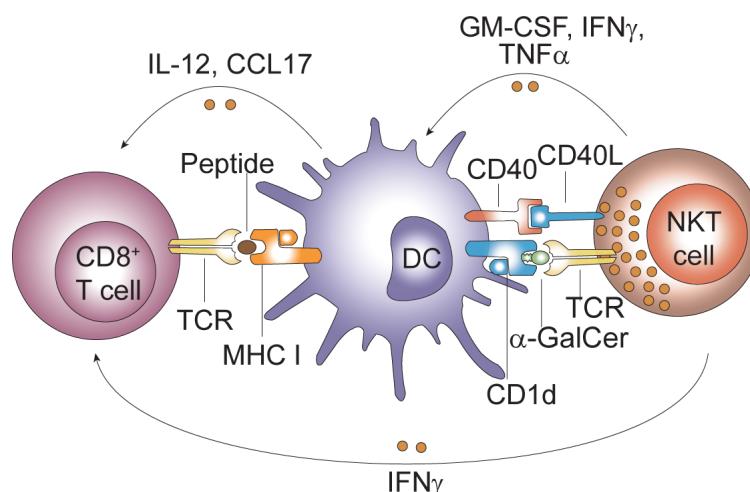


Figure 1.1 Alternative activation of APCs through the activation of NKT cells through the presentation of a lipid antigen (α -GalCer) on CD1d. The APC then activates CD8⁺ T cells to cause downstream immune responses. DCs are a subset of APCs. Reproduced from Hayman et al.⁴³ with permission from Springer Nature.

One common example of an NKT cell antigen/vaccine adjuvant is α -galactosylceramide (α -GalCer, **1**, Figure 1.2).⁴³ The synthetic glycolipid was developed from structure-activity relationship studies on a class of marine sponge-derived glycolipids.^{43, 51} The lipid chains of α -GalCer sit within the CD1d hydrophobic binding pockets and the polar head group hydrogen-bonds to surface residues on CD1d and the T cell receptor on the NKT cell.⁵² The lipid antigen has been widely used as a vaccine adjuvant in research and several pre-clinical studies.^{6, 49, 53-57}

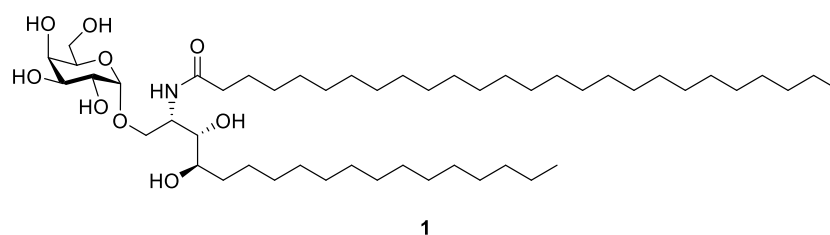


Figure 1.2 Structure of NKT cell agonist α -GalCer (**1**).

1.4 Conjugate Vaccines

As discussed earlier, subunit vaccines, such as peptide vaccines, often suffer from low immunogenicity, which can be overcome by combination of the antigen with an immune stimulating component such as an adjuvant or a carrier protein. While adjuvants enhance immune responses by activating cells of the innate immune system, carrier proteins can perform multiple functions, including multi-valent presentation of the antigenic component and the provision of classical T cell help. The presentation of peptide fragments on MHC class II molecules to CD4⁺ T cells leads to the activation of APC's.⁵⁸⁻⁶⁰ It is the covalent linkage of the antigen to the carrier protein or adjuvant that gives conjugate vaccines their particular advantage: the two components are presented in the same location at the same time, which promotes stimulation of and antigen uptake by the same immune cells.^{43, 61-66}

The first conjugate vaccine was described by Avery and Goebel in 1929, who demonstrated that the poor immunogenicity of polysaccharides could be overcome by their attachment to carrier proteins.⁶⁷ Since then, the field of conjugate vaccines has grown substantially. The first conjugate vaccines approved in the late 1980's were for *Haemophilus influenzae* type b (Hib).⁶⁸⁻⁷¹ These contain a capsular polysaccharide from Hib covalently linked to various carrier proteins, such as tetanus and diphtheria toxoids, and outer membrane proteins.⁶³ Conjugation of weakly immunogenic polysaccharides to immune stimulating moieties can produce

successful vaccines. In a related approach also involving conjugation, the poor immunogenicity of peptide antigens can be overcome by conjugation to adjuvants such as PRR ligands.^{62, 64, 72}

An important aspect in the design of conjugate vaccines is the choice of conjugation strategy for linking the antigen and immune stimulating component (e.g. adjuvant). The best strategies are highly chemoselective and reliable, such that they allow easy conjugation of the separate components. “Click” reactions, as defined by Sharpless et al. in 2001, lend themselves well to this application.⁷³ Click reactions must be high-yielding, wide in scope, produce easily removed by-products, able to be conducted in easily removable or benign solvents, and give products that are stable under physiological conditions. Some examples of click reactions include cycloadditions of unsaturated species (especially 1,3-dipolar cycloaddition reactions), nucleophilic substitution chemistry (particularly ring-opening reactions), carbonyl chemistry of the “non-aldol” type (e.g. formation of ureas and oximes), and additions to C-C multiple bonds.

Click chemistry has frequently been used in the development of drugs including conjugate vaccines⁷⁴⁻⁸² as well as antibody-drug-conjugates⁸³⁻⁸⁵ (ADCs). Some popular click reactions used in these contexts are copper(I)-catalysed azide-alkyne cycloaddition (CuAAC), strain-promoted azide-alkyne cycloaddition (SPAAC) and oxime ligation (Figure 1.3). Like other click reactions, these approaches allow easy chemoselective connection of moieties under mild conditions.

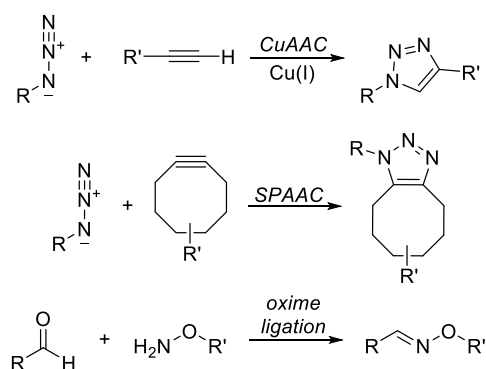


Figure 1.3 General mechanisms for click reactions common in ADC and conjugate vaccine development.

The most widely used click reaction is the copper catalysed reaction of azides with alkynes to form triazoles (CuAAC).⁸⁶ This reaction was first reported in 2002 by both Sharpless et al.⁸⁷ and Meldal et al.⁸⁸ Since then the reaction has been applied in many fields including drug development, organic synthesis, and dendrimer and polymer chemistries. CuAAC reactions have been used to link components in conjugate vaccines.^{74, 79, 81, 82} However, concerns exist

around the potential in vivo effects of any residual copper catalyst and the formation of reactive oxygen species (ROS). This is especially problematic when using a peptide substrate in a CuAAC reaction, as there is potential for ROS to oxidise susceptible amino acid residues.^{81, 89}

While CuAAC reactions use copper to catalyse the reaction of azides with alkynes, SPAAC reactions utilise the ring strain of a substituted cyclooctyne as the driving force for the conjugation reaction. Strain-promoted azide-alkyne cycloaddition was first described by Bertozzi et al.⁹⁰ in 2004, since then it has shown great success in the field of bioconjugates, including the synthesis of conjugate vaccines.^{76-78, 81, 91-93} Requiring no catalyst, SPAAC has distinct advantages over other click strategies such as CuAAC, with no ROS formation or possibility for residual catalyst to influence in vivo activity. However, the relatively large multicyclic moiety formed during the SPAAC reaction, which remains present in the bioconjugate, could influence the overall biophysical properties or metabolism of the bioconjugate in unpredictable ways.

Another strategy for conjugation of biomolecules is oxime ligation. Reaction of an aldehyde or ketone with an amino-oxy species produces the stable oxime bond.⁹⁴ Oxime ligation is less popular than other click reactions, possibly because the synthesis and storage of aldehyde and amino-oxy containing species can be challenging.⁹⁵ However, oxime formation is very effective. Indeed, the reaction is so facile that care must be taken to prevent the inadvertent reaction of the amino-oxy species with trace amounts of carbonyl species commonly found in many solvents.

1.5 Cleavable Linkers

Many conjugate vaccines are large systems that have multiple antigens and adjuvants (or carrier proteins) covalently bonded together, often via the click chemistry techniques described above. The components are usually irreversibly bound together, which is generally not a problem for larger protein-based constructs that are designed to induce antibody responses. However, when using small molecule adjuvants, such as the NKT cell agonist α -GalCer (**1**), care must be taken to attach the antigen in a manner that does not disrupt receptor interactions.^{68, 96}

α -GalCer does have some scope for derivatisation. Crystallographic data of the CD1d- α -GalCer-T cell receptor complex shows that the galactose 6''-OH position is solvent exposed (Figure 1.4).^{52, 97-100} This has prompted the synthesis of α -GalCer derivatives with modifications

at the primary hydroxyl group,¹⁰¹ which could allow antigen conjugation through this position. Nonetheless, with the exception of the 6''-OH position, the chemical structure of the glycolipid adjuvant is relatively fixed when considering receptor binding interactions. So the adjuvant must be disconnected from the rest of the vaccine construct before it can bind to CD1d on DCs and T cell receptors on NKT cells.⁴³

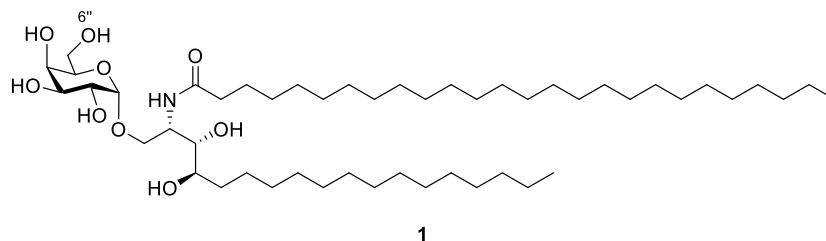


Figure 1.4 Structure of NKT cell agonist α -GalCer (**1**) with the solvent exposed 6''OH position labelled.

Cleavable linkers allow the vaccine components to be linked until they arrive at the desired destination, at which point they dissociate, allowing them to effectively interact with the appropriate receptors and cellular components. Cleavable linkers can be activated by chemical triggers such as changes in temperature, pH, and reductive potential.¹⁰² Alternatively, there are many enzymes that can be utilised to cleave conjugate linkers, examples include esterases, cysteine proteases such as cathepsin B, and hydrolytic lysosomal enzymes such as β -glucuronidases.

Lysosomal protease cathepsin B is abundant in APCs,¹⁰³⁻¹⁰⁹ making it an ideal trigger for the cleavage of a conjugate vaccine containing the adjuvant α -GalCer (**1**). A popular substrate for cathepsin B is valine-citrulline-*para*-amino-benzyl carbamate (Val-Cit-PABC, Figure 1.5).

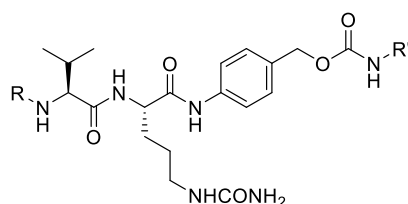


Figure 1.5 Structure of commonly used cathepsin B substrate Val-Cit-PABC.

This linker, and others, was first described by Dubowchik and co-workers in 1998.¹⁰⁶ They synthesised model compounds using these linkers with anti-cancer drug doxorubicin (DOX) as a payload e.g. compound **2** shown in Figure 1.6. The compounds were incubated with cathepsin B and the release rate of doxorubicin was measured. Half-lives of cleavable constructs ranged from 8 to 2040 minutes, depending on the dipeptide linker used. Interestingly, when model

compounds lacking the PABC group (e.g. **3**, Figure 1.6) were incubated with cathepsin B, no enzymatic cleavage was observed.^{104, 105} However, hydrolysis was reinstated when the PABC group was replaced with another amino acid, such as in Z-Val-Cit-Gly-DOX (**4**), but this meant that the active drug was released with a glycine residue still attached. These results suggest a non-sterically demanding group is required adjacent to the enzymatic cleavage site for enzymolysis to occur on substrates that contain bulky groups (e.g. DOX).

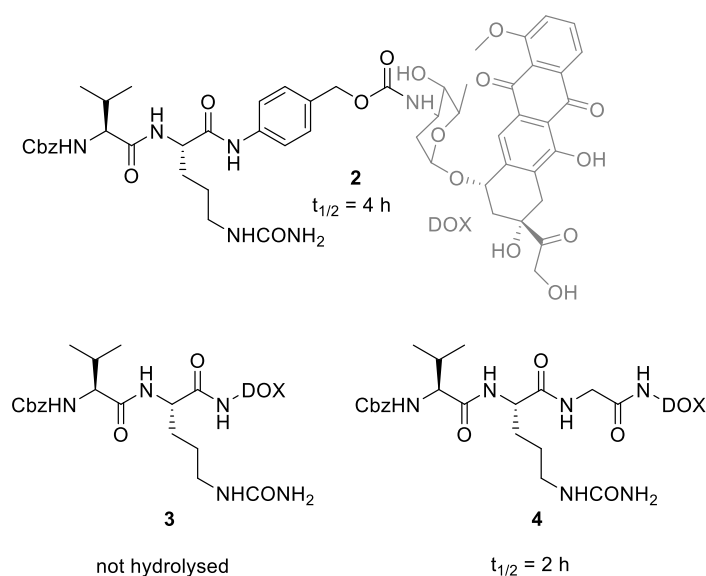


Figure 1.6 Structures of compounds **2-4** synthesised by Dubowchik et al.¹⁰⁴ Where DOX = doxorubicin.

1.6 Self-Immolative Spacers

The steric congestion around an enzyme cleavage site can be relieved by introducing a “self-immolative spacer” such as the PABC linker shown above.^{108, 110-112} These are designed to allow the correlated cleavage of a distant bond after activation by breaking an initial bond, often via enzymatic cleavage (Figure 1.7). The scission of the first bond reveals a reactive site on the immolative spacer, which then undergoes a decomposition reaction to release the distal moiety. The spacer is dismantled during the process, hence the term immolative. Non-immolative spacers are also effective at increasing cleavage rates but are not traceless and are therefore ineffective when the drug design requires the release of an unmodified drug.¹⁰⁴

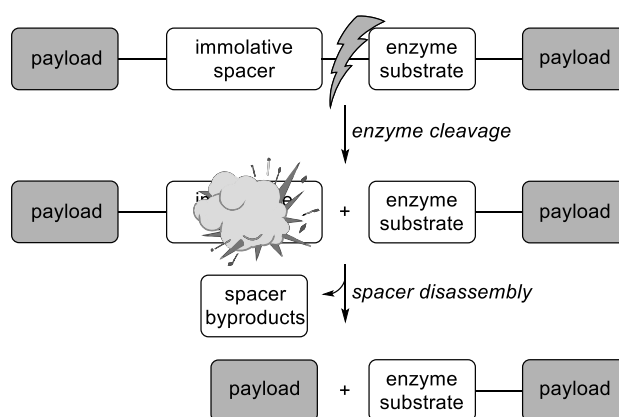
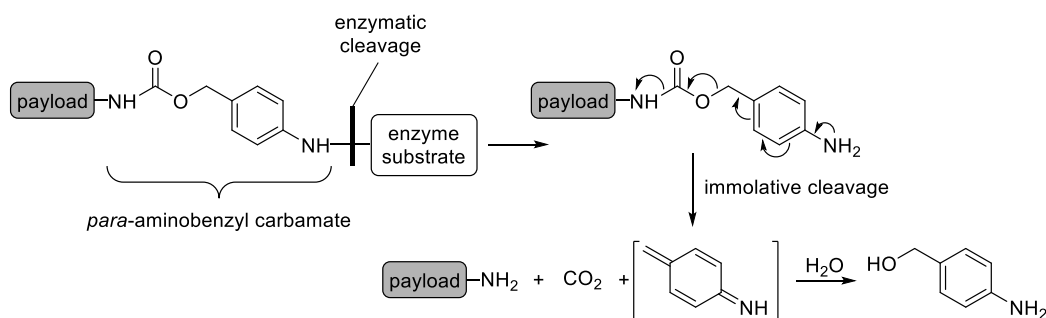


Figure 1.7 Enzyme mediated cleavage followed by spacer self-immolation.

In 1981 Katzenellenbogen et al. reported the use of *para*-amino-benzyl carbamate (PABC) as a self-immolative spacer (Scheme 1.1).¹¹³ Enzyme mediated cleavage reveals the free aniline moiety, which then undergoes spontaneous collapse to form an azaquinone methide, one molecule of carbon dioxide and the payload as a free amine. The reactive azaquinone methide can then react with a nucleophile (e.g. water) in a Michael-type addition to reform the aniline motif.¹¹⁴ Quinone methides are also known to react with enzymes and nucleic bases, which could have adverse effects *in vivo*.¹¹² However, conjugates containing similar immolative spacers have been well tolerated in clinical trials.^{85, 108, 115, 116}



Scheme 1.1 Mechanism of self-immolation for *para*-aminobenzyl carbamate-based spacers.

Since 1981, a substantial amount of work has gone into the development and optimisation of self-immolative spacer systems.^{83, 85, 108, 112, 117-119} Most spacers, like PABC, contain an aromatic system and immolate via an “electronic cascade”. The other main class of immolative spacers exploits cyclisation for the disassembly process. Rates of release can be tuned by the addition of substituents or other modifications of the self-immolative system. Polymeric and dendrimer immolative systems have also been developed, which allow release of multiple payloads, thus amplifying the triggering signal.^{108, 120-130} With the vast numbers of immolative systems reported in the literature, it is impressive that the first immolative spacer (PABC) is still the most widely used.^{108, 110}

1.7 Lead Vaccine Conjugate CI258

Many of the aspects described above are incorporated into the synthetic pre-clinical malaria vaccine **CI258**, the current lead malaria vaccine in the Painter research group at the Ferrier Research Institute, New Zealand (Figure 1.8). Conjugate vaccine **CI258** contains a peptide antigen and a prodrug of the lipid adjuvant α -GalCer (**1**). The conjugate also contains a linker that incorporates a Val-Cit dipeptide, an immolative spacer (PABC), and a short hydrocarbon chain to allow conjugation to the peptide through oxime ligation. A single injection of **CI258** into animals generates high numbers of liver tissue resident memory CD8⁺ T cells specific to the NVFDFNNL peptide antigen. These cells are able to protect animals from challenge with malaria sporozoites in a model in which only one other complicated vaccine design has been shown to work effectively.¹³¹

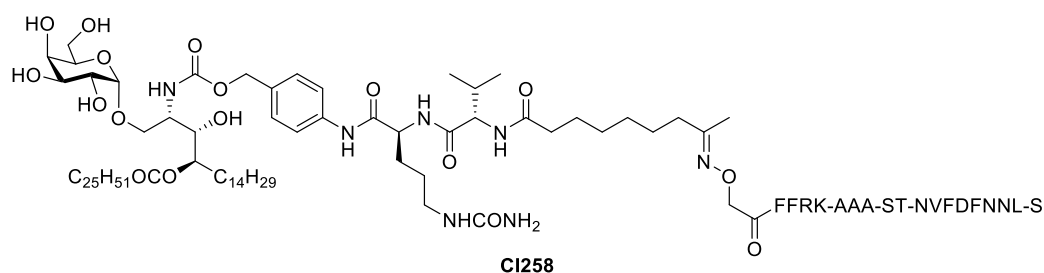


Figure 1.8 Structure of current lead vaccine **CI258**.

The specific design of **CI258** contains a murine malaria peptide epitope. However, the general vaccine design is compatible with many peptide antigens, including those designed to treat cancer, allergy and influenza.⁷⁸⁻⁸¹ In each case the peptide sequence is terminated with a short cleavage region (FFRK) at the N terminus of the epitope, which is designed to enhance peptide release from residual linker components. This allows processing of the peptide so that the epitope can be released and presented on MHC molecules (Scheme 1.2). The peptide chain is further functionalised with the N-terminal addition of amino-oxy acetic acid. The resulting amino-oxy peptide can be conjugated to the rest of the vaccine via chemoselective oxime ligation to a ketone at the end of a short hydrocarbon chain.¹³²⁻¹³⁴

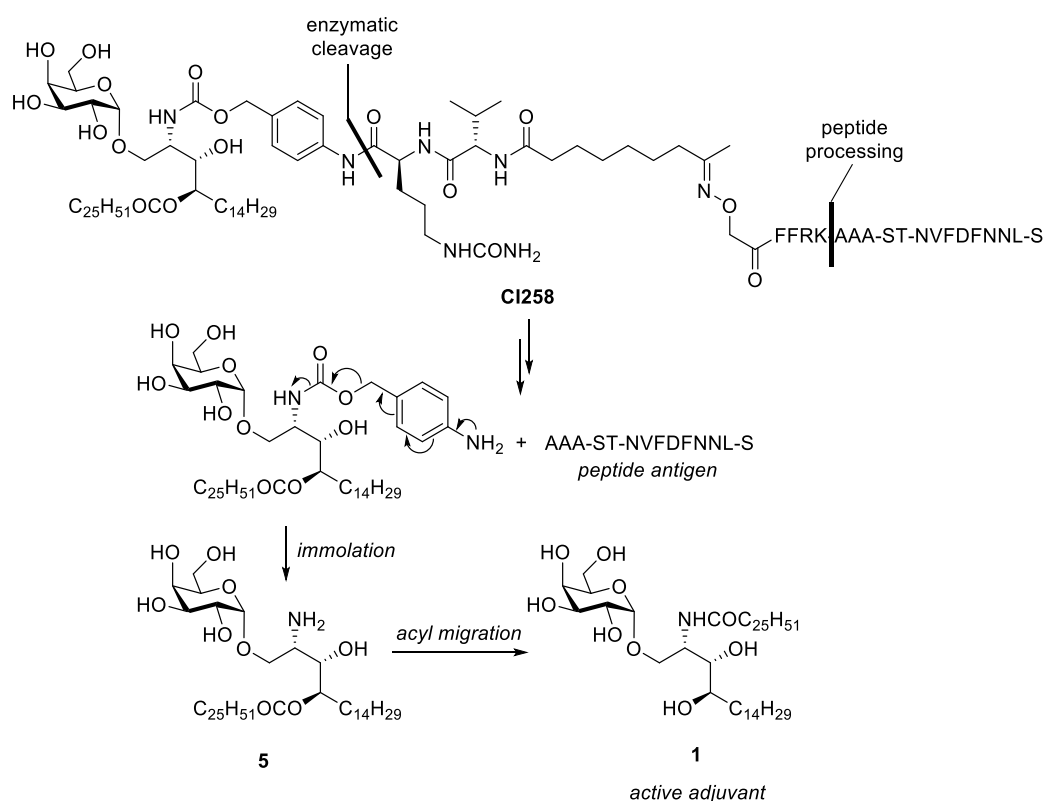
The central section of **CI258** contains a dipeptide linker and an immolative spacer.[†] The dipeptide linker (i.e. Cit-Val) used in **CI258** is a commonly used cathepsin B substrate. The

[†] From now on, the dipeptide linker will be depicted and described in the C→N direction (opposite to the conventional direction), this allows the sugar and the peptide antigen sequence to be drawn in the standard formats.

linker is hydrolysed at the carboxyl end of the citrulline residue, revealing the free aniline moiety, which spontaneously undergoes an electronic cascade to ultimately release α -GalCer (Scheme 1.2).

The vaccine design utilises a unique prodrug approach to allow attachment of the linker-peptide construct to the lipid adjuvant. Active adjuvant α -GalCer (**1**) can undergo a 2-N \rightarrow 4-O acyl migration of the C₂₆ fatty acid under acidic conditions, allowing subsequent attachment of the linker via the newly exposed amine handle.^{79, 80} After in vivo enzymatic cleavage and consequent immolative release of the conjugate, the α -GalCer prodrug (m α -GalCer, **5**) undergoes the reverse O \rightarrow N acyl migration to reform the active lipid antigen (Scheme 1.2).^{79,}

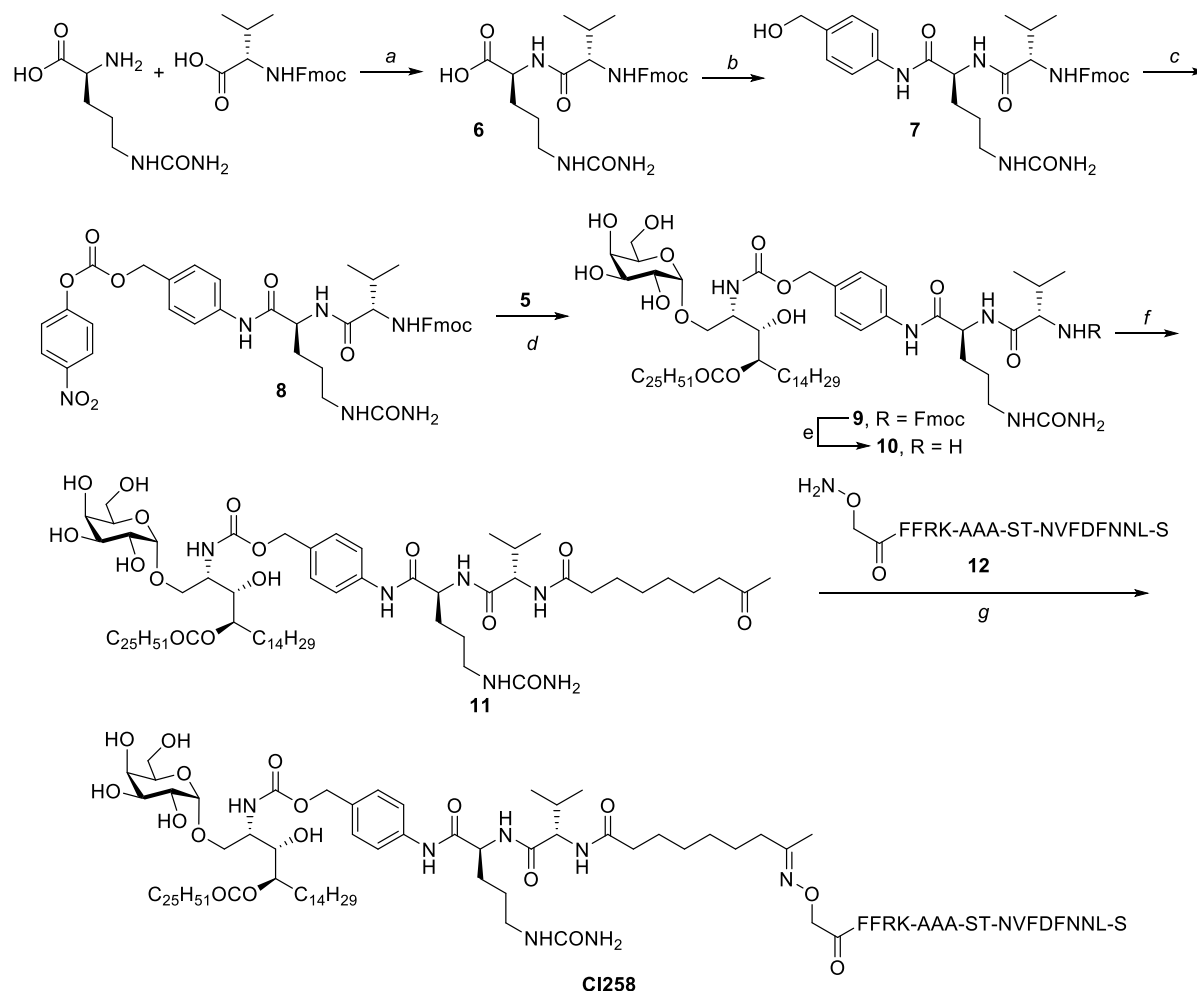
80



Scheme 1.2 Breakdown of conjugate vaccine **CI258** to release active adjuvant α -GalCer (**1**) and antigen containing peptide sequence.

The synthesis of **CI258** began with the formation of the dipeptide linker (Scheme 1.3). Citrulline was coupled to Fmoc-protected valine to give dipeptide **6** before the addition of the PABA immolative spacer. Alcohol **7** was then activated as the *para*-nitro phenyl (*p*NP) carbonate (**8**). Reaction with m α -GalCer (**5**) produced **9**, which was then Fmoc deprotected to

give **10**. Coupling to 8-oxo-nonanoic acid furnished the linker with the requisite ketone moiety (**11**), which was then reacted with amino-oxy peptide **12** to give the target vaccine (**CI258**).



Scheme 1.3 Synthesis of **CI258**. Reagents and conditions: a) isobutyl chloroformate, Et₃N, THF, 1 h, -14 to 15 °C, then NaHCO₃, 0 °C, to rt, 3 h, 70%; b) PABA, EEDQ, 2:1 CH₂Cl₂/CH₃OH, 30 °C to rt, 42 h, 80%; c) bis (*para*-nitrophenyl) carbonate, DIPEA, DMF, rt, o/n, 75%; d) pyridine, Et₃N, rt, o/n, 52%; e) piperidine, DMF, 0 °C to rt, 30 min, 81%; f) HBTU, DIPEA, DMF, rt, o/n, 85%; g) **12**, aniline/H₂O/TFA/THF/CH₃OH, 50 °C, o/n, 57%. Currently under review in Science Immunology.

For the lipid adjuvant to be released, three things must occur: enzymatic cleavage, spacer self-immolation and acyl chain rearrangement. The rate of this in vivo processing has not been probed in our system and is likely able to be optimised with respect to vaccine activity. The first processing step is the enzymatic cleavage by cathepsin B (Figure 1.9). The citrulline and valine residues are in the P1 and P2 positions, respectively, with the PABC group of **CI258** in the P1' position. The rate of the enzymatic cleavage is likely dependent on a few factors: the structure of the dipeptide (P1-P2), the group at P1' (i.e. immolative or non-immolative linker), and the physical properties of the construct (i.e. if it is available for enzymatic digestion).

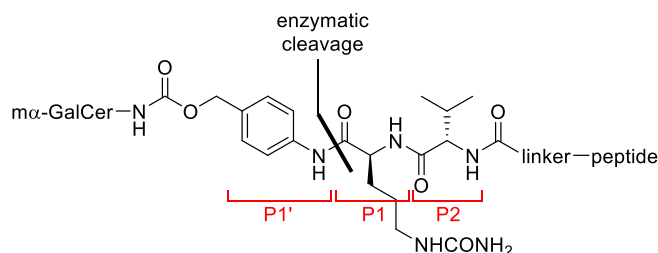


Figure 1.9 Diagram of generic conjugate showing enzymatic cleavage site.

1.8 Proposed Work

The overarching hypothesis for this thesis is that the overall rate of release of the components of **CI258** is important for its activity. This will be probed through this synthesis and analysis of compounds **12** to **15** (Figure 1.10). The synthesis of epimeric pair of advanced intermediates (**L-12** and **D-12**) will allow the impact of the stereochemistry at P1 to be probed. Synthesis of model compound **13** will allow us to explore the effect of removing the PABC immolative spacer. Synthesis of hydrophilic compounds such as **14** and **15** will investigate the influence of biodistribution on cleavage rate. In summary, we aim to synthesise a variety of compounds to probe the effect of enzymatic cleavage rate on vaccine efficacy.

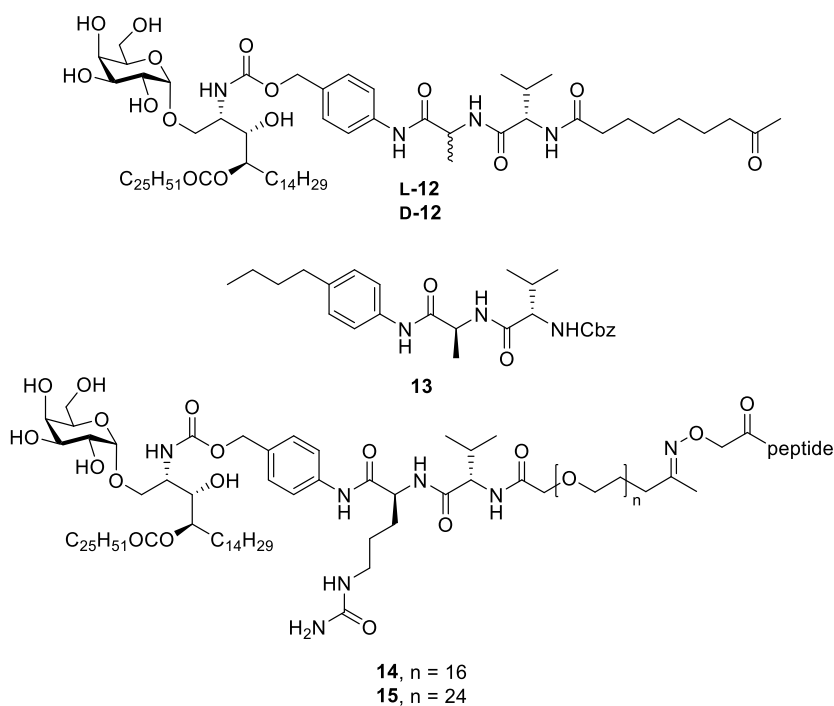


Figure 1.10 Structures of targets **12-15**. Where peptide = FFRK-AAA-ST-NVDFNNL-S.

Chapter 2 Investigating the Effect of P1

Stereochemistry

2.1 Target Compounds L- and D-12

Ongoing research from the Painter and Hermans research groups has shown that activity was abolished in a prodrug incorporating the same immolative linker used in **CI258** when one of the amino acids was replaced by its unnatural D-enantiomer.¹³⁵ The observation was attributed to a lack of enzymatic cleavage at the dipeptide linker. We chose to explore this in a α -GalCer conjugate system, with the synthesis of epimers **L-** and **D-12** (Figure 2.1). These advanced ketone intermediates can be conjugated to a variety of peptide antigens to explore these outcomes in different vaccine systems.

These targets contain the dipeptide linker Ala-Val, which cleaves at a comparable rate to that of Cit-Val.¹³⁶⁻¹³⁸ The Ala-Val linker has been selected for these targets because it has been reported in the literature¹³⁶ and noted in the Painter group that compounds containing it are more chemically tractable than those with Cit-Val. The more lipophilic nature of the methyl side chain makes the linkers (and intermediate compounds) more amenable to synthesis and purification.

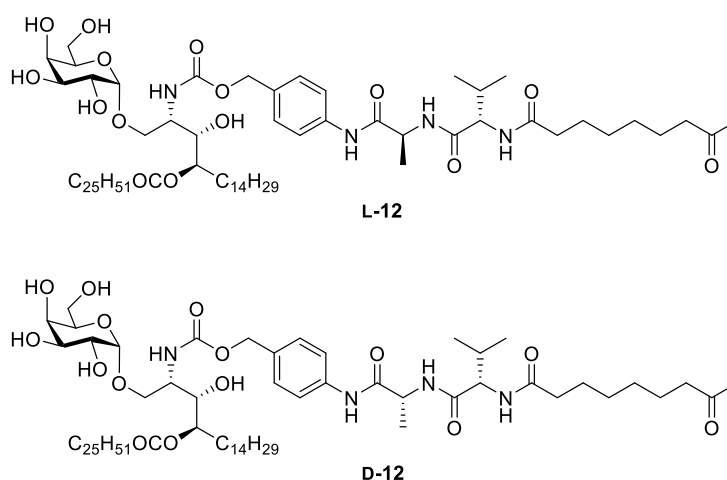
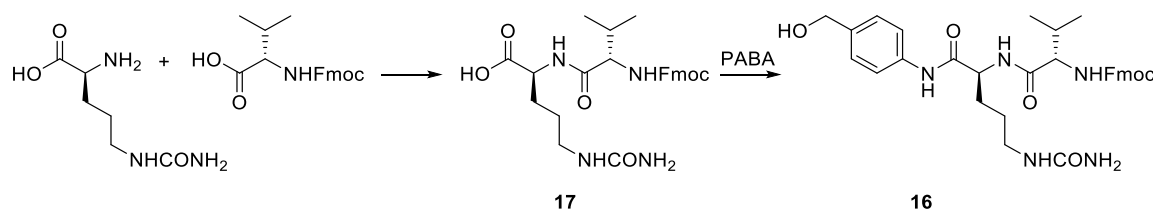


Figure 2.1 Structures of ketone targets **L-** and **D-12**.

2.2 Stereospecific Synthesis of Linkers

To accurately understand the effect of changing the stereochemistry of an amino acid, the synthesis of the short peptide linker must be highly stereospecific, otherwise any activity shown by the unnatural D-compound could be caused by contamination with the L-analogue. In the published synthesis of the PABA-Cit-Val-Fmoc peptide linker (**16**), the two amino acids are coupled together to give dipeptide **17** before the addition of *para*-aminobenzyl alcohol (Scheme 2.1).⁷⁹ This method is based on a procedure reported by Dubowchik et al.¹⁰⁴ and has been used extensively in the literature, which includes some of our own work.^{104, 139} This synthesis is in the N→C direction with respect to P1 (citrulline).



Scheme 2.1 Standard synthesis of PABA-Cit-Val linker (**16**) proceeds via the N→C direction with respect to P1.

In unpublished data, some epimerisation of the citrulline residue has been observed (up to 6%) when using this method in the synthesis of our conjugate vaccines. Figure 2.2 shows LC-MS SIM chromatograms of two PABA-Cit-Val-Fmoc epimers synthesised from commercially obtained citrulline samples. It can be clearly seen that some epimerisation (~1-3%) has occurred during this particular synthesis.

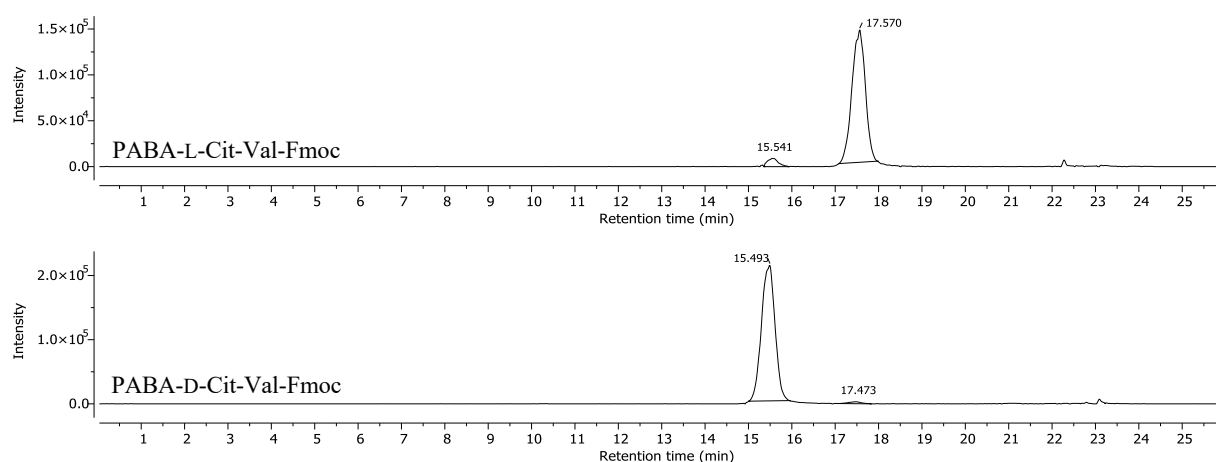
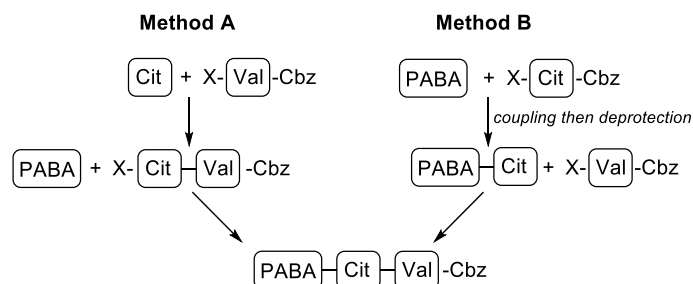


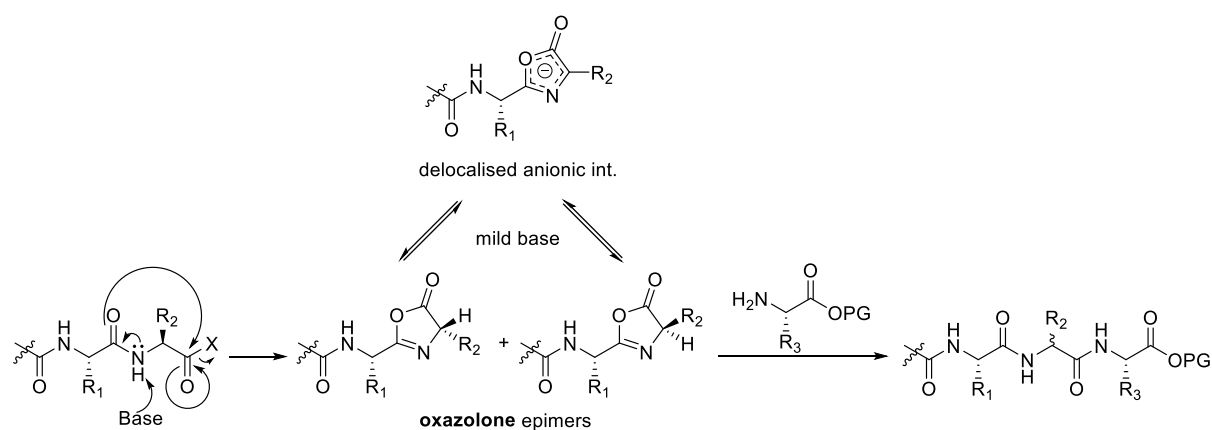
Figure 2.2 LC-MS data (SIM = 602.3 *m/z*) of PABA-Cit-Val-Fmoc epimers. Using HPLC Condition A (see section 6.1.2).

In 2018, Mondal et al.¹⁴⁰ also reported a substantial amount of epimerisation (up to 50%) at P1 (citrulline) when they followed the same linker synthesis. They proposed an alternative method (Scheme 2.2B), where the *para*-aminobenzyl alcohol is coupled to the first amino acid (citrulline) *before* the attachment of the second amino acid (valine). They report that this alternative method greatly reduces epimerisation.



Scheme 2.2 The original and widely used N→C method for linker synthesis first reported by Dubowchik et al.¹⁰⁶ (Method A) compared with the C→N method reported by Mondal et al.¹⁴⁰ (Method B).

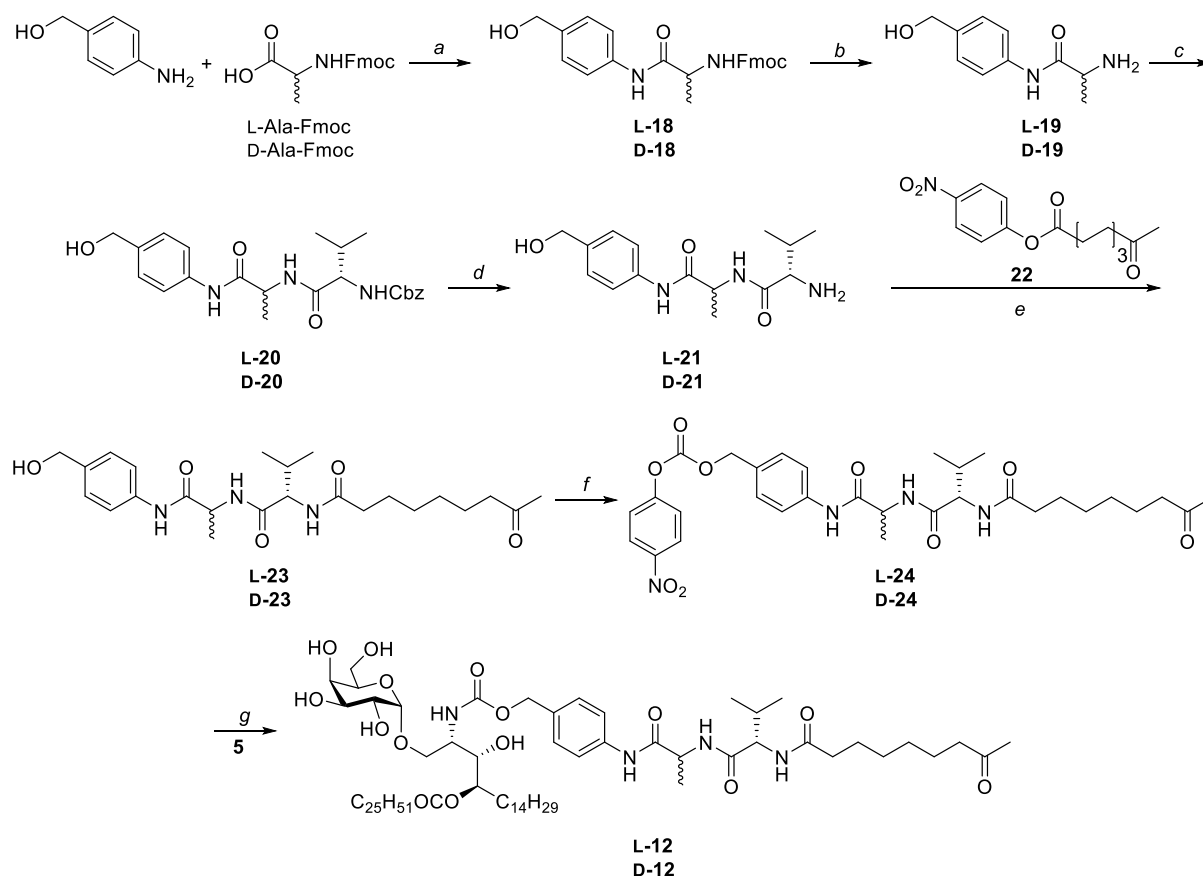
The method reported by Mondal et al. is in the C→N direction, the preferred direction for peptide synthesis. This direction is favoured because carboxylic acids are activated while the N-termini are protected as carbamates, which reduces the chance of racemisation through oxazolone formation. The formation of this unwanted species is enhanced when the activated acid is instead part of the growing peptide chain, as the nitrogen on the nearby amide bond can participate in an intramolecular attack on the activated carbonyl group (Scheme 2.3).



Scheme 2.3 Amino acid racemisation through oxazolone formation is favoured when the activated acid is part of the growing peptide chain. Where X is an activating group.

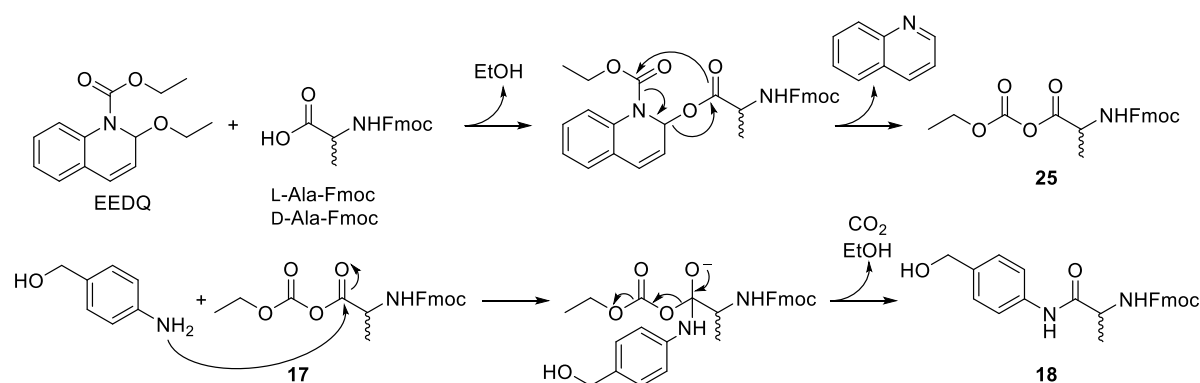
2.3 Synthesis of Ketone Epimers L- and D-12

The synthesis towards epimers **L-** and **D-12** is shown in Scheme 2.4. This synthesis follows the newer method proposed by Mondal et al.¹⁴⁰ where PABA is coupled to P1 (alanine) before the attachment of P₂ (valine). The synthesis of each target epimer begins with commercially purchased enantiomerically pure Fmoc protected alanine, allowing analysis of the optical purity of diastereomers **L-** and **D-12** and subsequent scrutiny of the stereospecificity of the synthesis. This scheme also differs from the reported synthesis of similar conjugate vaccines (Scheme 1.3) in that the ketone linker is installed before the addition of the α -GalCer prodrug component. This change reduces the number of chemical steps involving the synthetically advanced α -GalCer moiety. The syntheses of the two epimers were conducted in parallel, therefore they will be discussed simultaneously herein.



Scheme 2.4 Synthesis of ketone epimers **L-** and **D-12**. Reagents and conditions: a) EEDQ, CH₂Cl₂/CH₃OH (10:1), rt, 4.5 h, L = 58%, D = 67%; b) piperidine, DMF, rt, 1 h (not isolated); c) NHS-Val-Cbz, DMF, rt, 2 days, L = 89%, D = 75%; d) H₂, Pd/C, CH₂Cl₂/CH₃OH (1:9), rt, 1.5 h, L = quant., D = 97%; e) **22**, rt, 1.25 h, then DIPEA, 2.5 h, L = 70%, D = 84%; f) bis-*p*-NP carbonate, DIPEA, DMF, rt, 3 days, L = 71%, D = 86%; g) **5**, Et₃N, py, rt, o/n, L = 61%, D = 54%.

The syntheses began with the gram-scale *N*-ethoxycarbonyl-2-ethoxy-1,2-dihydroquinoline (EEDQ) promoted coupling of PABA to L-Ala-Fmoc and D-Ala-Fmoc, giving amides **L-18** (58%) and **D-18** (67%) respectively.^{125, 141, 142} The mechanism for this reaction is shown in Scheme 2.5,¹⁴³ where the activation of the acid proceeds via activated mixed anhydride **17**. The moderate reaction yields are due to poor recovery of the target materials from multiple triturations from Et₂O and CH₃OH/CH₂Cl₂. Column chromatography was attempted on **L-18** but the target amide was largely insoluble in the chromatography solvents (EtOAc/CH₂Cl₂). Additionally, the excess PABA starting material was not fully removed, leaving trituration as the more viable purification method. As expected, all data collected for the two enantiomers were the same, except for the optical rotation data, which were measured to be $[\alpha]_D^{20}$ -17.4° and +18.5° (c 1.00, DMF) for the L- and D- isomers, respectively. Analysis of the ¹H NMR data of the amides showed the expected downfield shift of the PABA protons *ortho* to the nitrogen compared to the PABA starting material.



Scheme 2.5 Reaction mechanism for the EEDQ promoted coupling of PABA to L- and D-Ala Fmoc to give **L-18** and **D-18**.

Fmoc deprotection to give amines **L-** and **D-19** proceeded quickly with 10% piperidine in DMF. An initial trial to purify the product by trituration from Et₂O was unsuccessful as target material loss was substantial. Given the only appreciable by-product was the Fmoc-piperidine adduct we deemed this purification step could be avoided. Thus, amine products **L-** and **D-19** were thereafter used directly in the next coupling reaction. The crude mixtures were analysed by HRMS-ESI and the protonated molecular ion was found at 195.1131 *m/z* (**L-19**) and 195.1140 *m/z* (**D-19**) consistent with the calculated value of 195.1134 *m/z*.

Amide coupling to NHS-Val-Cbz was conducted in DMF at room temperature over two days. The isolation of target materials **L-** and **D-20** was hindered by their low solubility in most solvents. The crude reaction mixture was added directly to a large volume of water, which

caused the formation of a white precipitate free of *N*-hydroxy succinimide. Two subsequent triturations from Et₂O further purified the target compounds. Filtration of the fine precipitates was troublesome, so when **D-20** was trituated, the solvent was instead removed by centrifugation (3 x 5 min at 4000 rpm). The two linkers were obtained in good to high yields, 89% and 75% for **L-** and **D-20** respectively. The ¹H NMR spectra of **L-** and **D-20** were very similar to one another and consistent with their structures (Figure 2.3). The side chain methyl resonances of the alanine and valine groups integrated for three and six protons respectively and the presence of the new peptide linkage was supported by the amide NH doublet at 8.13 ppm for **L-20** (8.31 ppm for **D-20**).

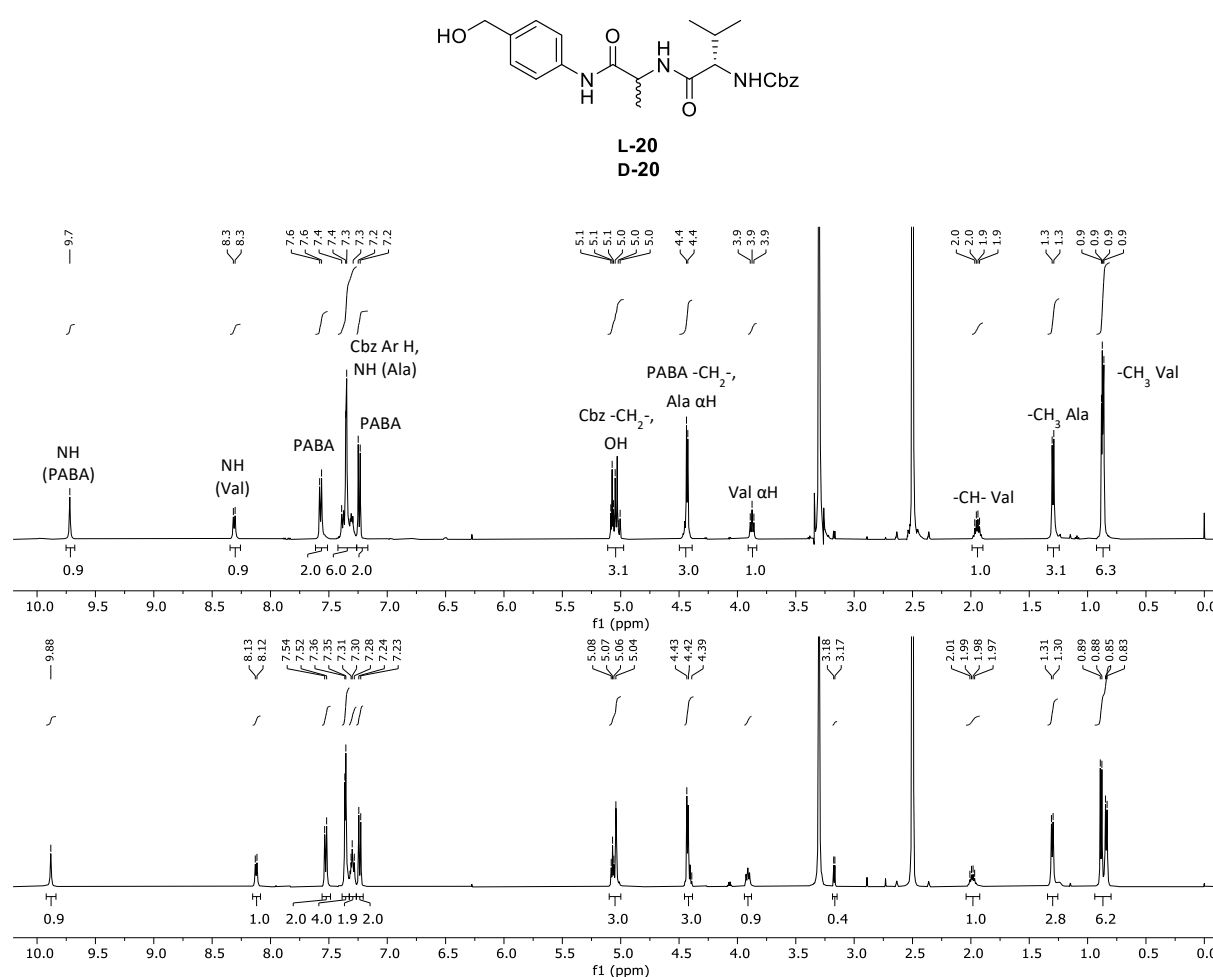


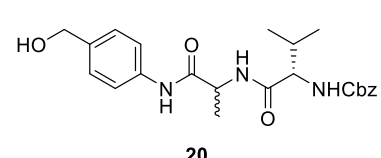
Figure 2.3 Comparison of the ¹H NMR spectra of the epimers **L-** and **D-20** in DMSO-*d*₆ at 500 MHz and 30 °C. The peak assignments for the two spectra are the same. Note that the valine methyl groups sometimes present as diastereotopic groups.

The stereochemical purity of diastereomers **L-** and **D-20** was assessed by reverse phase HPLC as this had been effective in the separation of the PABA-Cit-Val-Fmoc epimers (see Figure 2.2). A mixed sample containing both diastereomers (**L-** and **D-20**) was used in the development

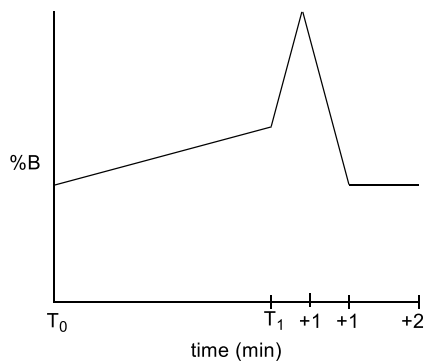
of the HPLC methods. Methods were developed by varying the solvent gradients over various times as indicated in Table 2.1.

Table 2.1 HPLC method development for the separation of **L-** and **D-20**, showing probed solvent gradients and resulting retention times. Using HPLC Condition B (see section 6.1.2), where solvent B is methanol.

entry	%B at T ₀	T ₁ (min)	%B at T ₁	R _t L-20 (min)	R _t D-20 (min)
1	40%	15.0	60%	10.7	10.9
2	45%	20.0	50%	11.5	11.7
3	45%	20.0	45%	12.4	12.7
4	40%	15.0	50%	13.6	13.8
5	40%	20.0	50%	15.7	16.0
6	40%	15.0	45%	16.9	17.1
7	42.5%	20.0	42.5%	17.8	18.2
8	40%	20.0	40%	22.3	22.3



20



Unfortunately, even after extensive efforts, including conditions that closely mimicked those that gave complete separation of PABA-Cit-Val-Fmoc epimers, we were unable to develop an HPLC method that achieved baseline resolution of the isomers **L-** and **D-20** (Figure 2.4). Although frustrated by this, the HPLC data of the individual isomers (not shown) show good peak shape with no visible evidence of isomeric contamination.

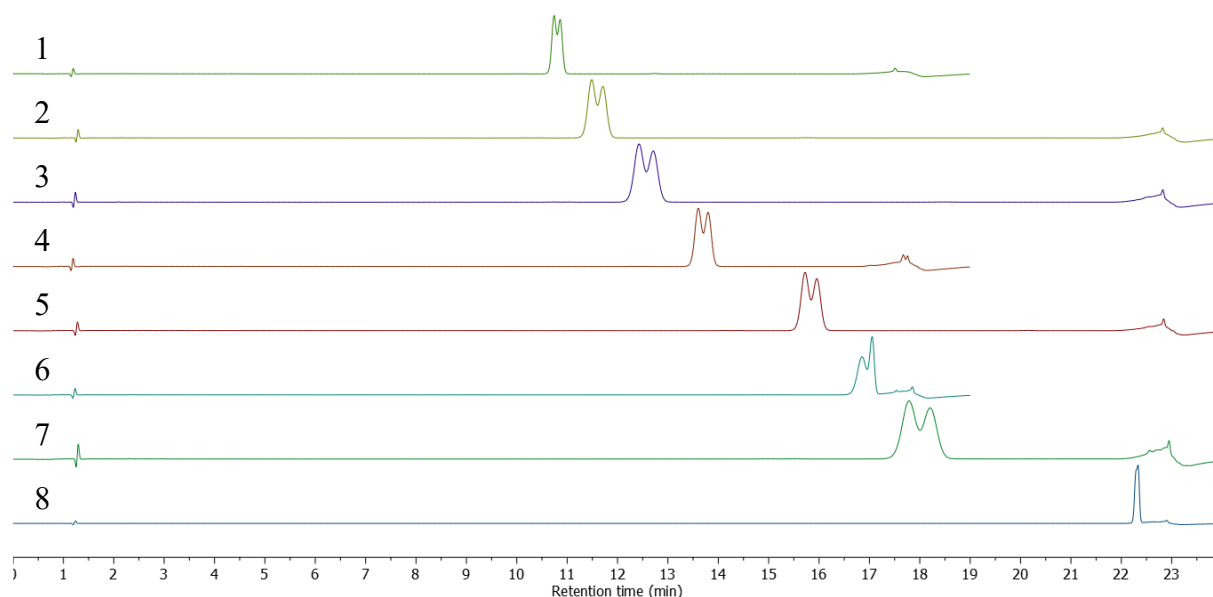


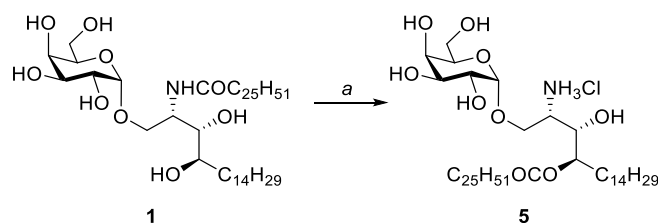
Figure 2.4 HPLC data (254 nm) of a 1:1 mixed sample of **L-** and **D-20** obtained with the methods shown in Table 2.1. Compound **L-20** is the fastest running peak in all samples.

The next step in the synthesis was Cbz deprotection of dipeptides **L-** and **D-20**. This was achieved with H₂ over a Pd/C catalyst. The Cbz protected starting materials (**L-** and **D-21**) were not fully soluble in the 10% CH₂Cl₂ in CH₃OH solvent mix. However, the reaction became homogenous as it progressed, indicating increased solubility of the product in this solvent mixture. Loss of the Cbz group was monitored by the appearance of a ninhydrin active spot on TLC. The reactions were filtered through Celite and concentrated in vacuo to give amines **L-** and **D-21** in excellent yields (quant. and 97% respectively). Once again, the NMR data of the two diastereoisomers were very similar to one another (not shown).

Attachment of 8-oxo-nonanoic acid was achieved through prior activation of the acid as a *p*NP ester (**22**).⁸¹ The activated acid was reacted with amine **L-** or **D-21** in DMF. After column chromatography (CH₃OH/CHCl₃) to remove the *para*-nitro-phenol by-product, ketone products **L-** and **D-23** were obtained in 70% and 84% yields respectively. The purified ketones were analysed by HRMS-ESI and the sodiated molecular ion was found at 470.2635 *m/z* (**L-23**) and 470.2636 *m/z* (**D-23**) consistent with the calculated value for [M + Na]⁺ of 470.2631 *m/z* supporting the large increase in mass incurred by the attachment of the nine carbon keto-acid.

The hydroxy termini of **L-** and **D-23** were then activated as the *p*NP carbonates by overnight reaction with bis (*para*-nitro phenyl) carbonate and DIPEA in DMF. Column chromatography in EtOAc/CH₂Cl₂ (to avoid potential methanolysis when using methanol as a chromatography solvent) afforded the *p*NP activated linkers **L-** and **D-24** in 71% and 86% yields respectively. The only notable difference between the ¹H NMR spectra of the two diastereoisomers was the position of the variable NH signals.

The next step in the synthesis was the attachment of the pro-adjuvant compound α -GalCer (**5**), which is first formed by the reaction of the active lipid adjuvant (α -GalCer, **1**)¹⁴⁴ with concentrated HCl in dioxane (Scheme 2.6).⁷⁸⁻⁸⁰ Following the literature method,⁸⁰ the amide starting material was first heated to 65 °C in freshly distilled dioxane until fully dissolved. Hydrochloric acid was then added, and the reaction was heated at 65 °C for a further 25 min whereupon the heating was removed, and the reaction was allowed to cool to rt. The emergence of a lower running spot on the silica TLC plate indicated that the formation of the polar amine product.



Scheme 2.6 Reaction of α -GalCer (**1**) with acid promotes acyl chain migration to form $m\alpha$ -GalCer (**5**). Reagents and conditions: a) HCl, dioxane, 65 °C, 20 min.

The formation of **5** was corroborated by the conversion of the amide starting material peak to an earlier running peak by C18 HPLC-CAD (Figure 2.5). Other peaks present in the chromatogram could be indicative of a regioisomer with the acyl chain on the other free hydroxyl group. Once cooled to rt, the reaction was concentrated in vacuo to give the crude hydrochloride salt of $m\alpha$ -GalCer (**5**) as a white solid, which was used without further purification.

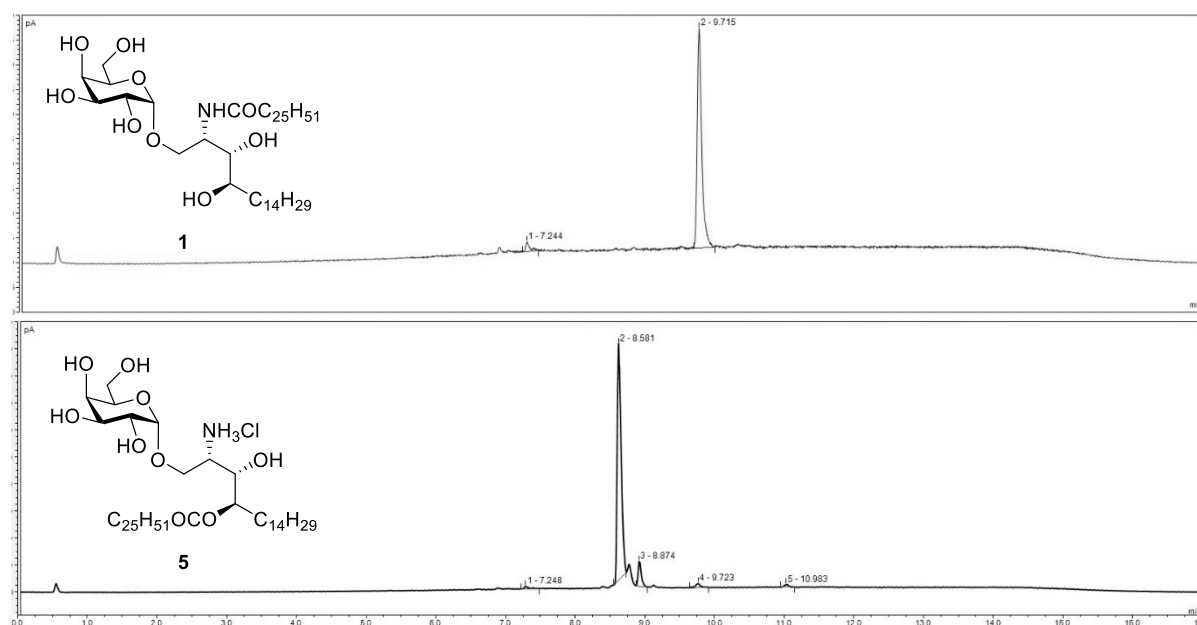


Figure 2.5 HPLC-CAD chromatograms showing conversion of α -GalCer (**1**) to $m\alpha$ -GalCer (**5**). Using HPLC Condition C (see section 6.1.2).

Subsequent coupling of $m\alpha$ -GalCer (**5**) to the two activated linkers (**L**- and **D-24**) was conducted in pyridine with 2.5 equivalents of Et₃N (Scheme 2.4). The reactions were stirred overnight at room temperature before purification by silica column chromatography (CH₃OH/CHCl₃). This gave the two adjuvant-linker compounds **L**- and **D-12** as white solids in 61% and 54% yields respectively. These moderate yields are typical in our research group for this reaction, which can be partially explained by the use of crude starting materials.⁸¹

Analysis of the ^1H NMR spectra of the two target compounds (**L-** and **D-12**) indicates a large upfield shift of the benzylic proton signals from 5.24 ppm in **L-** and **D-24** to 4.95 ppm in **L-** and **D-12**, indicating successful carbamate formation (Figure 2.6). The two spectra are very similar to one another, with only a slight difference in the chemical shift of the valine αH signals.

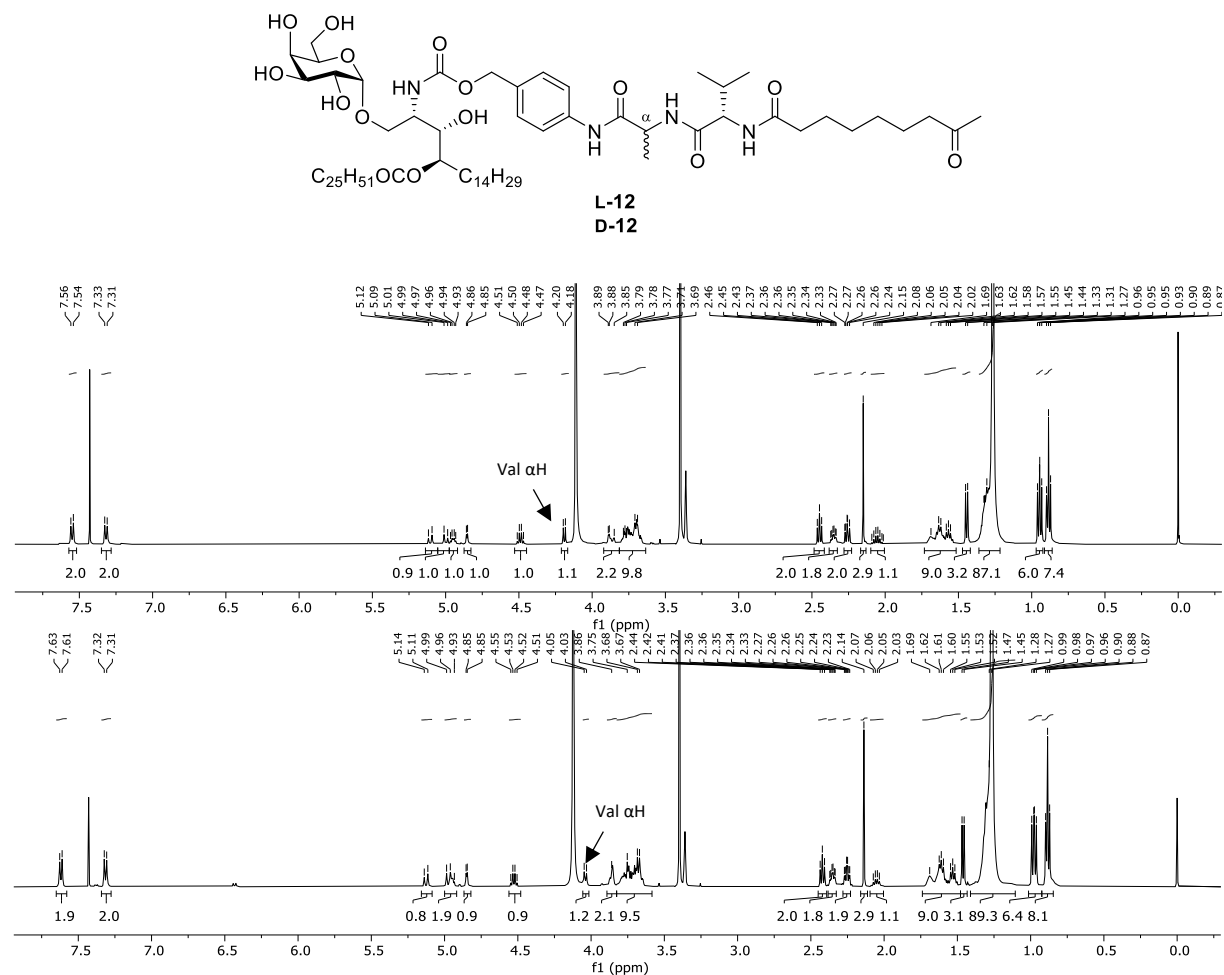
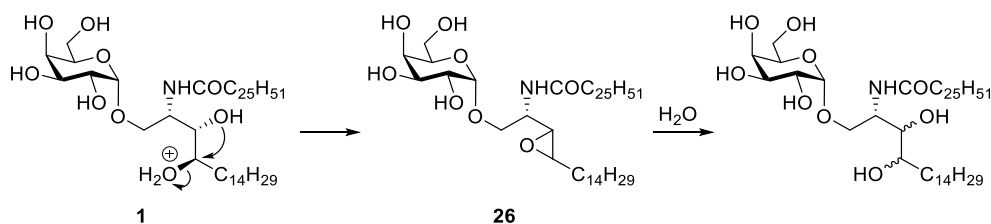


Figure 2.6 ^1H NMR spectra of **L-** and **D-12** in 2:1 $\text{CDCl}_3/\text{CD}_3\text{OH}$ at 500 MHz and 30 °C. Arrows indicate the position of the valine αH signal.

Analysis of the HR-MS data of the two ketones showed the sodiated target material peaks at 1353.9734 and 1353.9736 m/z for **L-** and **D-12** respectively, this closely matches the calculated mass for $\text{C}_{75}\text{H}_{134}\text{N}_4\text{O}_{15}\text{Na}$ of 1353.9743 m/z . However, compounds **L-** and **D-12** could not be fully purified and were found to be contaminated with a compound tentatively assigned as epoxide **26** (Scheme 2.7), as evidenced in the HR-MS with a peak at 840.7300 m/z (calcd. for $\text{C}_{50}\text{H}_{98}\text{NO}_8$, 840.7287 m/z). Epoxide **26** could have formed under the acidic conditions of the earlier rearrangement of α -GalCer (**1**). The epoxide can be formed by intramolecular attack of either hydroxyl group, thus a mixture of epoxide isomers may be formed, which, when

hydrolysed would give rise to a diol where scrambling of the stereochemistry at C3' and C4' has occurred.



Scheme 2.7 Epoxide **26** formed via intramolecular displacement of protonated hydroxyl group on α -GalCer (**1**) could then be hydrolysed with a loss of stereochemical information at C3' and C4'.

Oddly, epoxide **26** has a similar retention time to $m\alpha$ -GalCer (**5**) on C18 (i.e. HPLC) as well as a similar NMR profile, making detection after the migration reaction difficult. Past observations from the Painter group indicate that this impurity can be removed by column chromatography on silica, but this extra purification step results in a lower overall yield. It isn't until after $m\alpha$ -GalCer (**5**) is coupled to a linker that the epoxide impurity becomes observable by HPLC. However, at this stage it can still be difficult to remove for solubility reasons.

In the case of ketones **L-** and **D-12**, analysis of the HPLC-CAD data indicates that there is approximately 5-6% of epoxide **26** present. The ketones have already passed through a normal phase silica column, which suggests that normal phase flash chromatography is insufficient to remove the epoxide contaminant. Reverse phase chromatography is also unlikely to be effective, as the ketones and the epoxide both elute from an HPLC column after a 100% methanol hold. Preparative HPLC could be used. However, as the conjugates formed in the next step are usually purified via preparative HPLC, we chose to wait until after conjugation to peptides to remove the epoxide contaminant. As the peptide conjugation was beyond the scope of this project, the target ketones **L-** and **D-12** were not purified further at this stage.

2.4 Summary and Future Work

In this section we have discussed the synthesis towards advanced intermediates **L-** and **D-12**. The synthesis followed a modified method¹⁴⁰ of the standard synthesis of PABA-dipeptide linkers. This modified method aimed to reduce possible epimerisation at the P1 stereocenter, which is especially important when investigating the effects of inverting stereochemistry at P1. One pair of early diastereomeric intermediates (**L-** and **D-20**) were analysed by HPLC to

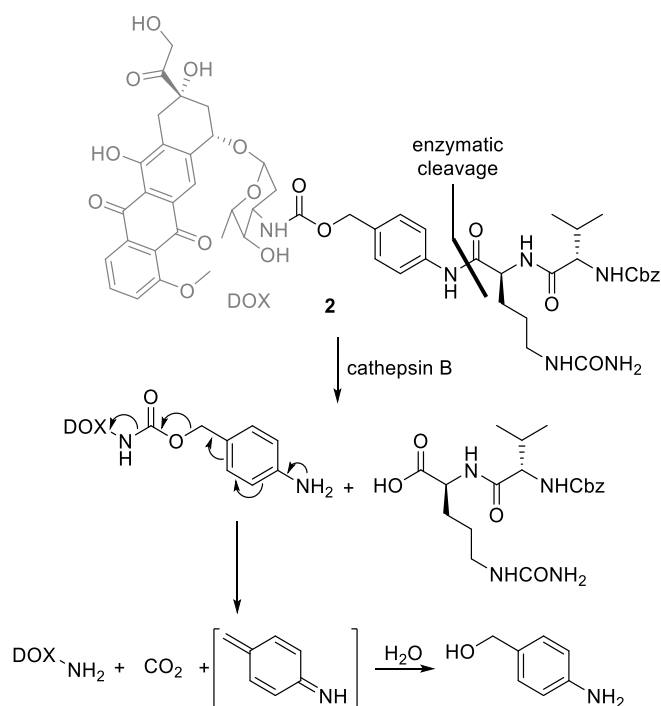
investigate the level of epimerisation taking place during the initial coupling reactions. Unfortunately, the analysis was inconclusive, only indicating that complete epimerisation had not occurred. Future analysis might involve spiking one isomer with ever increasing doses of the other to estimate the level of detection of the other isomer in the individual products as well as changing HPLC columns and solvent systems.

The synthetic approach coupled the pro-adjuvant α -GalCer (**5**) to a fully elaborated linker that differed from the published route.⁷⁸⁻⁸⁰ This was slightly advantageous in that fewer overall manipulations were required with synthetically intractable lipid moiety present. However, the additional step in the literature method provides an extra opportunity to remove any impurities, so may be more advantageous overall. In general, the syntheses were successful, with slightly higher yields obtained for the D-Ala analogues as these reactions were carried out after the corresponding L-Ala reactions, allowing any knowledge gained from the first reactions to be applied to the later ones.

The targets **L-** and **D-12** were obtained on the milligram scale (14 and 12 mg respectively) but were contaminated with a small amount of epoxide **26**. Future work in this area includes further purification, mostly likely after conjugation to various peptide antigens or through introduction of silica chromatography after the migration step. Both the ketones and their resulting conjugates will be tested in cathepsin B assays to determine whether the D-Ala linker has an effect on the enzymatic cleavage rate and subsequent release of α -GalCer.

Chapter 3 Removing the Immolative Linker

Immolative spacers such as *para*-amino benzyl carbamate (PABC) are commonly used to relieve steric crowding around enzymatic cleavage sites.^{108, 110, 111} For example as mentioned in the introduction of this thesis, model doxorubicin (DOX) prodrug **2** utilises the PABC group to separate the bulky anthracycline from the enzymatic cleavage site (Scheme 3.1).^{104, 106} When the PABC group was omitted such as in compound **3** (Figure 1.6), no release of the doxorubicin payload was observed.¹⁰⁴ Interestingly, cleavage was once again observed when the PABC group was replaced by a glycine (**4**). This suggests that for enzymolysis to occur on substrates with bulky payloads (e.g. DOX), a non-sterically demanding group is required adjacent to the enzymatic cleavage site.



Scheme 3.1 Hydrolysis of DOX-PABC-Cit-Val-Cbz (**2**) by cathepsin B allows release of the doxorubicin amine payload.¹⁰⁴

The necessity of the PABC spacer in our vaccine conjugate system (Figure 1.8) has not been explored. As the acid sensitivity of the carbamate linkage can be synthetically limiting (e.g. not compatible with automated solid phase peptide synthesis), it could be advantageous to remove the PABC unit entirely.¹⁴⁵⁻¹⁴⁷ This was probed by the synthesis of model compound **13** (Figure 3.1), which contains an Ala-Val dipeptide directly attached to a model payload, 4-butylaniline.

As for ketones **L-** and **D-12**, alanine is used in place of citrulline for ease of synthesis. The Cbz group at the N terminus of the dipeptide is well tolerated by cathepsin B.^{104, 106} Once synthesised, model compound **13** will be assessed for enzymatic cleavage in a cathepsin B assay.¹³⁵

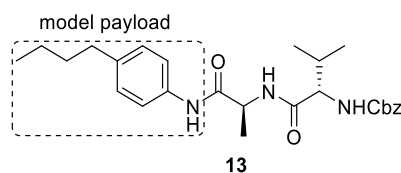
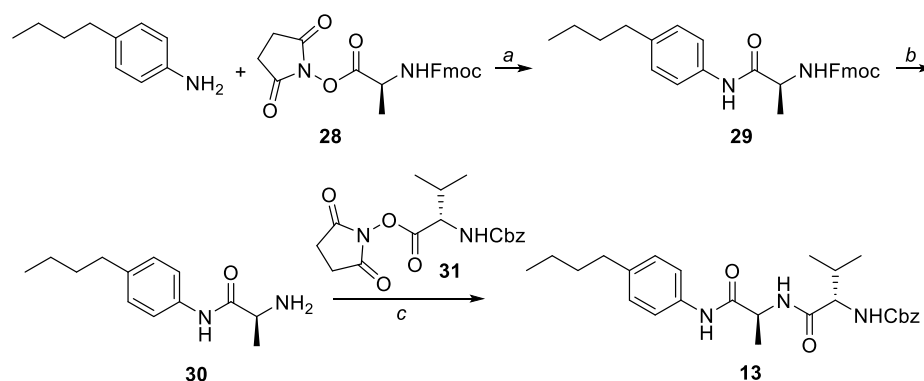


Figure 3.1 Structure of model PABC-free compound **13**.

3.1 Synthesis of Model Linker **13**

The synthesis of model compound **13** began with the reaction of NHS activated alanine (**28**)¹⁴⁸ with 4-butylaniline (Scheme 3.2). Purification of amide **29** by column chromatography using PE/EtOAc was problematic due to solubility issues. The issue was easily solved when CH₂Cl₂ was used in place of PE, thus affording amide **29** in good yield. The coupling was evident by an increase in molecular weight where the parent ion (465.2159 *m/z*) was consistent with [29 + Na]⁺. The aromatic proton signals in the ¹H NMR spectrum were downfield compared to those of 4-butylaniline due to the attachment of the electron-withdrawing amide group (Figure 3.2). A one proton singlet at 5.30 ppm was attributed to the new amide proton resonance. Also observed was the expected upfield shift of the alanine alpha proton signal from 4.79 to 4.34 ppm.



Scheme 3.2 Synthesis of PABC-free model **13**. Reagents and conditions: a) THF, rt, 2 days, 84%; b) 10% piperidine in DMF, rt, 30 min, 89%; c) **31**, THF, rt, 5 h, 68%.

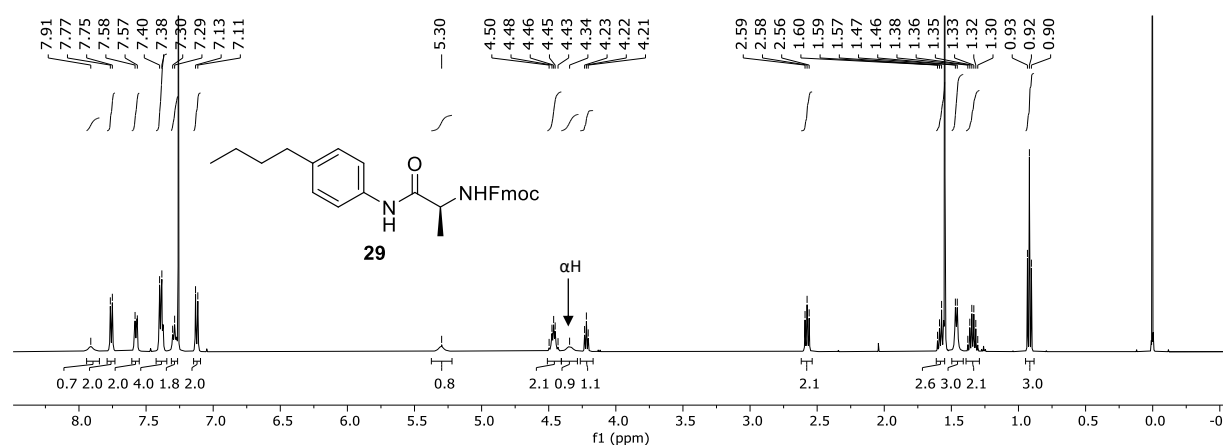


Figure 3.2 ^1H NMR spectrum of amide **29** in CDCl_3 at 500 MHz and 30 $^\circ\text{C}$.

Fmoc deprotection of amide **29** with 10% piperidine in DMF then yielded amine **30** in an 89% yield after silica column chromatography using $\text{CH}_3\text{OH}/\text{CHCl}_3$ with triethylamine. The formation of amine **30** was supported by the appearance of a more polar, ninhydrin positive spot on TLC. The ^1H NMR spectrum further corroborates this, with the loss of the Fmoc related peaks and the upfield shift of the alanine α proton from 4.34 to 3.58 ppm (Figure 3.3). Additionally, the decrease in mass to 221.1651 m/z by HR-MS (calcd for $\text{C}_{13}\text{H}_{21}\text{N}_2\text{O}$, 221.1654) further supports the loss of the Fmoc protecting group.

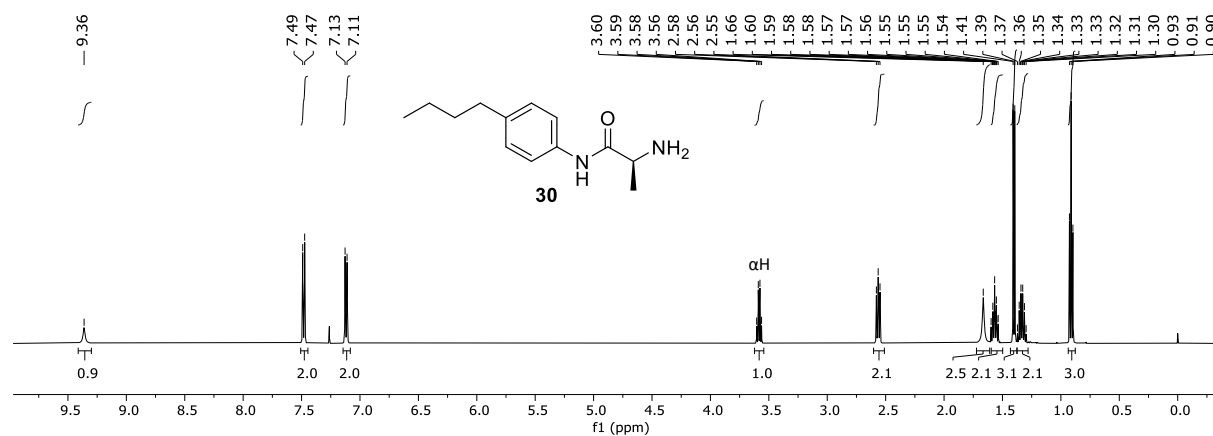


Figure 3.3 ^1H NMR spectrum of **30** in CDCl_3 at 500 MHz and 30 $^\circ\text{C}$.

Reaction of amine **30** with NHS activated Cbz protected valine (**31**)¹⁴⁹ gave crude linker **13**. As with amide **29**, column chromatography was unsuccessful with PE/EtOAc as solvents but substituting CH_2Cl_2 for PE allowed compound **13** to be easily purified and obtained in a 68% yield. The amide coupling was supported by the downfield shift of the alanine α proton signal to 4.67 ppm in the ^1H NMR spectrum of **13** (Figure 3.4). Additionally, the side chain methyl resonances of the alanine and valine groups integrated for three and six protons respectively.

The successful reaction was further corroborated by the large increase in mass to 476.2521 m/z (calcd for $C_{26}H_{35}N_3O_4Na$, 476.2525).

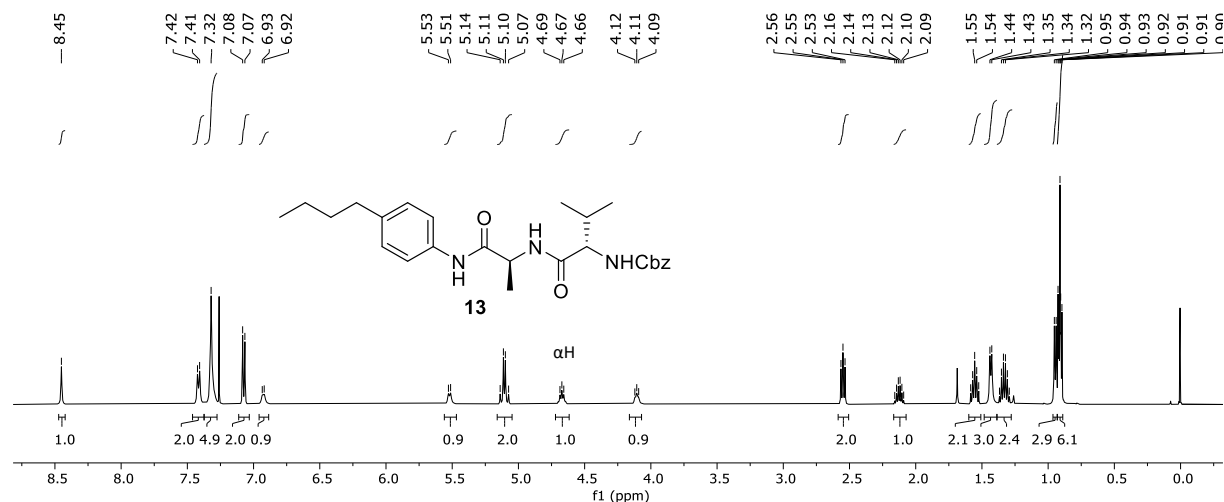


Figure 3.4 ¹H NMR spectrum of **13** in CDCl₃ at 500 MHz and 30 °C.

3.2 Cathepsin B Assay of Model Linker **13**

Model linker **13** was analysed for cleavage by cathepsin B in a biochemical assay.[‡] Full experimental details of the assay are provided in Section 6.1.1. Briefly: the substrate is incubated overnight in an ammonium acetate/EDTA/dithiothreitol buffer solution with the cathepsin B enzyme. Analysis by LC-MS and comparison to a control sample (incubated without enzyme) shows level of enzymatic cleavage. In the case of compound **13**, after 24 hours at 37 °C all of the amide substrate had been cleaved into 4-butylaniline and Ala-Val-Cbz (Figure 3.5). This clearly suggests that in this system the carbamate functionality in the PABC immolative spacer is not required for cleavage by cathepsin B.

[‡] Kindly carried out by co-worker Dr Susanna Chan.¹³⁵ DOI: 10.1021/acscchembio.9b00902

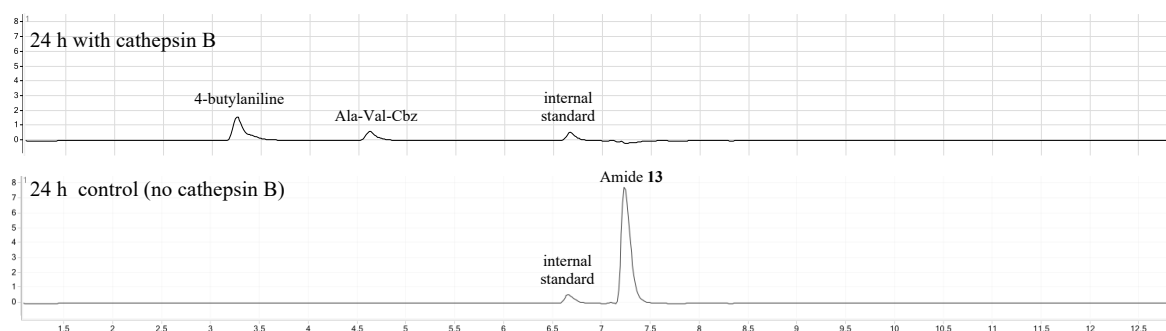


Figure 3.5 24 h time point LC-MS selected ion chromatograms for cathepsin B assay of **13**. Top: incubated with cathepsin B. Bottom: control, without cathepsin B. Internal standard is phytosphingosine.

3.3 Summary and Future Work

Model compound **13** was synthesised in three steps from NHS-activated amino acids in a 51% overall yield. The reactions proceeded well, with the only difficulties arising from solubility issues during purification. Incubation with cathepsin B in an enzymatic assay indicated that the PABC-free model compound (**13**) could be cleaved by cathepsin B. This suggests that the carbamate functionality in the PABC group is not needed in this context, therefore the next step is to synthesise the PABC-free intermediate compound **32** followed by PABC-free conjugate **33** (Figure 3.6). These compounds will be synthesised sequentially, with the results of the synthesis and enzymatic analysis of intermediate **32** determining whether or not conjugate **33** will be synthesised. If cathepsin B is capable of cleaving **33**, this could result in the removal of the PABC group from future conjugates.

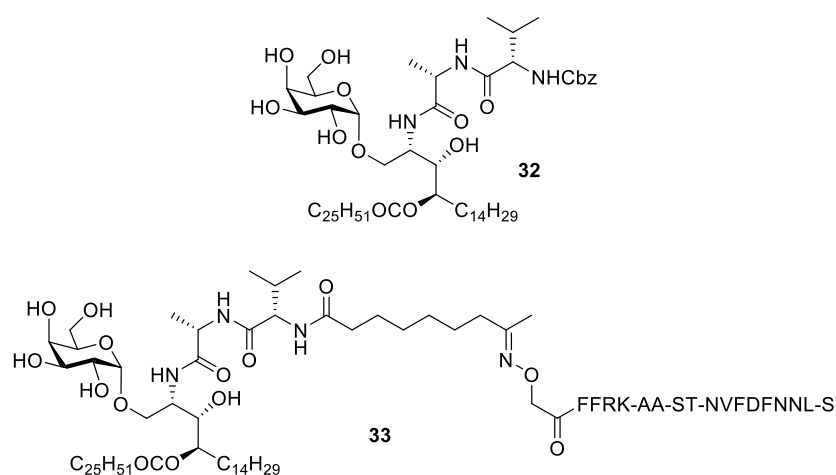


Figure 3.6 Structures of PABC-free compounds **32** and **33**.

Chapter 4 Efforts Towards Altering

Biodistribution

For a drug molecule to have its desired effect a sufficient concentration of the active pharmaceutical ingredient must reach its site of action. The efficiency of the delivery is dependent on a multitude of factors (e.g. adsorption, distribution, elimination, metabolism, excretion, and toxicity) that are collectively called the pharmacokinetics (PK) properties of the drug. Both drug potency and PK properties determine the overall efficacy of the drug.

In drug development, one PK optimisation method is to investigate the relationship between logP (solubility/biodistribution of the drug) and activity. This can be difficult to achieve for small molecule drugs because any variation in the chemical structure to change the solubility (and therefore biodistribution) would likely also change drug-receptor interactions. The conjugate vaccines used in this research comprise of two components that require processing before they can interact with their target receptors. The components are coupled together through a linker that is assumed to not be involved in any receptor interactions. Therefore, we hypothesise that we should be able to alter the in vivo biodistribution properties of these conjugate compounds by varying the chemical composition of the linker, without disruption of the receptor binding interactions.

A related observation is that the rate of in vitro biochemical cleavage of the vaccine constructs by cathepsin B is often slower for vaccines that are less soluble in aqueous media (unpublished work by Chan et al.). To probe the effect solubility and biodistribution have on cathepsin B cleavage we chose to investigate increasing the hydrophilicity of the vaccine conjugates by the installation of a discrete polyethylene glycol (PEG)[§] linker between the two active components. Replacement of the 8-oxo-nonanoic acid linker gives target compounds **14** (n = 16) and **15** (n = 24) (Figure 4.1). This modification to the vaccine design is traceless with respect to the active components and therefore shouldn't affect the drug-receptor interactions. However, the

[§] Note that the term polyethylene glycol or PEG is here used for any length of a repeating ethylene glycol sequence or derivative thereof.

increase in water solubility may increase the overall rate of processing by proteasomal enzymes (such as cathepsin B), which will likely impact the vaccine's activity.

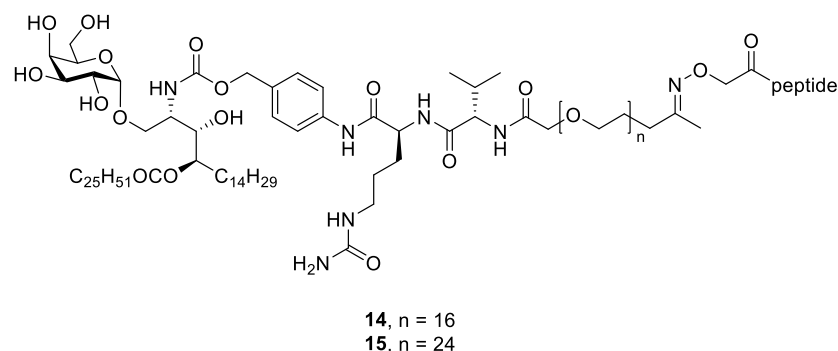


Figure 4.1 Structures of PEG based vaccines **14** and **15**. Where peptide = FFRK-AAA-ST-NVDFNNL-S.

4.1 LogP Analysis

Once target compounds are synthesised, their physical properties will be assessed before any biological analysis. The main physical property we wish to measure is the partition coefficient, known as logP. LogP is a measurable, although an imperfect proxy of hydrophilicity. It is defined as a measure of a compound's affinity for the aqueous phase over the organic phase (usually *n*-octanol):

$$\log P = \log_{10} \left(\frac{C_{n\text{-octanol}}}{C_{\text{water}}} \right)$$

where $C_{n\text{-octanol}}$ and C_{water} are the concentration of the compound in *n*-octanol and water respectively.

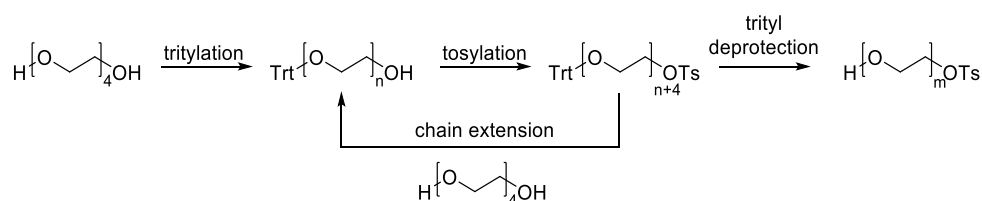
Historically, logP was measured by the shake-flask method, which required dissolving the analyte in a volume of *n*-octanol and water, then shaking the vessel and measuring the concentration of the analyte in each solvent.^{150, 151} This method can be difficult for analytes with very large or very small logP values, as their solubility in the aqueous or organic phases respectively are so low that it is difficult to measure their concentrations accurately. Moreover, this method is suboptimal when limited amounts of analyte are available, which would be the situation in this case. Computational methods to predict logP values exist, but these can be unwieldy for large compounds. We instead plan to approximate the logP values of our targets through HPLC methods,¹⁵²⁻¹⁵⁴ which in comparison to the original shake-flask methods, tend to be much more time and material efficient. Some HPLC methods for determining logP involve

measuring the change in analyte retention time across a range of concentrations of isocratic eluents.¹⁵³ An alternative is to compare retention times using a gradient method with gradient retention equations and indexes.¹⁵²

4.2 Discrete PEG Linkers

To help with the interpretation of any results we require discrete vaccine molecules, with defined structures. However, PEG chains are usually produced by polymerisation, which gives heterogenous samples with chains of varying lengths.¹⁵⁵ The polymerisation process can be controlled to give PEG chains with low polydispersity, but polymerisation will not yield monodisperse samples of a single chain length. In contrast, standard chemical methods can be used to synthesise “discrete” PEGs, where the number of repeating ethylene glycol units is highly defined. Discrete PEGs are commercially available, but as chain length increases their cost becomes prohibitive, therefore we chose to synthesise our own discrete PEG-based linkers.

Of the many reported syntheses of discrete PEGs, most require chromatography at every step to maintain high purity.¹⁵⁵⁻¹⁵⁸ This can be challenging, often requiring extensive optimisation of the chromatographic conditions.¹⁵⁸⁻¹⁶⁰ Although chromatography allows for the synthesis of highly pure monodisperse chains, we followed the simple chromatography-free iterative synthesis of Kinbara and coworkers.¹⁶¹⁻¹⁶³ Their strategy depends on the stronger organic phase affinity of mono-tosylated PEGs over that of PEG diols, which allows the diols to be selectively removed by aqueous separation. The synthesis begins with mono-trityl protected tetraethylene glycol, which is iteratively activated as the mono-tosylate before extension by reaction with tetraethylene glycol diol (Scheme 4.1). Bis-tritylated side-products are generated in the first tritylation step and in every chain extension step. However, they are converted to water soluble diols in the final trityl-deprotection step, which allows them to be easily washed out during the final aqueous workup.



Scheme 4.1 Iterative synthesis of discrete PEGs as described by Kinbara et al.¹⁶³

This approach allows us to obtain mono-tosylated discrete PEG chains that we envisaged could easily be derivatised into bifunctional linkers for use in our conjugates. The standard linker currently used in our conjugate vaccines is 8-oxo-nonanoic acid, which contains an acid functionality at one end and a methyl ketone at the other. We wished to retain this pattern of functionality to develop related analogues. In other words, we aimed to derivatise the discrete PEG chains such that they have a carboxylic acid group at one end and a methyl ketone at the other (Figure 4.2).

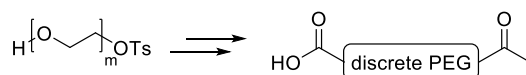
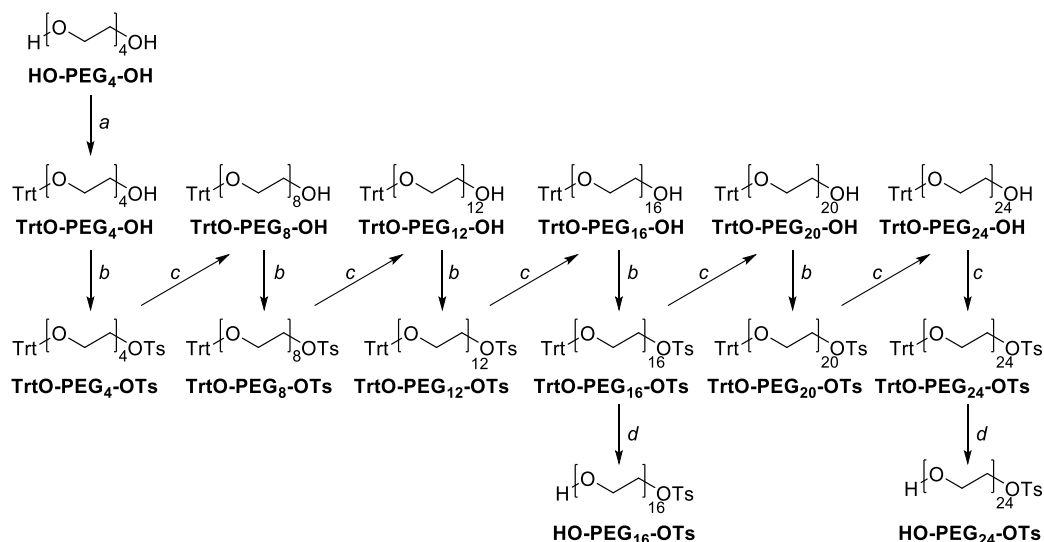


Figure 4.2 General structure of discrete PEG keto-acid linker targets.

4.3 Iterative Synthesis of Discrete PEG Chains

The synthesis of the discrete PEG linkers began with the synthesis of discrete mono-tosylated PEGs **HO-PEG₁₆-OTs** and **HO-PEG₂₄-OTs** (Scheme 4.2).¹⁰²⁻¹⁰⁴ Water was removed from tetraethylene glycol samples immediately before use by azeotropic co-evaporation with toluene, but the hygroscopic nature of the PEG chains was not found to be a major issue. As the intermediate compounds were not purified, no intermediate yields are reported here.



Scheme 4.2 Iterative synthesis towards **HO-PEG₁₆-OTs** and **HO-PEG₂₄-OTs**. Reagents and conditions: a) TrtCl, Et₃N, rt, 3 h; b) NaOH, THF, H₂O, 0 °C, 30 min, then TsCl, 0 °C, 6.5 h; c) NaH, tetraethylene glycol, THF, 0 °C, then tosylate, THF, 75 °C, 5 h; d) *p*TsOH, CH₃OH, rt, o/n.

The synthesis began with the reaction of TrtCl with a seven-fold excess tetraethylene glycol and Et₃N to give **TrtO-PEG₄-OH** as a pale-yellow oil. A slight over integration of the aromatic region in the ¹H NMR spectrum of **TrtO-PEG₄-OH** can be explained by the presence of the expected side-product **TrtO-PEG₄-OTrt** (Figure 4.3). HPLC analysis of the crude material supported the presence of ~14% bis-tritylated material (Figure 4.4). As mentioned earlier, this unreactive side-product was not removed until the final de-tritylation step. All compounds produced during this iterative synthesis were used crude, so the stoichiometry for all subsequent reactions were based on the initial limiting trityl chloride reagent.

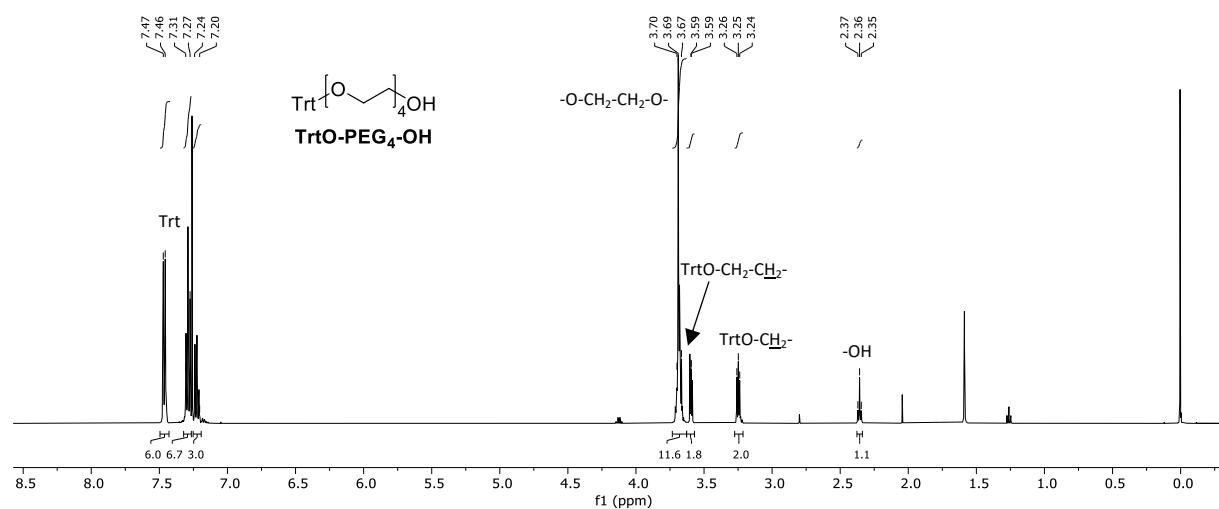


Figure 4.3 ¹H NMR spectrum of **TrtO-PEG₄-OH** in CDCl₃ at 500 MHz and 30 °C. Some residual EtOAc is present.

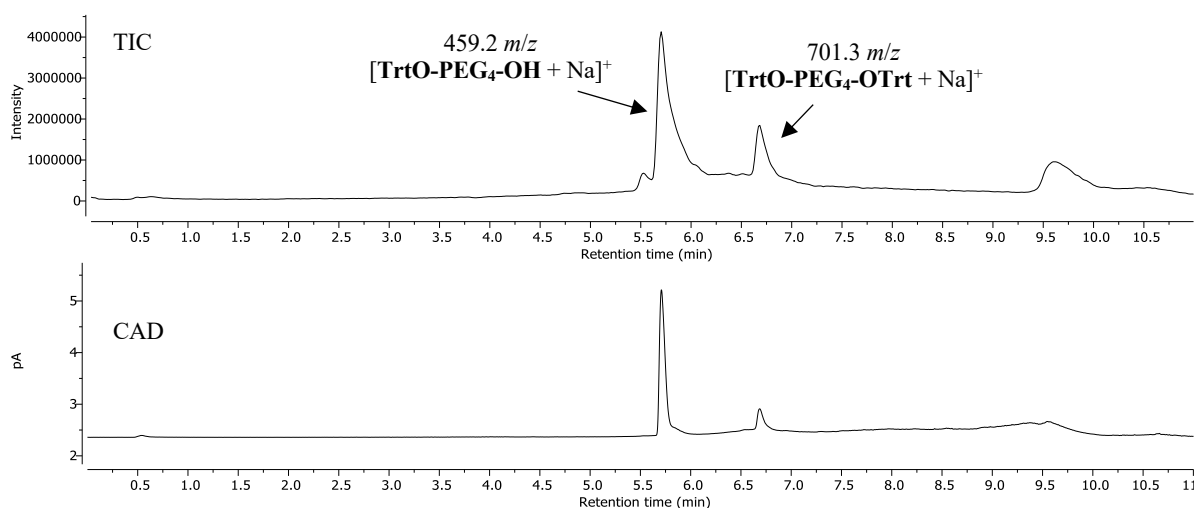


Figure 4.4 TIC (top) and CAD (bottom) chromatograms of crude **TrtO-PEG₄-OH** indicating presence of bis-tritylated **TrtO-PEG₄-OTrt**. Using HPLC Condition D (see section 6.1.2).

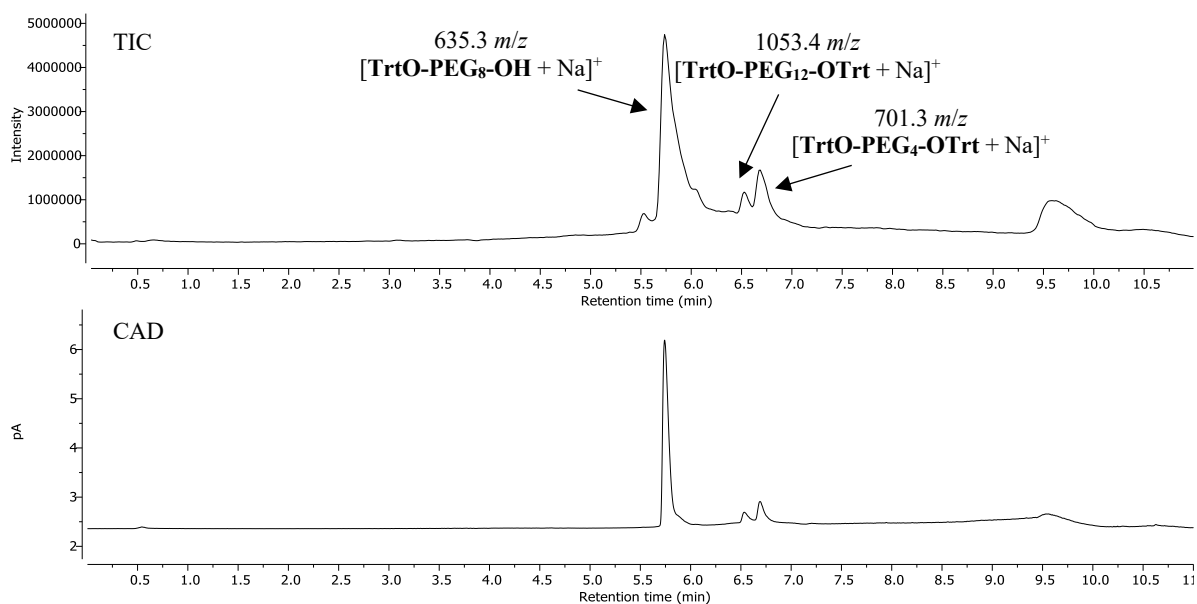


Figure 4.6 TIC (top) and CAD (bottom) chromatograms of crude **TrtO-PEG₈-OH** indicating presence of bis-tritylated **TrtO-PEG₄-OTrt** and **TrtO-PEG₈-OTrt** side-products.

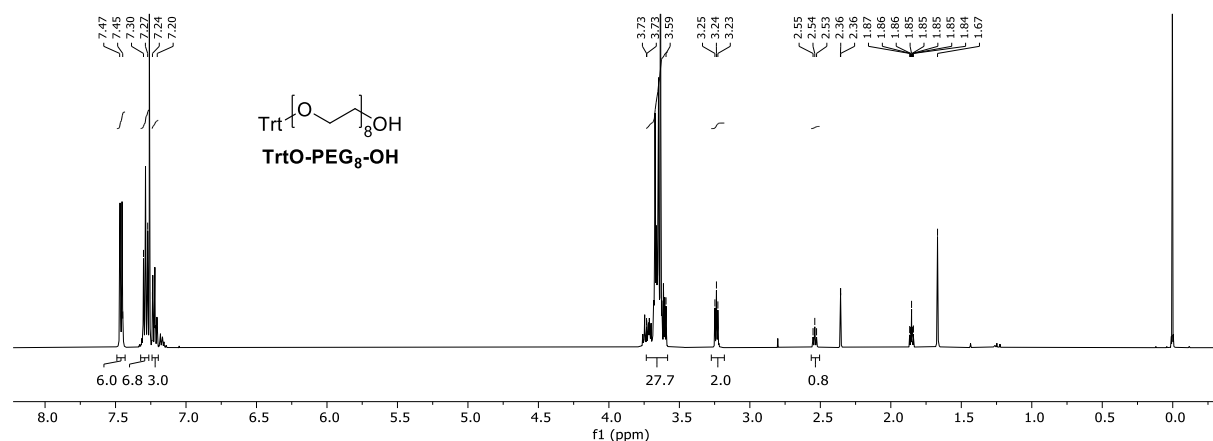


Figure 4.7 ^1H NMR spectrum of **TrtO-PEG₈-OH** in CDCl_3 at 500 MHz and 30 °C. Some residual THF is present.

With **TrtO-PEG₈-OH** in hand, the tosylation and chain extension steps were repeated until **TrtO-PEG₁₆-OTs** was obtained. Data for these steps are reported in the experimental section of this thesis. The data obtained of intermediate compounds were as expected and matched literature when the bis-tritylated impurities were taken into account.¹⁶³

Trityl deprotection of **TrtO-PEG₁₆-OTs** using TsOH in CH_3OH yielded **HO-PEG₁₆-OTs**, which was separated from the diol contaminants by organic extraction. **HO-PEG₁₆-OTs** was obtained in a 16% yield over nine steps. LC-MS analysis of the crude white solid indicated the presence of some of the shorter chain tosylate **HO-PEG₁₂-OTs** (Figure 4.8). Unfortunately, the

retention times of the two compounds were too similar to quantify the impurity by HPLC, which likely originated from an incomplete coupling during one of the chain extension steps.

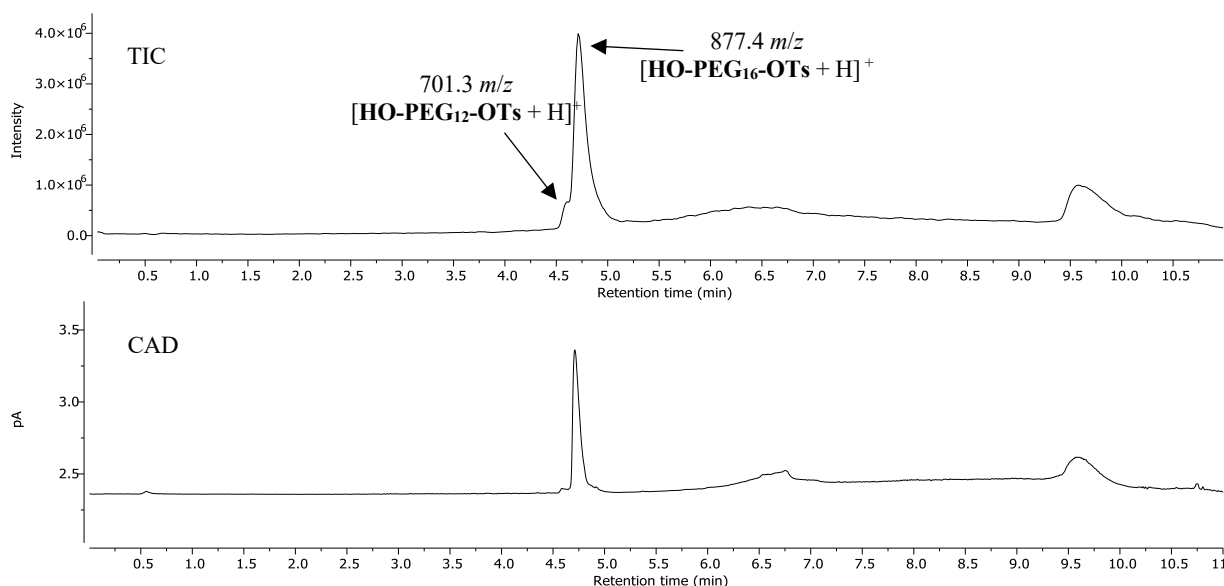


Figure 4.8 TIC (top) and CAD (bottom) chromatograms of crude **HO-PEG₁₆-OTs** indicating the presence of **HO-PEG₁₂-OTs**.

The ¹H NMR spectrum of **HO-PEG₁₆-OTs** is shown in Figure 4.10A. The lack of any other chemically distinct signals suggests that **HO-PEG₁₂-OTs** is the only impurity present in this sample. Given the extremely similar chemical and physical properties of the two compounds, no attempts were made to separate them. However, if this synthesis were to be repeated, more care would be taken to ensure complete coupling during the chain extension steps. This would be achieved by closer analysis of the TLC and LC-MS data of the reaction mixtures.

In a similar fashion, **TrtO-PEG₁₆-OTs** was taken forward through further chain extension and tosylation steps until **TrtO-PEG₂₄-OTs** was obtained. Analytical data of crude intermediate compounds were as expected. Detritylation of **TrtO-PEG₂₄-OTs** using the same method as above gave **HO-PEG₂₄-OTs** with an overall yield of 13% over 13 steps. Analysis of the LC-MS chromatogram of **HO-PEG₂₄-OTs** shows the presence of two shorter chain mono-tosylates (Figure 4.9). Once again, the relative amount of these impurities was difficult to determine. The ¹H NMR spectrum of **HO-PEG₂₄-OTs** is shown in Figure 4.10B. As for **HO-PEG₁₆-OTs**, the lack of any signals chemically distinct from the target material suggests that the only impurities are the aforementioned shorter chain tosylates.

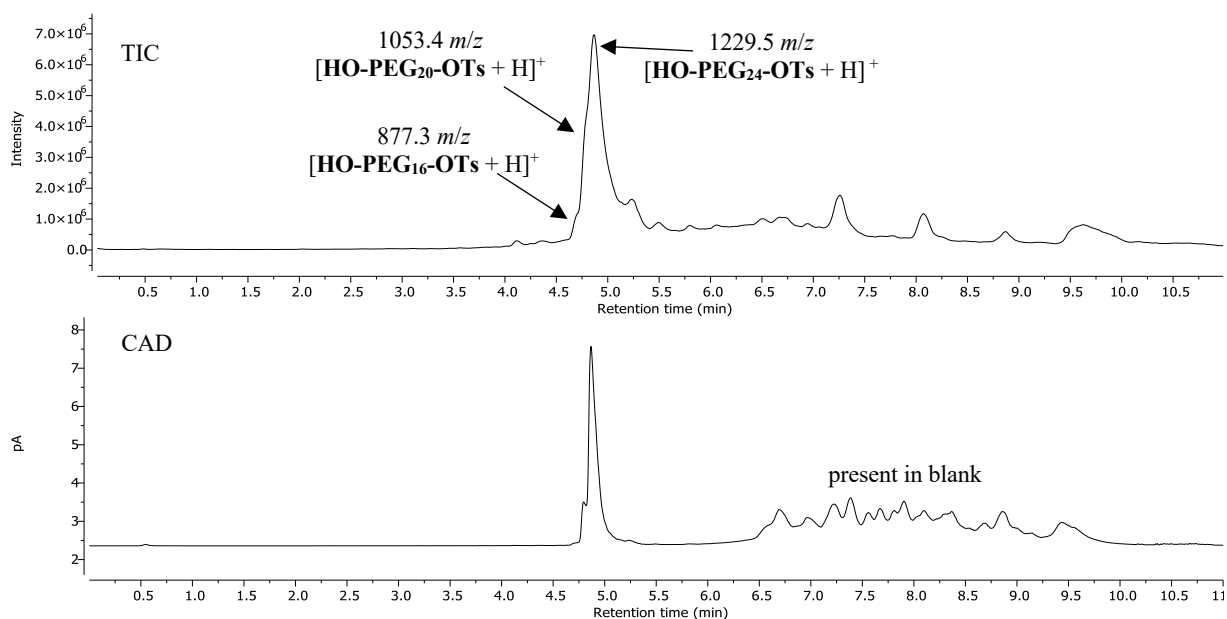


Figure 4.9 TIC (top) and CAD (bottom) chromatograms of crude **HO-PEG₂₄-OTs** indicating presence of **HO-PEG₁₆-OTs** and **HO-PEG₂₄-OTs**. Later eluting peaks were present in blank run also and are not related to the sample.

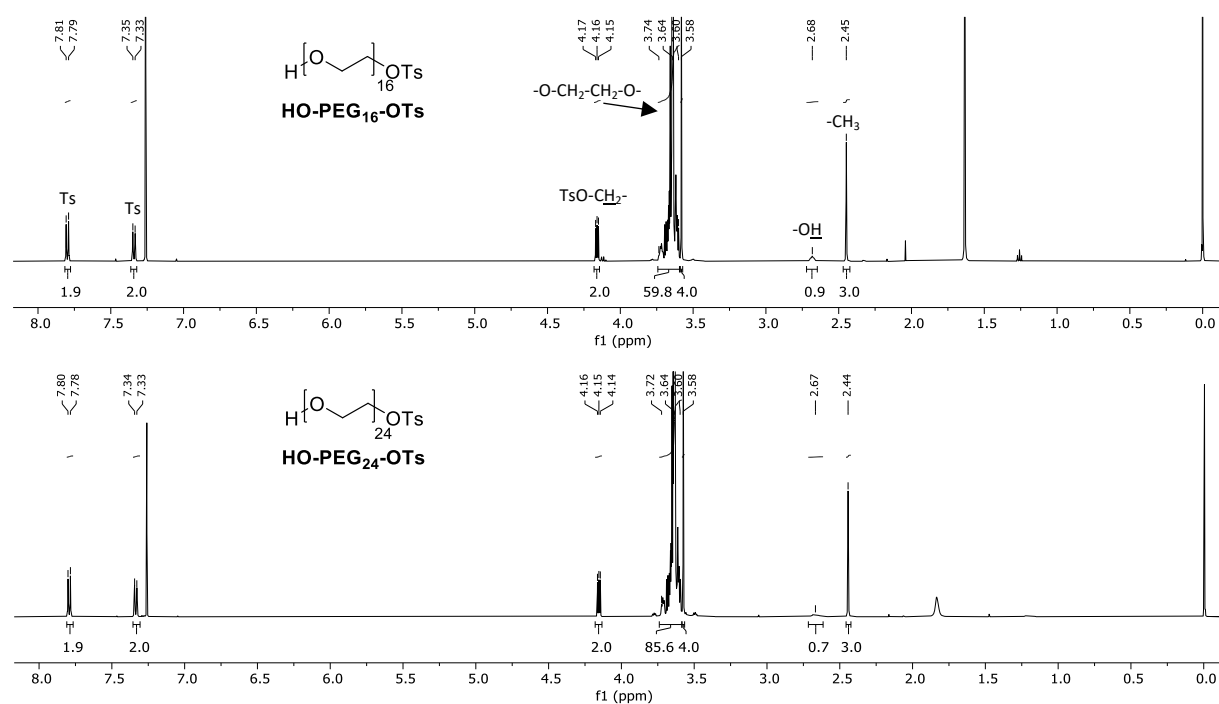


Figure 4.10 ¹H NMR spectra of **HO-PEG₁₆-OTs** (A) and **HO-PEG₂₄-OTs** (B) in CDCl₃ at 500 MHz and 30 °C. Some residual EtOAc is present. Assignments are the same for both spectra.

4.4 HPLC Analysis of Intermediates

Once the discrete PEG chains have been derivatised and the linkers incorporated into vaccine conjugates, their lipophilicity (logP) would be determined via HPLC methods. However, when some of the above intermediates were routinely analysed by RP-HPLC, an interesting trend was observed. In Figure 4.11, it can be clearly seen that the retention time of mono-tritylated compounds (**TrtO-PEG_n-OH**) increases with increasing chain length. This relationship is the opposite of what was originally anticipated.

For small drug molecules, an increase in retention time on RP-HPLC generally correlates to an increase in logP, i.e. a decrease in hydrophilicity.¹⁵² This would suggest that the PEG chains are increasing in hydrophobicity as they get longer, an unlikely result. A more likely explanation is that the increased number of ethylene groups increase the interactions between the analyte and the solid phase. This unfortunately indicates that HPLC methods may not be the optimal way to investigate the logP values of these PEG based compounds.

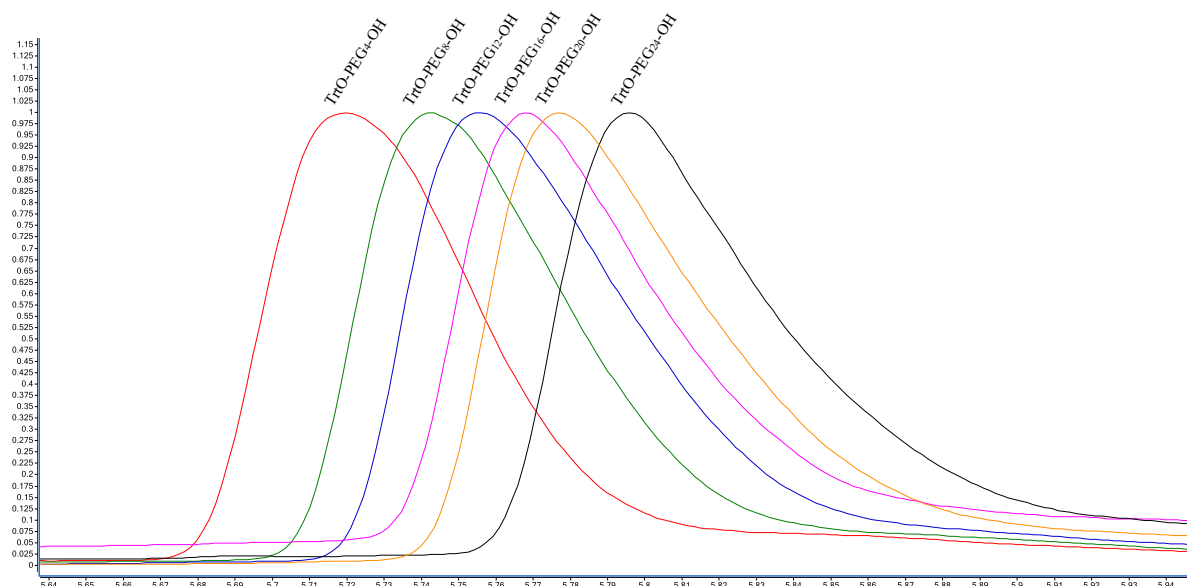


Figure 4.11 Sections of overlaid LC-CAD chromatograms of crude **TrtO-PEG_n-OH** compounds. Using HPLC Condition D (see section 6.1.2).

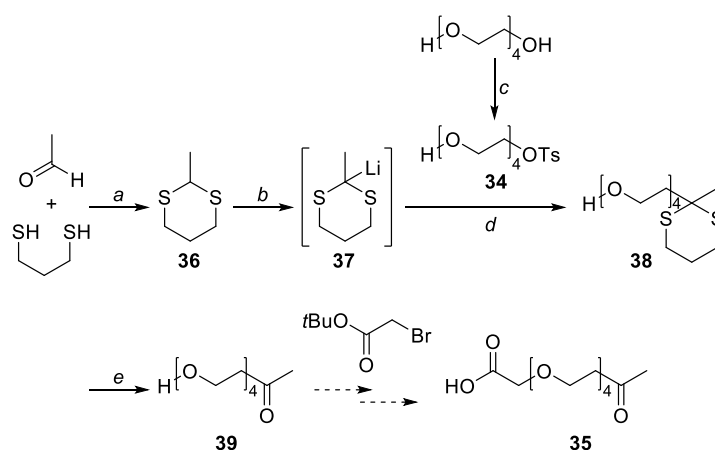
4.5 Derivatisations of Discrete PEG Linkers

We next endeavoured to derivatise the mono-tosylate PEGs **HO-PEG₁₆-OTs** and **HO-PEG₂₄-OTs**. As previously mentioned, for consistency with our previous work,^{79, 80} we sought linkers with a terminal carboxylic acid and a methyl ketone at the other end for

conjugation and coupling purposes. Due to the limited quantities of the previously synthesised mono-tosylate PEG intermediates, tetraethylene glycol mono-tosylate (**34**) was used as a model discrete PEG throughout this work.

4.5.1 Corey-Seebach Reaction to Install Protected Ketone

The first proposed derivatisation strategy utilises a key Corey-Seebach *umpolung* reaction to install the ketone moiety protected as a dithiane (Scheme 4.3).¹⁶⁴⁻¹⁶⁶ Deprotection, followed by installation of the acid group should allow the desired bifunctional PEG linker (**35**) to be obtained.



Scheme 4.3 Synthesis of dithiane **38** with deprotection to ketone **35**. Reagents and conditions: a) $\text{BF}_3 \cdot \text{Et}_2\text{O}$, CH_2Cl_2 , 0°C , 1.5 h, 92%; b) BuLi , THF, 0°C , 5 min; c) TsCl , NaOH , 1:1 $\text{H}_2\text{O}/\text{THF}$, 0°C , 25 min, 73%; d) **34**, 0°C to rt, 1.5 h, 63%; e) MeI , CaCO_3 , MeCN , H_2O , 50°C , 5.5 h, <2%.

As mentioned earlier, mono-tosylate **34** was used as a model discrete PEG throughout this synthesis. Tetraethylene glycol was converted into **34** by reaction with 4-toluenesulfonyl chloride and NaOH in a mixture of water and THF.¹⁶⁷ After silica column chromatography the tosylate was isolated as a colourless oil in a 73% yield.

Dithiane **36** was prepared in a 92% yield from 1,3-propanedithiol and acetaldehyde.^{164, 168} Care had to be taken to minimise the unpleasant onion-like odour of the dithiol starting material. This was achieved through the use of a bleach bath inside the fume hood and frequent glove changes. The odour of dithiane **36** was less pungent, but still required careful manipulation and storage. The ^1H NMR spectrum of crude **36** matches literature well, with the distinctive dithioacetal H-2 resonance at 4.12 ppm (Figure 4.12).^{164, 169}

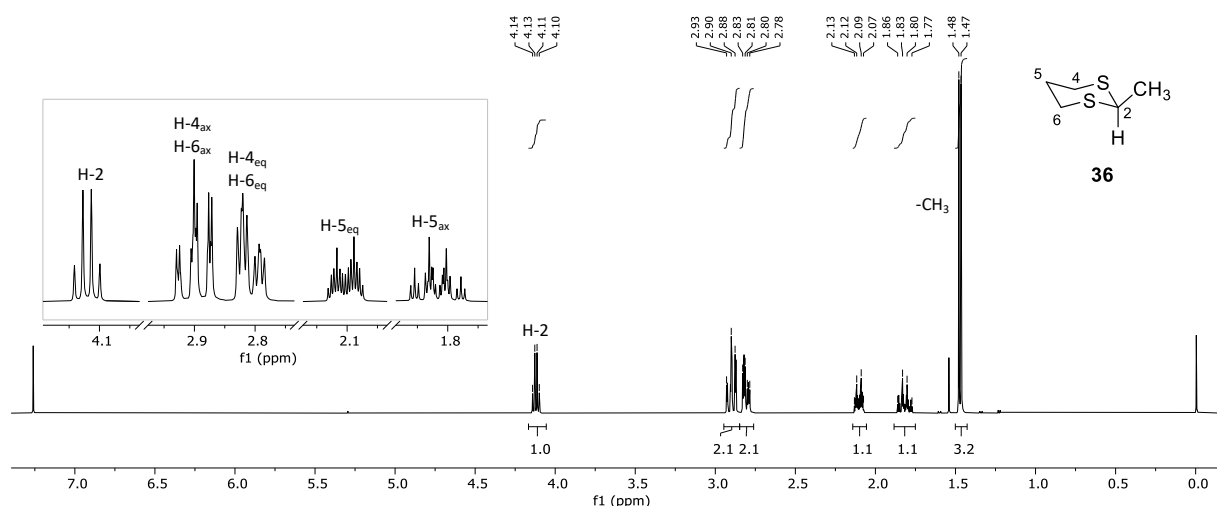


Figure 4.12 ^1H NMR spectrum of dithiane **36** in CDCl_3 at 500 MHz and 30 °C. Insert shows detail of complex multiplets. Peaks have been tentatively assigned as axial or equatorial based on J_{HH} coupling constants.

Lithiated dithiane **37** was formed in situ by reaction of dithiane **36** with 1.2 equivalents butyllithium at 0 °C for 5 minutes before the dropwise introduction of tosylate **34** and warming to room temperature allowed the formation of protected ketone **38** (63% yield). Analysis of the ^1H NMR spectrum of **38** clearly indicates the loss of the tosylate signals and the H-2 signal at 4.12 ppm (Figure 4.13). The successful reaction was further corroborated by the large upfield shift of the H-a resonance (4.17 to 2.27 ppm), and its strong 3-bond HMBC coupling to the methyl carbon.

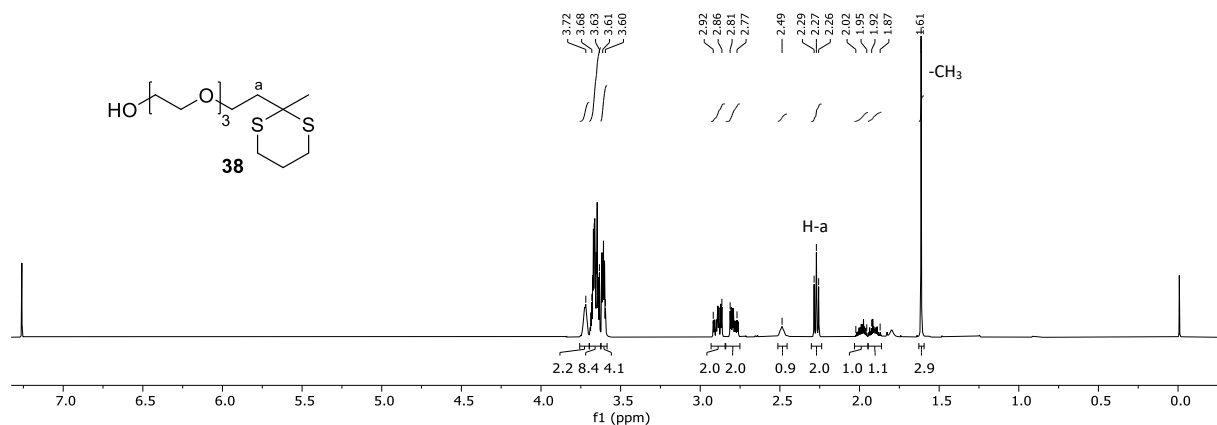


Figure 4.13 ^1H NMR spectrum of protected ketone **38** in CDCl_3 at 500 MHz and 30 °C.

With protected ketone **38** in hand, attention turned to the removal of the dithiane protecting group. Dithianes are a commonly used and easily installed protecting group.¹⁷⁰⁻¹⁷² However, the wide range of deprotection strategies and the substantial amount of optimisation reported in the literature suggests that removal of the protecting group is frequently problematic.¹⁷³⁻¹⁷⁸ We trialled multiple methods for the deprotection of dithiane **38**. Oxidants (2,2,6,6-

tetramethylpiperidin-1-yl)oxyl (TEMPO) and (diacetoxyiodo)benzene^{173, 179-181} or the related oxidant [bis(trifluoroacetoxy)iodo]benzene^{173, 175} led only to decomposition of the dithiane starting material. Dess-Martin periodinane (DMP) has been reported to successfully remove thioacetals in the presence of primary alcohols.¹⁸²⁻¹⁸⁴ However in our hands using DMP only yielded very small amounts of impure target ketone **39** (<2% yield). Deprotection with methyl iodide gave a similar result.¹⁸⁵⁻¹⁹⁰

The ¹H NMR spectrum of the purified ketone **39** formed by reaction with MeI is shown in Figure 4.14. The strong downfield shifts of the methyl signal (1.61 to 2.18 ppm) and H-a (2.27 to 2.71 ppm) is indicative of successful deprotection. The HR-MS data further corroborated this, with the observed ion at 243.1211 *m/z* consistent with the calculated value for [M + Na]⁺ of 243.1208 *m/z*. However, ultimately only 0.6 mg of the ketone was obtained (2% yield).

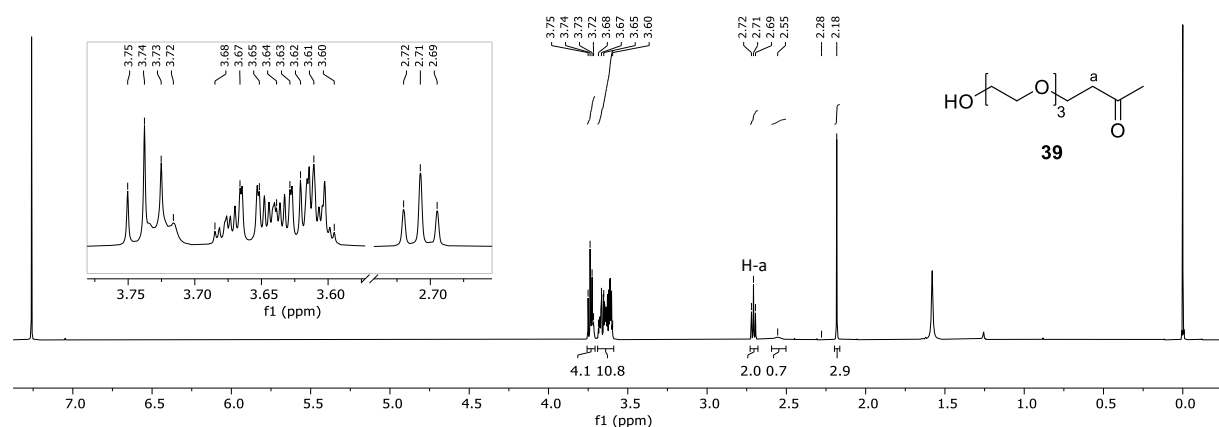
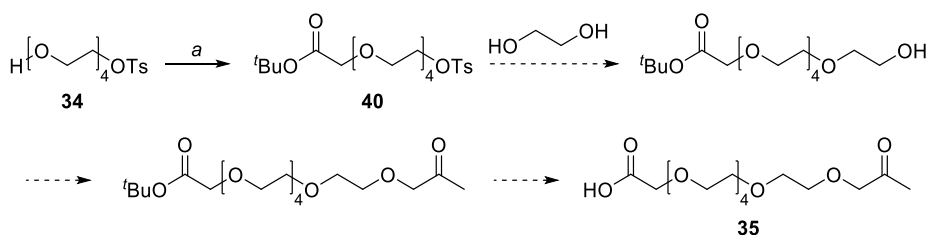


Figure 4.14 ¹H NMR spectrum of ketone **39** in CDCl₃ at 500 MHz and 30 °C. Inset shows detail of the complex multiplets.

Given the large number of dithiane deprotection strategies available in the literature and that our probed deprotection strategies gave complex mixtures or very low yields of the desired ketone we chose to shift away from this dithiane approach.

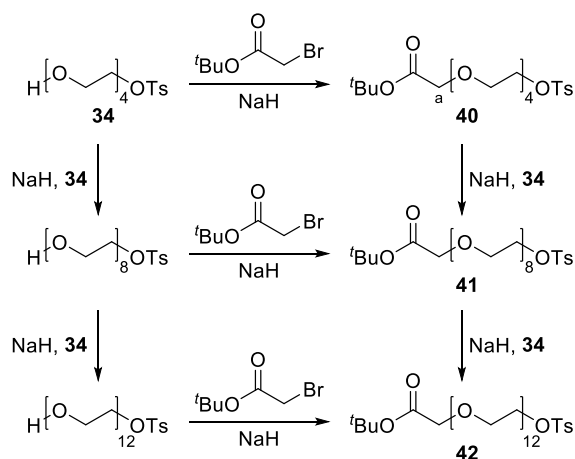
4.5.2 Converting the Hydroxyl Terminus to an Acid

Our next approach to derivatising the discrete PEG tosylates is shown in **Scheme 4.4**, where the free hydroxyl group is manipulated before the displacement of the tosyl group with ethylene glycol, eventually leading to discrete PEG linker **35**.



Scheme 4.4 Proposed derivatisation of model discrete PEG linker **34**. Dashed arrows indicate reactions not conducted. Reagents and Conditions: a) *tert*-butyl bromoacetate, NaH, THF, 0 °C, 1 h, 22%.

The reaction of alcohol **34** with *tert*-butyl bromoacetate gave a pale-yellow oil. When the crude material was analysed by LC-MS and NMR, only a small amount of protected acid **40** was detected, instead the major products were longer chain analogues **41** and **42** (Scheme 4.5). This suggests that the alkoxide formed during this reaction has the propensity to react with itself, or other tosylated compounds in Williamson ether type reactions. This gives side-products with the same functionality as the target material but four or eight tetraethylene glycol units longer.



Scheme 4.5 Formation of side-products **41** and **42** during the reaction of alcohol **34** with *tert*-butyl bromoacetate.

When the reaction was conducted at a lower concentration (0.05 mol L⁻¹ instead of 0.11 mol L⁻¹) the ratio of target material (**40**) to side-products increased substantially. Purification via silica column chromatography was partially successful, giving impure target material **40** in a 22% yield, containing approximately 10% of side-products **41** and **42** (Figure 4.15).

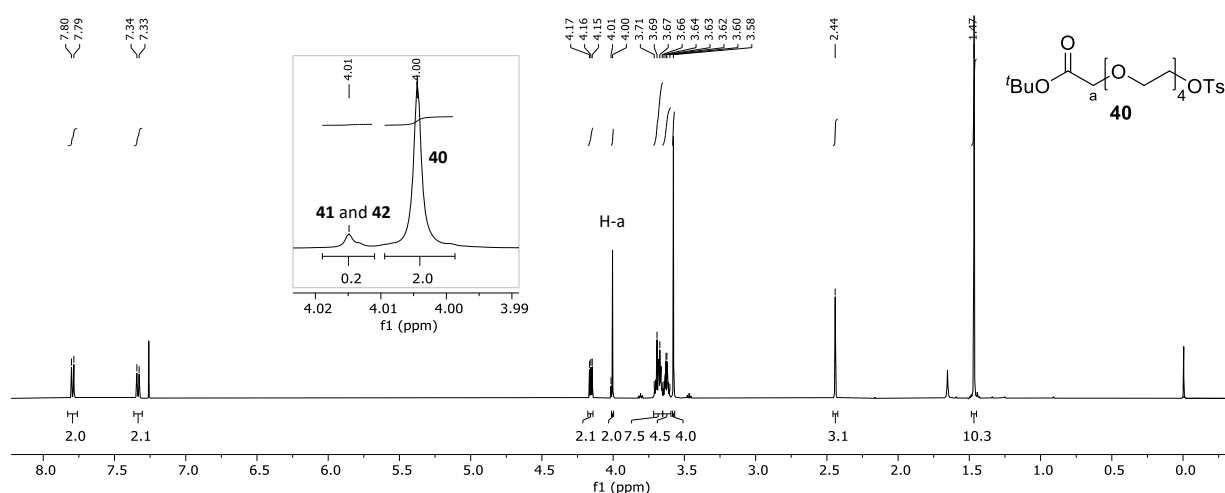
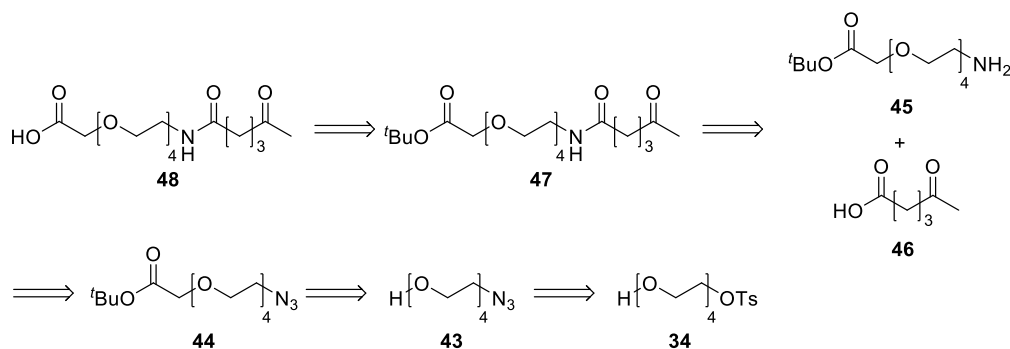


Figure 4.15 ^1H NMR spectrum of impure **40** after silica column chromatography with insert showing presence of side-products **41** and **42**. Spectrum recorded in CDCl_3 at 500 MHz and 30 $^\circ\text{C}$.

While target material **40** could be partially purified from the longer chain side-products by silica column chromatography, it is unlikely that this would be possible for the longer PEG chain analogues ($n = 16$ and 24), thus this approach was deemed unsuitable for the derivatisation of the discrete PEG linkers.

4.5.3 Acylation to Install Ketone Moiety

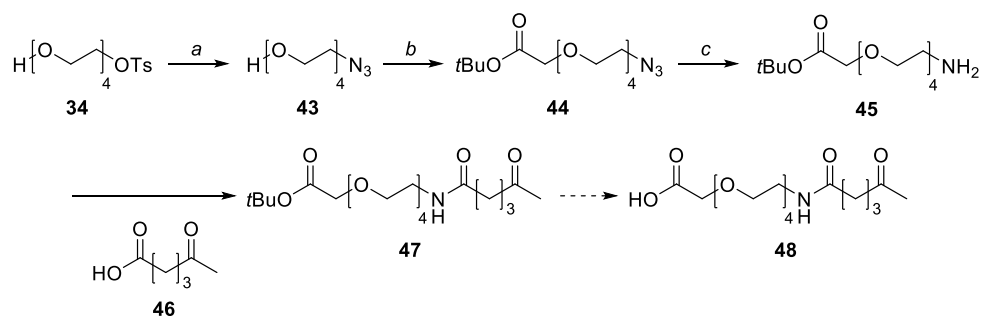
An alternative strategy displaces the tosylate group on **34** with an azide (Scheme 4.6). This allows the addition of an acid functional group onto **43** to give **44**. Reduction of the azide to amine **45** allows coupling to short ketone contained acid (**46**) to give ketone **47**. Deprotection would give the keto-acid PEG based linker **48**. This linker is not comprised of only ethylene glycol repeat units, but we anticipate that this will still allow us to investigate the biodistribution of our conjugate vaccines.



Scheme 4.6 Retrosynthetic analysis of the synthesis of keto-acid linker **48**.

Synthesis towards PEG linker 48

The synthesis towards **48** began with the reaction of tosylate **34** with sodium azide (Scheme 4.7).^{163, 191} The reaction went smoothly and gave azide **43** in a high yield. It should be noted that the aqueous workup required to remove reaction by-products could be problematic when working with the longer chain discrete PEGs. The NMR data of **43** matches that previously reported in the literature.¹⁶²



Scheme 4.7 Second proposed synthetic route towards keto-acid functionalised PEG linkers. Synthesis of amine **45** followed by attempted acylation with levulinic acid to furnish amide **48**. Dashed arrows indicate reactions not conducted. Reagents and conditions: a) NaN_3 , DMF, 70°C , 1.5 h, 94%; b) NaH , THF, 0°C , 30 min, then *t*Bu-bromo acetate, -78°C to rt, 2.5 h, 89%; c) PPh_3 , H_2O , THF, rt, 28 h, 45%.

Subsequent conversion of alcohol **43** into ester **44** by reaction with *tert*-butyl bromo acetate at 0°C ¹⁹²⁻¹⁹⁵ was accompanied by the formation of a substantial amount of a side-product of a higher molecular weight than the target material. Through NMR and MS analysis, the side product was given the proposed structure **49** and proposed to have formed by over reaction of the starting material **43** with the product **44** (Figure 4.16).¹⁹⁶ The ^1H NMR spectrum of the side-product does not contain a *tert*-butyl methyl signal and the $-\text{CH}_2-\text{N}_3$ signal has twice the integration relative to the methylene alpha to the carbonyl group. Also indicative of *n*-alkyl ester formation is the appearance of the $\text{COO}-\text{CH}_2$ peak at 4.31 ppm.

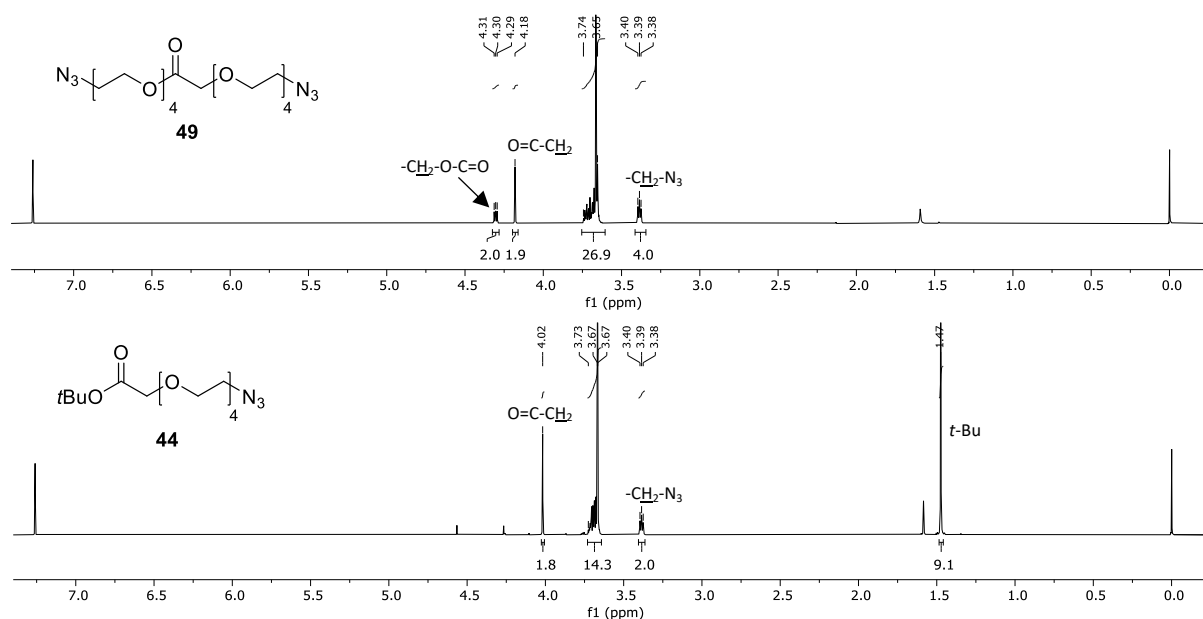


Figure 4.16 ^1H NMR spectra of side-product **49** and target ester **44** in CDCl_3 at 500 MHz and 30 $^\circ\text{C}$.

The LC-MS data of a crude reaction sample is shown in Figure 4.17. Compound **49** elutes a little faster than the ester target material (**44**) and has a much larger mass.

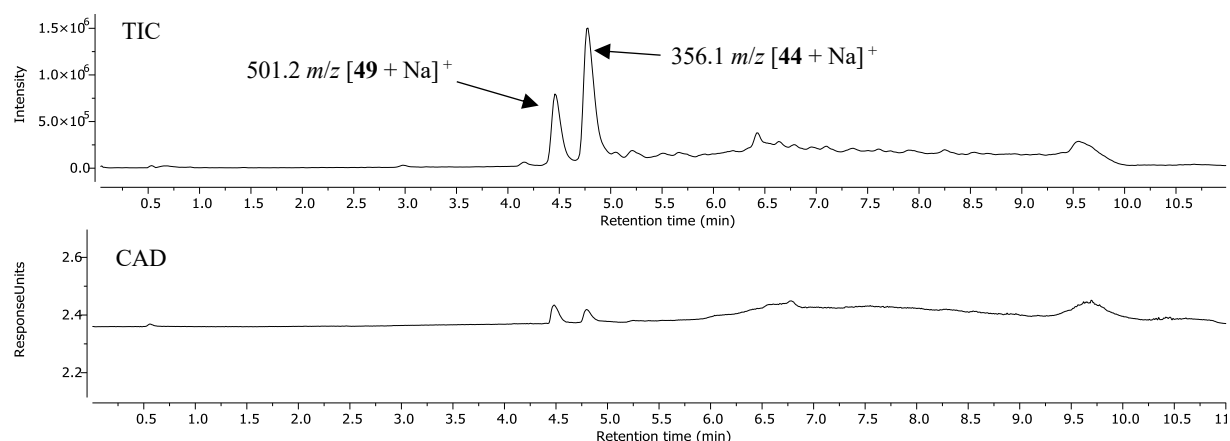


Figure 4.17 TIC (top) and CAD (bottom) HPLC chromatograms of crude **44** indicating substantial presence of compound **49**. Using HPLC Condition D (see section 6.1.2).

A search of similar reactions in the literature suggests that some researchers have encountered related side-products formed through the removal of a *tert*-butyl ester.¹⁹⁶ Paul et al.¹⁹⁷ report the deprotection of *tert*-butyl esters under similar conditions, where they suggest that the reaction of NaH with DMF produces the highly basic dimethylamide anion. Whereas, Filali et al.¹⁹⁸ propose that NaH instead reacts with trace amounts of H_2O , giving very nucleophilic anhydrous hydroxide. Whichever the prevailing mechanism, the result is that the usually stable *tert*-butyl ester is removed, allowing transesterification to form compound **49**.

After some optimisation, the formation of **49** was minimised by simply lowering the initial temperature of the reaction from 0 °C to -78 °C. The reaction was then allowed to warm to room temperature over 3.5 h to give target ester **44** in an 89% crude yield, without any noticeable formation of compound **49**.

Two methods were then probed for the conversion of azide **44** to amine **45**. Palladium catalysed hydrogenolysis^{199, 200} of azide **44** was successful in forming amine **45** but suffered from the formation of side-products, postulated to be the corresponding ethyl ester or ethyl amine derivatives of the target amine. These side-products were not investigated further as concurrent efforts towards at the Staudinger reduction of azide **44** looked more favourable.

Initial attempts at a Staudinger reduction^{192, 201-205} used dilute HCl and toluene during the aqueous workup to separate the target amine (**45**) from PPh₃ and PPh₃O. However, as evidenced by LCMS (Figure 4.18), some hydrolysis of the *tert*-butyl ester (**50**) was observed.

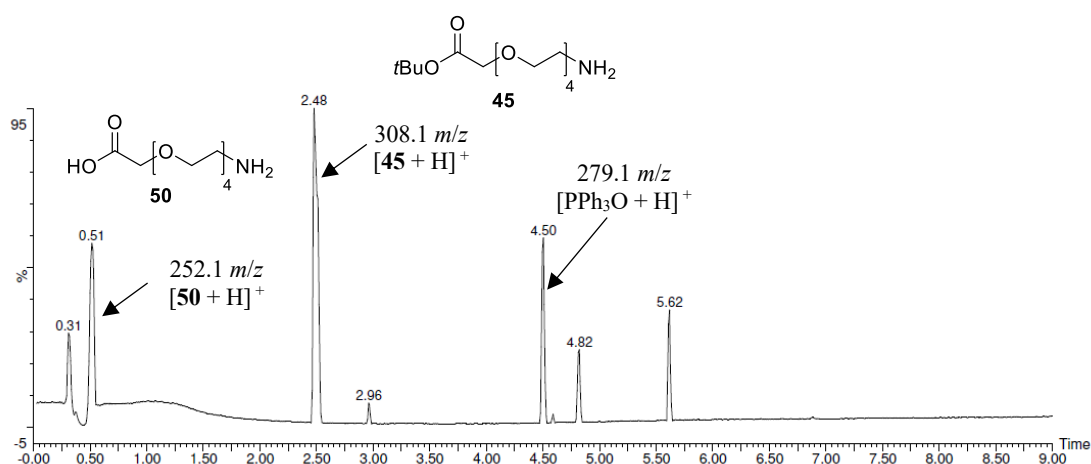


Figure 4.18 LCMS chromatogram of crude amine **45** indicating presence of hydrolysed acid **50**. Using LC-MS Conditions D (see section 6.1.2).

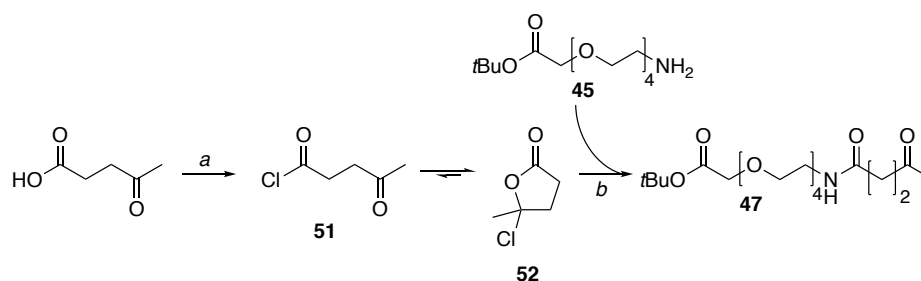
A second attempt at Staudinger reduction of azide **44** was diluted into only water and then extracted with toluene to remove the triphenylphosphine oxide by-product. This prevented the hydrolysis of the *tert*-butyl ester. However, a substantial amount of the target amine (**45**) was also lost during this procedure, giving only a moderate yield (45%). Analysis of the ¹H NMR spectrum of amine **45** showed the expected upfield shift of the two methylene groups closest to the nitrogen as well as a new signal for the amino group

With amine **45** in hand attention turned the attachment of a keto-acid. Due to the difficulties encountered so far in the functionalisation of the model PEG tetraethylene glycol, we anticipated that the limited quantities of the discrete PEG chains synthesised earlier in this work

might render them unsuitable for use in this process. We therefore chose to purchase commercially available discrete PEG chains that are prefunctionalised with amino and carboxylic acid termini. The amino functionality on these PEGs could then be reacted directly with a short ketone containing acid to generate our desired PEG keto-acid linkers. The small keto-acid compound would have to be pre-activated for reaction with the commercial PEG as in situ activation could lead to polymerisation of the PEG chain. We therefore then turned our attention to the activation of short chain keto-acids.

Levulinic Acid

The literature contains many reports of the reaction of 4-oxo-pentanoic acid (levulinic acid) with oxalyl chloride and DMF²⁰⁶⁻²⁰⁸ or thionyl chloride²⁰⁹⁻²¹³ to give levulinoyl chloride (**51**) (Scheme 4.8). In our hands, activation with oxalyl chloride and catalytic DMF appeared to work as expected (gas evolution upon addition of DMF) until the ¹H and ¹³C NMR spectra of the product were collected (Figure 4.19). Analysis of the ¹H NMR spectrum indicates five distinct proton environments, inconsistent with the proposed structure of **51**. The ¹³C NMR spectrum is also unusual, with only one carbonyl peak (174.5 ppm) and an unusual quaternary carbon resonance at 104.2 ppm. Further evaluation of the literature found reports of the spontaneous cyclisation of keto-acid chlorides such as **51** to form chlorolactones such as γ -chloro- γ -valerolactone (**52**).²¹³⁻²¹⁵ This clearly explains the anomalous NMR data, with the four multiplets in the ¹H NMR spectrum arising from the two cyclic methylenes and the ¹³C NMR resonance at 104.2 ppm resulting from the quaternary chlorolactone carbon. Interestingly, the NMR spectra of **52** nonetheless matches well with that reported in the literature for linear acid chloride **51**.²⁰⁶



Scheme 4.8 Formation of chlorolactone **52**. Reagents and conditions: a) oxalyl chloride, DMF, CH₂Cl₂, rt, 3 h, 69%; b) **45**, Et₃N, CH₂Cl₂, 0 °C to rt, o/n, not isolated.

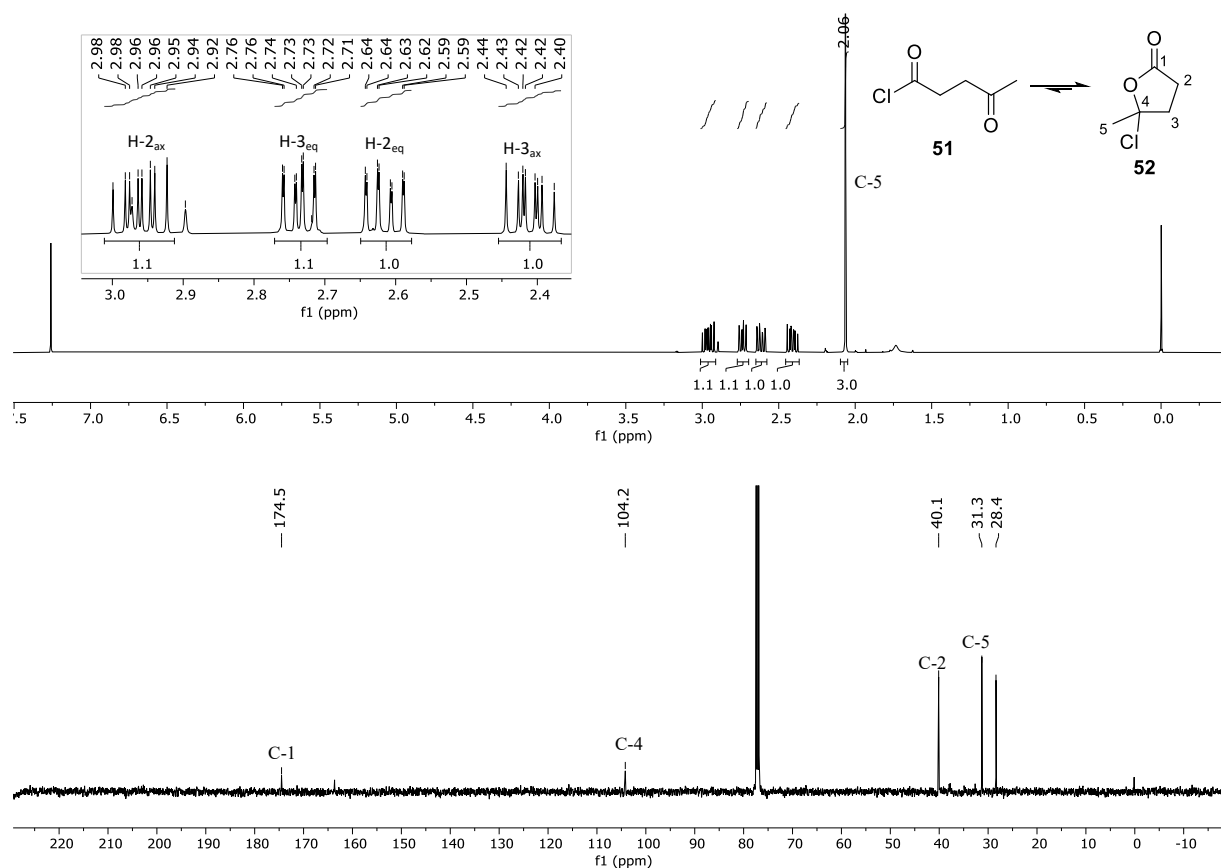
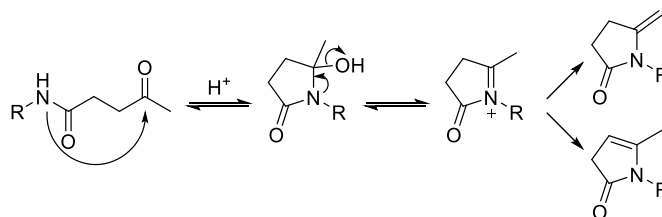


Figure 4.19 ^1H NMR (top) and ^{13}C NMR (bottom) spectra of **52** in CDCl_3 at 500 MHz and 30 °C, suggesting five distinct proton environments, only one carbonyl resonance (174.5 ppm) and the quaternary carbon (C-4) resonance at 104.2 ppm. Some residual DMF is present in both spectra.

Given the apparent success in the literature of the reaction of activated species **51/52** with nucleophiles (regardless of its linear/cyclised form), we chose to continue with the synthesis using chlorolactone **52**. The chlorolactone was moderately unstable – decomposing when stored neat or in solution at -20 °C overnight – so it was used without further purification.

The activated acid was reacted directly with model PEG-amine **45** in CH_2Cl_2 at room temperature overnight. Trituration from THF to remove Et_3NHCl and column chromatography gave amide **47**, as evidenced by ^1H NMR and HR-MS: the ^1H NMR signal of the methylene protons next to the amine nitrogen shifted downfield from 2.87 to 3.40 ppm, and the HR-MS of the columned material was observed to be 428.2260 m/z , consistent with the calculated value for $[\text{M} + \text{Na}]^+$ of 428.2260 m/z . However, the material was still contaminated with unidentifiable impurities. A direct coupling of levulinic acid to amine **45** using DCC gave similar results.²¹⁶⁻²¹⁸ Although we felt that these reactions could be improved, amides of levulinic acid have been reported to undergo unwanted intramolecular cyclisation (Scheme 4.9).²¹⁹ This issue is reported to be especially evident during oxime ligations and the reaction

yields can suffer drastically as little ketone is available for conjugation. Therefore, we chose to stop using levulinic acid in this work.



Scheme 4.9 Mechanism proposed by Agten et al. for the formation of unwanted cyclic species from levulinic amides.²¹⁹

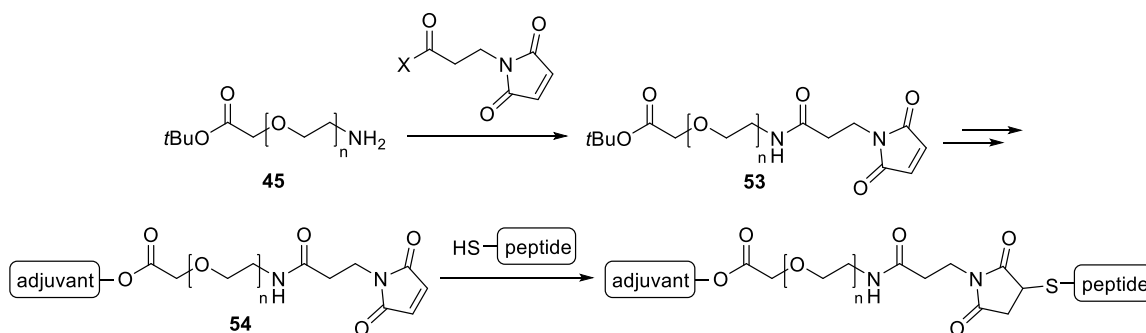
4.6 Summary and Future Work

In this section we have discussed our efforts towards the synthesis of conjugate vaccines with increased hydrophilicity. This work began with the iterative synthesis of discrete PEG chains. This was successful and yielded good amounts of **HO-PEG₁₆-OTs** and **HO-PEG₂₄-OTs** (~500 mg of each). These intermediates were of sufficient purity to be used in further preliminary work.

Functionalisation of the discrete PEG chains was investigated using model discrete PEG monotosylate tetraethylene glycol. Initial attempts at derivatisation were through the instalment of the ketone moiety protected as the dithiane (Scheme 4.3). This approach worked well until the dithiane deprotection step, where none of the probed methods were successful.

In an alternative route, the mono-tosylate of tetraethylene glycol was converted into C-protected amino acid **47** through the displacement of the tosylate with azide and subsequent reduction to the amine, followed by introduction of a protected acetic acid moiety (Scheme 4.7). Levulinic and pyruvic acids were then investigated as potential small molecule ketone donors. The activation of these short carboxylic acids was overall unsuccessful. Therefore, the derivatisation of discrete PEG chains to obtain the desired keto-acid functionalities was not achieved.

With attempts at forming a discrete keto-acid PEG linker unsuccessful, focus will now shift to the formation of alternative discrete PEG linkers for use in other ligation strategies. For example, the use of thiol-maleimide click chemistry to attach the functionalised PEG linker to a thiol containing peptides. This would require the synthesis of a maleimido-acid discrete PEG linker, which we envisage could be synthesised as shown in Scheme 4.10.



Scheme 4.10 Proposed synthetic strategy towards maleimide//thiol click chemistry-based conjugates. Where X is an activating group.

Discrete C-protected amino acid PEG component **45** could be synthesised via the iterative processes and subsequent derivatisation procedures previously described herein. The amino terminus of **45** could be functionalised with a maleimide moiety to give protected acid **53**. The linker could then be functionalised at the carboxylic acid terminus with the pro-adjuvant component to give a pro-drug with the general structure **54**. The maleimido construct could then be “clicked” together with a thiol functionalised peptide antigen, which would be obtained via the addition of a thiol containing species (such as cysteine) to the end of the peptide chain.

Chapter 5 Concluding Remarks

In vivo processing of current lead vaccine **CI258** releases the malaria peptide antigen and active adjuvant α -GalCer (**1**). The aim of this thesis was to probe the relationship between the chemical structure of the vaccine and the rate at which the construct is cleaved. The overarching goal of this project is to understand how the rate of release of the immunological components from **CI258** affects its activity. The synthesis of **L-12**, **D-12** and **13** alongside work towards the synthesis of **14** and **15** furthered our knowledge in this field (Figure 5.1).

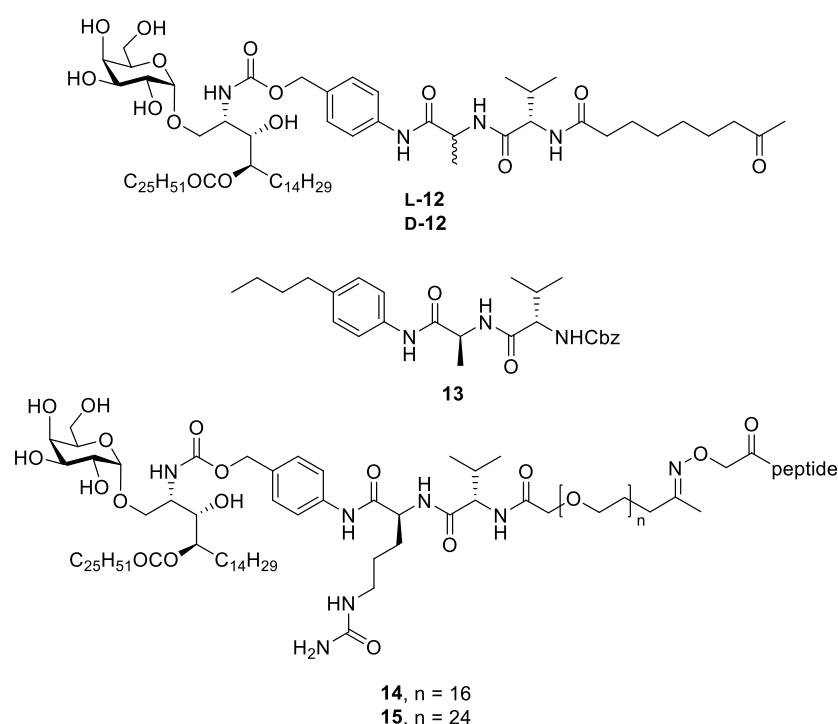


Figure 5.1 Structures of synthesised targets **L-** and **D-12** and **13** and unobtained targets **14** and **15**. Where peptide = FFRK-AAA-ST-NVDFNNL-S.

5.1 Investigating the Effect of Stereochemistry at P1

The synthesis of **L-** and **D-12** followed a modified method¹⁴⁰ of the standard synthesis of PABA-dipeptide linkers.^{104, 106} This aimed to reduce the potential for epimerisation at the P1 stereocenter (alanine). HPLC analysis of earlier intermediates was inconclusive in determining the level of epimerisation taking place during the synthesis. Future work to determine the level of epimerisation using this method will likely include more detailed HPLC analysis. Targets

L- and **D-12** were contaminated with a known by-product of an earlier reaction. In continuing with this work, the intermediates (**L-** and **D-12**) will be conjugated to various peptides before purification. Both the ketone intermediates and the resulting conjugates will be tested in cathepsin B assays to determine whether the D-Ala linker has an effect on the rate of enzymatic cleavage.

5.2 Removing the Immolative Linker

Immolative spacers such as PABC enhance the cleavage of conjugate systems by distancing the site of enzymatic cleavage from bulky payloads. The necessity of the PABC group in our vaccine conjugate system was explored by the synthesis of model compound **13**, which contains an Ala-Val linker directly attached to a model payload, 4-butaniline. **13** was synthesised in three steps from NHS-activated amino acids in a 51% overall yield. Incubation of **13** with cathepsin B was successful in allowing the release of the model payload. This supports the hypothesis that the PABC group is not a requirement for cathepsin B cleavage. These results encourage the synthesis of a PABC-free analogue of **CI258**, thus removing the acid sensitive carbamate linkage, which could allow the development of conjugates able to be fully synthesised by solid phase peptide synthesis.

5.3 Efforts Towards Altering Biodistribution

Biodistribution is an important factor in determining the efficacy of a drug, influencing where and how a drug is processed. The biodistribution of conjugate vaccines such as **CI258** could be altered by using linkers with different physical properties. Altering the linker component would allow the biodistribution to be changed without affecting the receptor interactions of the active components. Our efforts towards the synthesis of hydrophilic vaccines **14** and **15** began with the iterative synthesis of discrete PEG compounds **HO-PEG₁₆-OTs** and **HO-PEG₂₄-OTs**. This process was successful and allowed the easy formation of long and reasonably pure discrete PEGs. Attempts to derivatise these chains into functional linkers were largely unsuccessful. Installation of the desired ketone moiety protected as a dithiane was hampered by difficulties in the subsequent removal of the protecting group. Introduction of the ketone through coupling of short keto-acids to an amine functionalised PEG chain also proved problematic.

Future focus in this project will shift to the formation of other discrete PEG linkers for use in alternative ligation strategies. For example, the use of thiol-maleimide click chemistry to attach the functionalised PEG linker to a thiol decorated peptide chain. Synthesis of the maleimido discrete PEG could be achieved through reaction of an amine functionalised PEG with an electrophilic maleimide source.

Chapter 6 Experimental

6.1 General Experimental

Anhydrous solvents were purchased commercially and used as received. Reagents were purchased from Sigma-Aldrich, Scharlau, or AK Scientific and, unless otherwise stated, used as received. Discrete PEGs were purchased from PurePEG. Moisture- and oxygen-sensitive liquids and solutions were transferred using stainless steel cannula or syringe and needle. Thin layer chromatography was performed on aluminum backed silica gel plates (Sigma-Aldrich). Normal phase silica gel column chromatography was either conducted manually using silica gel (60 Å) or on an X2 automated system using Silicycle Inc. SiliaSep™ silica cartridges and the specified eluents. NMR spectra were recorded on a Bruker AVANCE III 500 MHz NMR with 5 mm broad-banded SmartProbe at 30 °C unless otherwise specified. Chemical shifts are referenced to the residual solvent peaks, in CDCl₃ to 7.26 ppm for ¹H NMR and 77.16 ppm for ¹³C NMR; in CD₃OD and CD₃OD/CDCl₃ mixtures to 3.31 ppm for ¹H NMR and 49.00 for ¹³C NMR. ¹H NMR shifts are reported to the nearest 0.01 ppm and coupling constants to the nearest 0.1 Hz. ¹H NMR data are reported using the following convention: ¹H NMR (frequency, solvent) δ/ppm: chemical shift (multiplicity, number of protons, coupling constant (Hz), assignment). ¹³C NMR shifts are reported to the nearest 0.1 ppm, except where necessary to differentiate between similar resonances, when they are reported to two decimal places. ¹³C NMR data are reported as: chemical shift (assignment). 2-D correlation spectra (COSY, HSQC, and HMBC) were used in the assignment of peaks in the ¹H and ¹³C spectra. High resolution mass spectrometry (HR-MS) measurements were conducted on a Waters Xevo G2-XS Q-TOF Tandem Mass Spectrometer (ESI) in either positive or negative ion mode as indicated. Compounds are given indicative names and atom numbers in this experimental to allow for ease of data assignment. These are not intended to be IUPAC systematic names or numbering systems.

6.1.1 Cathepsin B Assay Conditions

Cathepsin B Assay conditions were conducted as follows. A stock solution of internal standard phytosphingosine (190 μ M) in DMSO was pre-mixed with ammonium acetate buffer (50 mM, pH 5.3) containing EDTA (2.5 mM) and dithiothreitol (2.5 mM) to a final phytosphingosine concentration of 6.3 μ M. The substrate conjugate (190 μ M in DMSO) was added to the pre-mixed buffer solution to give a final substrate concentration of 12.7 μ M. Cathepsin B from human liver (Sigma) dissolved in ammonium acetate buffer (50 mM, pH 5.3, EDTA (2.5 mM), dithiothreitol (2.5 mM)) was added to the reaction mixture to give a final cathepsin B concentration of 2.9 units/mL. For the control reaction (without enzyme) the same volume of buffer was added. The reaction mixtures were then incubated at 37 °C. An aliquot of 10 μ L was taken from the reactions at the 24 time point and analysed by LCMS.

6.1.2 Liquid Chromatography Conditions

Liquid chromatography data were collected under four different conditions on four different instruments:

Condition A

Agilent 1260 and 1290 Infinity II HPLC modules coupled to an Agilent LC/MSD - electrospray ionisation (ESI) single quadrupole and an Agilent 1290 Infinity II evaporative light scattering detector. Using a Poroshell C18 5 μ m column. Solvents, A: water + 0.1% formic acid and B: methanol. Gradient (%B): T0 = 50%, T20 = 57%, T22 = 100%, T23 = 50%, T26 = 50%. T = 40 °C. Flow rate = 0.5 mL/min.

Condition B

Instrument as for condition A. Using a Poroshell EC-C18, 2.7 μ m, 4.6 x 100 mm column. Solvents, A: water + 0.1% formic acid and B: methanol. After the specified gradient all runs increase to 100% methanol over 1 min, then decreased to the starting %B over 1 minute before a two-minute hold at the same %B. T = 40 °C. Flow rate = 1.0 mL/min.

Condition C

Agilent 1260 Infinity II coupled to an Agilent XT single quadrupole mass spectroscopic detector using ESI. Using a Phenomenex Kinetex 2.6 μ m C18 100 Å LC 50 x 3 mm column.

Solvents, A: water + 0.05% TFA and B: methanol + 0.05% TFA. Gradient (%B): T0 = 50%, T5 = 100%, T13 = 100%, T17 = 50%. T = 40 °C. Flow rate = 0.5 mL/min.

Condition D

Agilent 1260 coupled to a Dionex Corona Ultra RS charged aerosol detector (CAD) and an Agilent 6130 single quadrupole mass spectroscopic detector using ESI. Using a Phenomenex Kinetex 2.6 μ m C18 100 Å LC 50 x 3 mm column. Solvents, A: water + 0.05% TFA and B: methanol. Gradient (%B): T0 = 5%, T5 = 100%, T8 = 100%, T11 = 5%. T = 40 °C. Flow rate = 0.5 mL/min.

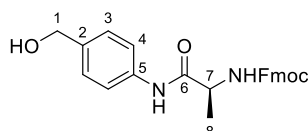
Condition E

Waters Xevo G2-XS Q-ToF mass spectrometer fitted with a Waters H-Class UPLC. Acquity UPLC BEH C18 column 1.7 μ 50 x 2.1 mm. Solvents, A: water and B: 0.1% formic acid in acetonitrile. Gradient (%B): T0 = 5%, T9 = 95%. T = 40 °C. Flow rate = 0.5 mL/min. This condition/instrument was used for all HR-MS analyses.

6.2 Synthetic Protocols

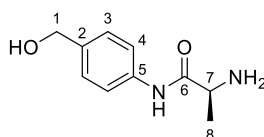
6.2.1 Synthesis of Ketone L-12

PABA-L-Ala-Fmoc (L-18)



PABA (1.162 g, 9.435 mmol) and EEDQ (3.27 g, 13.1 mmol) were added to a solution of Fmoc-L-Ala-COOH (1.99 g, 6.39 mmol) in anhydrous $\text{CH}_2\text{Cl}_2/\text{CH}_3\text{OH}$ (100 mL/10 mL) at rt under Ar. The reaction was stirred for 4.5 h in the dark before concentration to yield a crude brown oil. Repeated precipitations from Et_2O and $\text{CH}_3\text{OH}+\text{CH}_2\text{Cl}_2/\text{Et}_2\text{O}$ gave PABA-L-Ala-Fmoc (**L-18**, 1.56 g, 3.74 mmol, 58%) as an off-white solid. R_f (70% EtOAc in PE + AcOH) 0.55. ^1H NMR (500 MHz, 1:1 $\text{CDCl}_3:\text{CD}_3\text{OD}$) δ 7.73 (d, $J = 7.6$ Hz, 2H, Fmoc), 7.60 (t, $J = 7.1$ Hz, 2H, Fmoc), 7.49 (d, $J = 8.1$ Hz, 2H, PABA), 7.35 (t, $J = 7.5$ Hz, 2H, Fmoc), 7.28 (d, $J = 8.3$ Hz, 4H, Fmoc and PABA), 4.55 (s, 2H, H-1), 4.38 (d, $J = 6.8$ Hz, 2H, Fmoc), 4.29 (q, $J = 7.0$ Hz, 1H, H-7), 4.19 (t, $J = 6.9$ Hz, 1H, Fmoc), 1.41 (d, $J = 7.2$ Hz, 3H, H-8). ^{13}C NMR (126 MHz, 1:1 $\text{CDCl}_3:\text{CD}_3\text{OD}$) δ 173.1 (C-6), 157.6 (C=O Fmoc), 144.6, 142.1, 128.4, 128.2, 127.8, 125.7, 121.0, 120.5, 67.6, 64.6 (C-1), 52.0 (C-7), 47.9 (Fmoc), 18.5 (C-8). HRMS–ESI (m/z): $[\text{M} + \text{Na}]^+$ calcd for $\text{C}_{25}\text{H}_{24}\text{N}_2\text{O}_4\text{Na}$, 439.1634; found, 439.1638. $[\alpha]_D^{20}$ -17.4° (c 1.00, DMF).

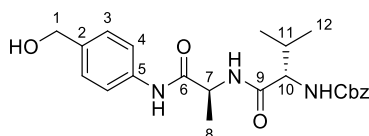
PABA-L-Ala-NH₂ (L-19)



Piperidine (1.8 mL, 18 mmol) was added to a solution of PABA-L-Ala-Fmoc (**L-18**, 1.375 g, 3.302 mmol) in DMF (16.2 mL) at rt under Ar. The reaction was stirred at rt for 1 h before concentration in vacuo. Repeated addition of DMF and further evaporation ensured complete removal of piperidine. PABA L-Ala-NH₂ (**L-19**) was used without further purification. Data

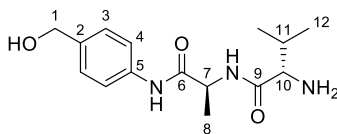
were collected on a separate sample of amine that was precipitated with Et₂O directly from the reaction mixture. R_f (65:30:4:0.5 CHCl₃, CH₃OH, H₂O, aq NH₃) 0.56. ¹H NMR (500 MHz, CD₃OD) δ 7.55 (d, *J* = 8.5 Hz, 2H, H-3), 7.31 (d, *J* = 8.3 Hz, 2H, H-4), 4.56 (s, 2H, H-1), 3.54 (q, *J* = 6.9 Hz, 1H, H-7), 1.35 (d, *J* = 6.9 Hz, 3H, H-8). ¹³C NMR (126 MHz, CD₃OD) δ 175.4 (C-6), 137.33, 137.2, 127.2 (C-f), 119.8 (C-g), 63.5 (C-1), 50.7 (C-7), 20.2 (C-8). HRMS–ESI (*m/z*): [M + H]⁺ calcd for C₁₀H₁₅N₂O₂, 195.1134; found, 195.1131.

PABA-L-Ala-Val-Cbz (L-20)



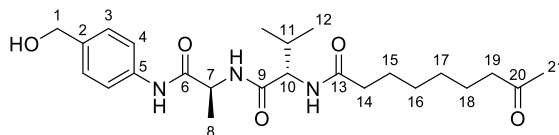
Crude PABA-L-Ala-NH₂ (**L-19**, 1.29 g, 2.72 mmol) and NHS-Val-Cbz (1.14 g, 3.26 mmol, 1.2 equiv) were dissolved in DMF (13.5 mL) and the reaction was stirred at rt under Ar for two days. The reaction was added dropwise to water (135 mL) and the flask was rinsed with water (50 mL). The resulting white precipitate was filtered. The precipitate was taken up in CH₃OH/CHCl₃ and triturated with Et₂O. This was repeated once more to give PABA-L-Ala-Val-Cbz (**L-20**, 1.04 g, 2.43 mmol, 89%) as an off-white solid. R_f (10% CH₃OH in CHCl₃) 0.46. ¹H NMR (500 MHz, DMSO-*d*₆) δ 9.88 (s, 1H, NH PABA), 8.12 (d, *J* = 7.1 Hz, 1H, NH Cbz), 7.53 (d, *J* = 8.4 Hz, 2H, PABA), 7.36 – 7.23 (m, 6H, Cbz and NH Ala), 7.24 (d, *J* = 8.3 Hz, 2H, PABA), 5.07 (t, *J* = 5.7 Hz, 1H, -OH), 5.05 – 5.02 (br s, 2H, Cbz), 4.43 – 4.39 (m, 3H, H-1 and H-7), 3.91 (t, *J* = 7.8 Hz, 1H, H-10), 1.99 (q, *J* = 6.8 Hz, 1H, H-11), 1.30 (d, *J* = 7.1 Hz, 3H, H-8), 0.88 (d, *J* = 6.8 Hz, 3H, H-12), 0.84 (d, *J* = 6.7 Hz, 3H, H-12). ¹³C NMR (126 MHz, DMSO-*d*₆) δ 170.91 (C=O), 170.85 (C=O), 156.2, 137.5, 137.4, 137.1, 128.3, 127.7, 127.6, 126.9 (PABA), 118.9 (PABA), 65.4 (Cbz), 62.6 (C-1), 60.0 (C-10), 48.9 (C-7), 30.3 (C-11), 19.1 (C-12), 18.1 (d, C-8 and -12). HRMS–ESI (*m/z*): [M + Na]⁺ calcd for C₂₃H₂₉N₃O₅Na, 450.2005; found, 450.2011.

PABA-L-Ala-Val-NH₂ (L-21)



A heterogeneous mixture of PABA-L-Ala-Val-Cbz (**L-20**, 506 mg, 1.18 mmol) and 10% Pd/C (96 mg, 0.090 mmol, 9 mol%) in CH₂Cl₂ (2.4 mL) and CH₃OH (21.6 mL) was stirred under an H₂ atmosphere for 1.5 h. The reaction mixture was filtered through Celite then concentrated in vacuo to give PABA-L-Ala-Val-NH₂ (**L-21**, 352 mg, 1.20 mmol, quant.) as a colourless oil. R_f (65:30:4:0.5 CHCl₃, CH₃OH, H₂O, aq NH₃) 0.66. ¹H NMR (500 MHz, CD₃OD) δ 7.53 (d, *J* = 8.2 Hz, 2H, H-3), 7.30 (d, *J* = 8.1 Hz, 2H, H-4), 4.56 (s, 2H, H-1), 4.51 (q, *J* = 7.1 Hz, 1H, H-7), 3.16 (d, *J* = 5.5 Hz, 1H, H-10), 1.99 (h, *J* = 6.7 Hz, 1H, H-11), 1.44 (d, *J* = 7.1 Hz, 3H, H-8), 0.98 (d, *J* = 6.8 Hz, 3H, H-12), 0.92 (d, *J* = 6.8 Hz, 3H, H-12). ¹³C NMR (126 MHz, CD₃OD) δ 176.9 (C-9), 173.1 (C-6), 138.74 (PABA), 138.70 (PABA), 128.6 (C-3), 121.3 (C-4), 64.8 (C-1), 61.5 (C-10), 50.8 (C-7), 33.5 (C-11), 19.8 (C-12), 18.3 (C-8), 17.7 (C-12). HRMS–ESI (*m/z*): [M + Na]⁺ calcd for C₁₅H₂₄N₃O₃Na, 294.1818; found, 294.1824.

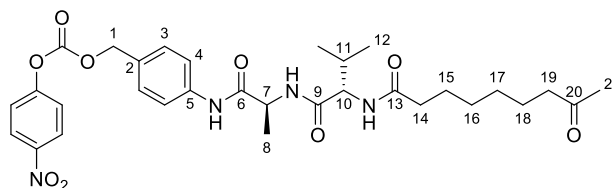
PABA-L-Ala-Val-ketone (L-23)



A solution of PABA-L-Ala-Val-NH₂ (**L-21**, 106 mg, 0.361 mmol) and pNP-activated 8-oxononanoic acid (**22**, 129 mg, 0.44 mmol, 1.2 equiv) in DMF (3.4 mL) was stirred at rt under Ar for 1 h 15 min before DIPEA (70 μL, 1.1 equiv) was added. The reaction was stirred for a further 2 h 20 min before concentration in vacuo. The crude yellow solid was purified by flash chromatography on silica gel (0-10% CH₃OH in CHCl₃) to give PABA-L-Ala-Val-ketone (**L-23**, 113 mg, 0.252 mmol, 70%) as a white solid. R_f (10% CH₃OH in CHCl₃) 0.38. ¹H NMR (500 MHz, 1:1 CDCl₃:CD₃OD) δ 7.50 (d, *J* = 8.1 Hz, 2H, PABA), 7.27 (d, *J* = 8.2 Hz, 2H, PABA), 4.55 (s, 2H, H-1), 4.48 (q, *J* = 7.0 Hz, 1H, H-7), 4.16 (d, *J* = 7.1 Hz, 1H, H-10), 2.42 (t, *J* = 7.4 Hz, 2H, H-19), 2.29 – 2.20 (t, *J* = 7.6 Hz, 2H, H-14), 2.11 (s, 3H, H-21), 2.05 (q, *J* = 6.8 Hz, 1H, H-11), 1.60 (p, *J* = 7.4 Hz, 2H, H-15), 1.53 (p, *J* = 7.3 Hz, 2H, H-18), 1.42 (d, *J* = 7.0 Hz, 3H, H-8), 1.31 – 1.27 (m, 4H, H-16 and -17), 0.93 (t, *J* = 7.4 Hz, 6H, H-12). ¹³C NMR (126 MHz, 1:1 CDCl₃:CD₃OD) δ 211.6 (C-20), 175.5 (C-13), 172.8 (C-9), 171.8 (C-2), 137.9

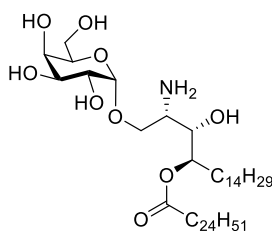
(PABA), 137.8 (PABA), 128.1 (PABA), 120.7 (PABA), 64.5 (C-1), 59.5 (C-10), 50.2 (C-7), 44.0 (C-19), 36.5 (C-14), 31.3 (C-8), 29.9 (C-21), 29.5, 29.3, 26.1 (C-15), 24.1 (C-18), 19.5 (C-19), 18.5 (C-12), 17.9 (C-8). HRMS–ESI (m/z): $[M + Na]^+$ calcd for $C_{24}H_{37}N_3O_5Na$, 470.2631; found, 470.2635.

***p*NP-PABC-L-Ala-Val-ketone (L-24)**



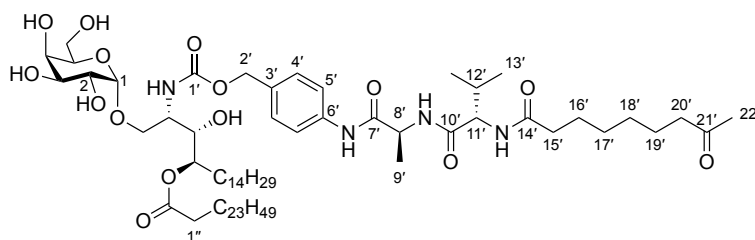
A mixture of PABA-L-Ala-Val-ketone (**L-23**, 104 mg, 0.232 mmol) and bis-*p*NP carbonate (79 mg, 0.26 mmol) were dried together under high vacuum. DMF (3 mL) was added at rt under Ar. DIPEA (50 μ L, 0.29 mmol) was then added. The reaction was stirred at rt under Ar for 4 h before more bis-*p*NP carbonate (~ 60 mg, 0.2 mmol) and DIPEA (50 μ L, 0.29 mmol) were added. The reaction was stirred under Ar at rt for a further 65 h (total reaction time of 3 days). The reaction was concentrated, and the oily yellow residue was purified by flash chromatography on silica gel (50-100% EtOAc in CH_2Cl_2) to give *p*NP-PABA-L-Ala-Val-ketone (**L-24**, 101 mg, 0.165 mmol, 71%) as a white solid. R_f (10% CH_3OH in $CHCl_3$) 0.58. 1H NMR (500 MHz, $CDCl_3$) δ 9.13 (s, 1H, NH PABA), 8.27 – 8.24 (m, 2H, *p*NP), 7.71 (d, $J = 7.8$ Hz, 1H, NH Ala), 7.64 (d, $J = 8.5$ Hz, 2H, H-4), 7.38 – 7.35 (m, 4H, *p*NP and H-3), 6.77 (d, $J = 8.6$ Hz, 1H, NH Val), 5.24 (s, 2H, H-1), 4.84 (p, $J = 7.2$ Hz, 1H, H-7), 4.56 – 4.52 (m, 1H, H-10), 2.38 (t, 2H, $J = 7.3$ Hz, H-19), 2.34 – 2.27 (m, 2H, H-14), 2.10 (s, 3H, H-21), 2.08 – 2.04 (m, 1H, H-11), 1.97 – 1.63 (m, 2H, H-15), 1.53 (p, $J = 7.3$ Hz, 2H, H-18), 1.47 (d, $J = 7.0$ Hz, 3H, H-8), 1.34 – 1.324 (m, 5H, H-16 and -17), 0.95 – 0.92 (m, 6H, H-12). ^{13}C NMR (126 MHz, $CDCl_3$) δ 209.1 (C-20), 173.8 (C-13), 172.1 (C-9), 171.0 (C-6), 155.7 (*p*NP), 152.6, 145.6 (*p*NP), 139.0 (PABA), 130.1 (PABA), 129.8 (PABA), 125.4 (*p*NP), 121.9 (*p*NP), 120.3 (PABA), 70.8 (C-1), 58.5 (C-10), 49.7 (C-7), 43.7 (C-19), 36.6 (C-14), 31.6 (C-11), 30.0 (C-21), 29.1, 29.0, 25.8 (C-15), 23.7 (C-18), 19.3 (C-12), 18.7 (C-12), 18.0 (C-8). HRMS–ESI (m/z): $[M + Na]^+$ calcd for $C_{31}H_{40}N_4O_9Na$, 635.2693; found, 635.2692.

m α -GalCer (**5**)



A suspension of α -GalCer (**1**, 110.5 mg, 0.1287 mmol) in dioxane (freshly distilled from 2,4-DNPH and HCl, 37 mL) was heated at 65 °C until all in solution. HCl (12 M, 125 μ L) was added and the reaction was heated at 65 °C for a further 20 min. The reaction was concentrated in vacuo to give crude m α -GalCer (**5**, 111 mg) as a white solid that was used immediately without any further purification. R_f (20% CH₃OH in CHCl₃) 0.16. ¹H NMR (500 MHz, 1:1 CDCl₃/CD₃OD) δ 4.90 – 4.89 (m, 2H), 4.14 (d, J = 10.4 Hz, 1H), 3.99 (br s, 1H), 3.92 (d, J = 8.7 Hz, 1H), 3.88 – 3.85 (m, 1H), 3.81 – 3.80 (m, 3H), 3.73 – 3.72 (m, 1H), 3.62 – 3.58 (m, 1H), 3.39 (br s, 1H), 3.36 (t, J = 1.7 Hz, 1H), 2.39 – 2.36 (m, 2H), 1.85 – 1.74 (m, 1H), 1.65 – 1.56 (m, 3H), 1.40 – 1.19 (br s, 69H), 0.89 (t, J = 6.9 Hz, 6H).

m α -GalCer-PABC-L-Ala-Val-ketone (**L-12**)

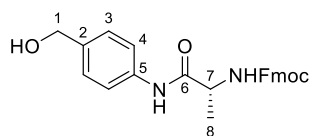


*p*NP-PABC-L-Ala-Val-ketone (**L-24**, 21.1 mg, 0.0344 mmol) and m α -GalCer (**5**, 15.1 mg, 0.0176 mmol) were dried together under vacuum. Pyridine (2 mL) and Et₃N (6 μ L, 0.04 mmol) were added at rt under Ar. The reaction was stirred at rt overnight before concentration under vacuum. The crude material was purified by flash chromatography on silica gel (0-20% CH₃OH in CHCl₃) to give impure m α -GalCer-PABA-L-Ala-Val-ketone (**L-12**, 13.7 mg, 10.3 nmol, 61%) as a white solid. R_f (10% CH₃OH in CHCl₃) 0.14. ¹H NMR (500 MHz, 2:1 CDCl₃/CD₃OD) δ 7.50 (d, J = 8.6 Hz, 2H, PABC), 7.27 (d, J = 8.4 Hz, 2H, PABC), 5.05 (d, J = 12.2 Hz, 1H, H-2'), 4.95 (d, J = 12.3 Hz, 1H, H-2'), 4.92 – 4.87 (m, 1H), 4.80 (d, J = 3.9 Hz, 1H, H-1), 4.44 (q, J = 7.0 Hz, 1H, H-8'), 4.14 (d, J = 7.3 Hz, 1H, H-11'), 3.84 – 3.80 (m, 2H), 3.77 – 3.59 (m, 10H), 2.40 (t, J = 7.4 Hz, 2H, H-20'), 2.30 (td, J = 7.4, 3.2 Hz, 2H, H-1''), 2.24

– 2.17 (m, 2H, H-15'), 2.10 (s, 3H, H-22'), 2.04 – 1.96 (m, 1H, H 12'), 1.64 – 1.49 (m, 9H, H-16' and -19'), 1.39 (d, $J = 7.1$ Hz, 3H, H-9'), 1.30 – 1.19 (m, 91H, CH₂), 0.91 – 0.88 (m, 6H, H-13'), 0.83 (t, $J = 6.9$ Hz, 8H, CH₃). ¹³C NMR (126 MHz, 2:1 CDCl₃/CD₃OD) δ 211.2 (C-21'), 174.9 (C-14'), 172.5 (C-10'), 171.4 (C-7'), 156.9 (C-1'), 138.2 (C-6'), 132.8 (C-3'), 129.0 (PABC), 120.3 (PABC), 100.3 (C-1), 75.0, 72.2, 70.8, 70.6 (C-2), 70.1, 69.3, 68.4, 66.7 (C-2'), 62.2, 59.0 (C-11'), 52.4, 50.0 (C-8'), 43.8 (C-20'), 36.3 (C-15'), 34.9 (C-1''), 32.2 (-CH₂-CH₃), 31.2 (C-12'), 29.9 (br, C-22' and CH₂), 29.6 (br), 29.5, 29.2, 29.1, 29.0, 25.8 (C-16'), 25.6, 25.3, 23.9 (C-19'), 22.9 (-CH₂-CH₃), 19.3 (C13'), 18.3 (C-13'), 17.7 (C-9'), 14.2 (CH₃). HRMS–ESI (m/z): [M + Na]⁺ calcd for C₇₅H₁₃₄N₄O₁₅Na, 1353.9743; found, 1353.9734.

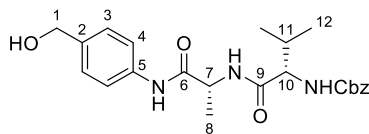
6.2.2 Synthesis of Ketone D-12

PABA-D-Ala-Fmoc (D-18)



PABA (595 mg, 4.83 mmol) and EEDQ (1.61 g, 6.44 mmol) were added to a solution of D-Ala-Fmoc (1.01 g, 3.24 mmol) in anhydrous CH₂Cl₂ (50 mL) and CH₃OH (5 mL) at rt under Ar. The reaction was stirred for 4.5 h in the dark before concentration to yield a crude brown oil. Precipitation from CH₃OH+CH₂Cl₂/Et₂O gave the PABA-D-Ala-Fmoc (**D-18**, 898 mg, 2.16 mmol, 67%) as an off-white solid. R_f (70% EtOAc in PE + AcOH) 0.55. ¹H NMR (500 MHz, 1:1 CDCl₃:CD₃OD) δ 7.74 (d, $J = 7.6$ Hz, 2H, Fmoc), 7.61 (t, $J = 6.6$ Hz, 2H, Fmoc), 7.49 (d, $J = 8.2$ Hz, 2H, PABA), 7.36 (t, $J = 7.6$ Hz, 2H, Fmoc), 7.28 (d, $J = 8.5$ Hz, 4H, Fmoc, PABA), 4.56 (s, 2H, H-1), 4.38 (d, $J = 6.9$ Hz, 2H, Fmoc), 4.29 (q, $J = 7.2$ Hz, 1H, H-7), 4.20 (t, $J = 6.9$ Hz, 1H, Fmoc), 1.41 (d, $J = 7.1$ Hz, 3H, H-8). ¹³C NMR (126 MHz, 1:1 CDCl₃:CD₃OD) δ 172.8 (C-6), 157.4 (C=O Fmoc), 144.4, 141.9, 128.3, 128.1, 127.7, 125.6, 120.9, 120.5, 67.5 (Fmoc), 64.5 (C-1), 51.8 (C-7), 47.8 (Fmoc), 18.6 (C-8). HRMS–ESI (m/z): [M + Na]⁺ calcd for C₂₅H₂₄N₂O₄Na, 439.1634; found, 439.1638. [α]_D²⁰ +18.5° (c 1.00, DMF).

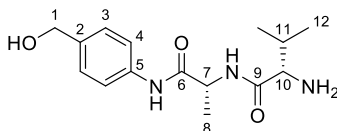
PABA-D-Ala-Val-Cbz (D-20)



Piperidine (0.95 mL, 9.5 mmol) was added to a solution of PABA-D-Ala-Fmoc (**D-18**, 795 mg, 1.91 mmol) in DMF (8.7 mL) at rt under Ar. The reaction was stirred at rt for 20 min before concentration in vacuo. Repeated addition of DMF and further evaporation ensured complete removal of piperidine. Amine **D-19** was then used without further purification. R_f (65:30:4:0.5 CHCl₃, CH₃OH, H₂O, aq NH₃) 0.56. HRMS–ESI (m/z): $[M + H]^+$ calcd for C₁₀H₁₅N₂O₂, 195.1134; found, 195.1140.

NHS-Val-Cbz (798 mg, 2.29 mmol, 1.2 equiv) and the above crude amine (**D-19**) were dried under vacuum before being dissolved in DMF (9.5 mL) and the reaction was stirred at rt under Ar for two days. The reaction was added dropwise to water (95 mL). The flask was rinsed with water (30 mL). The resulting white precipitate was filtered. The precipitate was triturated with Et₂O. This was repeated once more to give PABA-D-Ala-Val-Cbz (**D-20**, 615 mg, 1.44 mmol, 75% over two steps) as an off-white solid. R_f (10% CH₃OH in CHCl₃) 0.48. ¹H NMR (500 MHz, DMSO-*d*₆) δ 9.71 (s, 1H, NH PABA), 8.31 (d, J = 7.5 Hz, 1H, NH Val), 7.57 (d, J = 8.2 Hz, 2H, PABA), 7.39 – 7.23 (m, 6H, Cbz and NH Ala), 7.24 (d, J = 8.5 Hz, 2H, PABA), 5.08 – 5.00 (m, 3H, -OH and Cbz), 4.45 – 4.43 (m, 3H, H-1 and -7), 3.87 (t, J = 7.8 Hz, 1H, H-10), 1.95 (h, J = 6.8 Hz, 1H, H-11), 1.30 (d, J = 7.1 Hz, 3H, H-8), 0.88 – 0.86 (m, 6H, H-12). ¹³C NMR (126 MHz, DMSO-*d*₆) δ 171.1 (C=O), 170.8 (C=O), 156.3, 137.6, 137.3, 137.3, 136.9, 128.3, 127.8, 127.6, 126.8 (PABA), 119.0 (PABA), 65.5 (Cbz), 62.6 (C-1), 60.5 (C-10), 48.8 (C-7), 30.1 (C-11), 19.1 (-CH₃), 18.4 (-CH₃), 18.1 (-CH₃). HRMS–ESI (m/z): $[M + Na]^+$ calcd for C₂₃H₂₉N₃O₅Na, 450.2005; found, 450.2005.

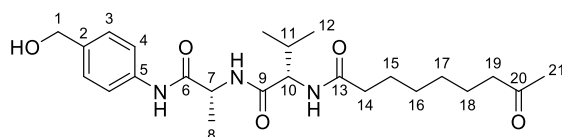
PABA-D-Ala-Val-NH₂ (D-21)



A heterogenous mixture of PABA-D-Ala-Val-Cbz (**D-20**, 483 mg, 1.13 mmol) and 10% Pd/C (99 mg, 0.093 mmol, 8 mol%) in CH₂Cl₂ (1 mL) and CH₃OH (9 mL) was stirred under an H₂

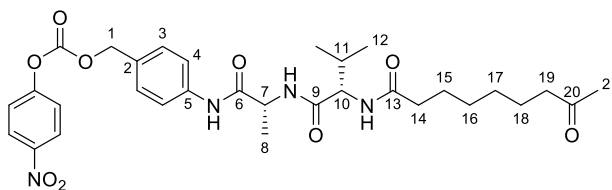
atmosphere for 2 h. The reaction mixture was filtered through Celite then concentrated to give PABA-D-Ala-Val-NH₂ (**D-21**, 322 mg, 1.10 mmol, 97%) as white solid. *R_f* (65:30:4:0.5 CHCl₃, CH₃OH, H₂O, aq NH₃) 0.66. ¹H NMR (500 MHz, CD₃OD) δ 7.54 (d, *J* = 8.5 Hz, 2H, H-3), 7.30 (d, *J* = 8.6 Hz, 2H, H-4), 4.56 (s, 2H, H-1), 4.52 (q, *J* = 7.1 Hz, 1H, H-7), 3.14 (d, *J* = 5.9 Hz, 1H, H-10), 1.96 (pd, *J* = 6.9, 5.8 Hz, 1H, H-11), 1.44 (d, *J* = 7.1 Hz, 3H, H-8), 0.97 (d, *J* = 6.9 Hz, 2H, H-12), 0.94 (d, *J* = 6.9 Hz, 1H, H-12). ¹³C NMR (126 MHz, CD₃OD) δ 176.9 (C-9), 173.2 (C-6), 138.8 (PABA), 138.6 (PABA), 128.6 (PABA), 121.4 (C-4), 64.8 (C-1), 61.6 (C-10), 50.8 (C-7), 33.4 (C-11), 19.7 (C-12), 18.3 (C-8), 17.9 (C-12). HRMS–ESI (*m/z*): [M + Na]⁺ calcd for C₁₅H₂₄N₃O₃Na, 294.1818; found, 294.1816.

PABA-D-Ala-Val-ketone (**D-23**)



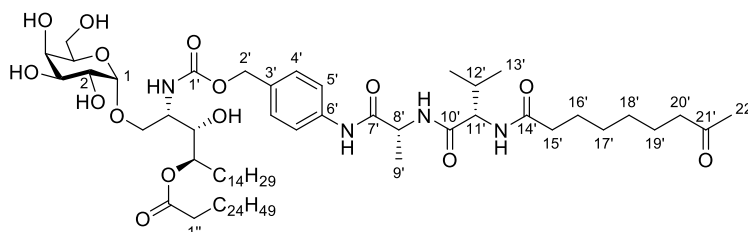
DIPEA (0.1 mL, 0.6 mmol, 1.2 equiv) was added to a solution of PABA-D-Ala-Val-NH₂ (**D-21**, 164 mg, 0.56 mmol) and pNP-activated 8-oxo-nonanoic acid (**22**, 198 mg, 0.68 mmol, 1.2 equiv) in DMF (5.4 mL) at rt under Ar. The reaction was stirred at rt for 2.5 h, before concentration in vacuo. The crude yellow solid was purified by flash chromatography on silica gel (0-10% CH₃OH in CHCl₃) to give PABA-D-Ala-Val-ketone (**D-23**, 210 mg, 0.469 mmol, 84%) as a white solid. *R_f* (10% CH₃OH in CHCl₃) 0.41. ¹H NMR (500 MHz, 1:1 CDCl₃:CD₃OD) δ 7.60 (d, *J* = 8.5 Hz, 2H, PABA), 7.27 (d, *J* = 8.3 Hz, 2H, PABA), 4.55 (s, 2H, H-1), 4.56 – 4.49 (m, 1H, H-7), 4.01 – 3.99 (m, 1H, H-10), 2.40 – 2.37 (m, 2H, H-19), 2.23 (td, *J* = 7.4, 3.8 Hz, 2H, H-14), 2.10 (s, 3H, H-21), 2.05 – 2.01 (m, 1H, H-11), 1.57 (p, *J* = 7.4 Hz, 2H, H-15), 1.49 – 1.46 (m, 2H, H-18), 1.44 (d, *J* = 7.3 Hz, 3H, H-8), 1.28 – 1.19 (m, 4H, H-16 and -17), 0.98 (d, *J* = 6.7 Hz, 3H, H-12), 0.95 (d, *J* = 6.8 Hz, 3H, H-12). ¹³C NMR (126 MHz, 1:1 CDCl₃:CD₃OD) δ 211.7 (C-20), 175.9 (C-6), 173.4 (C-13), 172.1 (C-9), 138.0 (PABA), 137.8 (PABA), 128.0 (PABA), 121.0 (PABA), 64.5 (C-1), 60.7 (C-10), 50.3 (C-7), 44.0 (C-19), 36.2 (C-14), 30.5 (C-11), 29.9 (C-21), 29.4, 29.3, 26.1 (C-15), 24.1 (C-18), 19.4 (C-12), 19.1 (C-12), 17.9 (C-8). HRMS–ESI (*m/z*): [M + Na]⁺ calcd for C₂₄H₃₇N₃O₅Na, 470.2631; found, 470.2636.

*p*NP-PABC-D-Ala-Val-ketone (**D-24**)



A mixture of PABA-D-Ala-Val-ketone (**D-23**, 94 mg, 0.21 mmol) and bis-*p*NP carbonate (128 mg, 0.421 mmol) were dried together under high vacuum. DMF (2 mL) was added at rt under Ar. DIPEA (80 μ L, 0.46 mmol) was then added. The reaction was stirred at rt under Ar for 18 h before concentration in vacuo. The oily yellow residue was purified by flash chromatography on silica gel (50-90% EtOAc in CH_2Cl_2) to give *p*NP-PABA-D-Ala-Val-ketone (**D-24**, 110 mg, 0.180 mmol, 86%) as a white solid. R_f (10% CH_3OH in CHCl_3) 0.56. ^1H NMR (500 MHz, CDCl_3) δ 8.93 (s, 1H, NH), 8.26 – 8.23 (m, 2H, *p*NP), 7.67 (d, J = 8.6 Hz, 2H, PABA), 7.37 – 7.33 (m, 4H, PABA and *p*NP), 7.09 (d, J = 7.9 Hz, 1H, NH), 6.45 (d, J = 7.4 Hz, 1H, NH), 5.24 (s, 2H, H-1), 4.68 (p, J = 7.1 Hz, 1H, H-7), 4.10 (t, J = 7.7 Hz, 1H, H-10), 2.37 (t, 2H, J = 7.3 Hz, H-19), 2.27 – 2.16 (m, 2H, H-14), 2.11 – 2.03 (m, 4H, H-21 and -11), 1.62 – 1.56 (m, 2H, H-15), 1.54 – 1.45 (m, 5H, H-18 and -8), 1.31 – 1.20 (m, 6H, H-16 and -17), 0.98 – 0.96 (m, 6H, H-12). ^{13}C NMR (126 MHz, CDCl_3) δ 209.3 (C-20), 174.4 (C-13), 172.6 (C-9), 170.5 (C-6), 155.7 (*p*NP), 152.6, 145.6 (*p*NP), 139.0 (PABA), 130.0 (PABA), 129.7 (C-3), 125.4 (*p*NP), 121.9 (*p*NP), 120.3 (C-4), 70.8 (C-1), 60.1 (C-10), 49.9 (C-7), 43.6 (C-19), 36.4 (C-14), 30.5 (C-11), 29.9 (C-21), 28.9, 28.8, 25.5 (C-15), 23.6 (C-18), 19.3 (C-12), 18.9 (C-12), 17.9 (C-8). HRMS–ESI (m/z): $[\text{M} + \text{Na}]^+$ calcd for $\text{C}_{31}\text{H}_{40}\text{N}_4\text{O}_9\text{Na}$, 635.2693; found, 635.2693.

α -GalCer-PABC-D-Ala-Val-ketone (**D-12**)

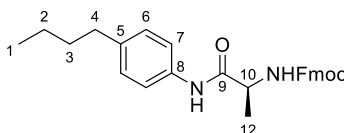


*p*NP-PABC-D-Ala-Val-ketone (**D-24**, 19.6 mg, 0.0320 mmol) and α -GalCer (**5**, 15.0 mg, 0.0175 mmol) were dried together under vacuum. Pyridine (2 mL) and Et_3N (6 μ L, 0.04 mmol) were added at rt under Ar. The reaction was stirred at rt overnight, before concentration under

vacuum. The crude material was purified by flash chromatography on silica gel (0-15% CH₃OH in CHCl₃) to give impure m α -GalCer-PABA-D-Ala-Val-ketone (**D-12**, 12.1 mg, 9.08 nmol, 54%) as a white solid. *R_f* (10% CH₃OH in CHCl₃) 0.30. ¹H NMR (500 MHz, 2:1 CDCl₃/CD₃OD) δ 7.57 (d, *J* = 8.2 Hz, 2H, PABC), 7.27 (d, *J* = 8.2 Hz, 2H, PABC), 5.08 (d, *J* = 12.2 Hz, 1H, H-2'), 4.94 – 4.88 (m, *J* = 12.3 Hz, 2H), 4.80 (d, *J* = 3.9 Hz, 1H, H-1), 4.48 (q, *J* = 7.1 Hz, 1H, H-8'), 3.99 (d, *J* = 8.0 Hz, 1H, H-11'), 3.83 – 3.60 (m, 12H), 2.37 (t, *J* = 7.4 Hz, 2H, H-20'), 2.30 (td, *J* = 7.5, 3.1 Hz, 2H, H-1''), 2.20 (td, *J* = 7.4, 3.0 Hz, 2H, H-15'), 2.09 (s, 3H, H-22'), 2.04 – 1.97 (m, 1H, H-12'), 1.64 – 1.47 (m, 9H, H-16' and -19'), 1.41 (d, *J* = 7.2 Hz, 3H, H-9'), 1.28 – 1.19 (m, 90H, -CH₂-), 0.94 – 0.91 (m, 6H, H-13'), 0.83 (t, *J* = 6.9 Hz, 8H, -CH₃). ¹³C NMR (126 MHz, 2:1 CDCl₃/CD₃OD) δ 211.3 (C-21'), 175.4, 174.9, 172.9 (C-10'), 171.7 (C-7'), 156.9 (C-1'), 138.2 (C-6'), 132.9 (C-3'), 129.0 (PABC), 120.6 (PABC), 100.3 (C-1), 75.0, 72.2, 70.8, 70.6 (C-2), 70.1, 69.3, 68.4, 66.7 (C-2'), 62.2, 60.0 (C-11'), 52.4, 49.9 (C-8'), 43.8 (C-20'), 36.1 (C-15'), 34.9 (C-1''), 32.2 (-CH₂-CH₃), 30.4 (C-12'), 29.9 (br, C-22' and -CH₂-), 29.6 (br, -CH₂-), 29.5, 29.1, 29.0, 25.8 (C-16'), 25.6, 25.3, 23.8 (C-19'), 22.9 (-CH₂-CH₃), 19.3 (C-13'), 18.8 (C-13'), 17.8 (C-9'), 14.2 (CH₃). HRMS–ESI (*m/z*): [M + Na]⁺ calcd for C₇₅H₁₃₄N₄O₁₅Na, 1353.9743; found, 1353.9736.

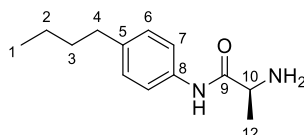
6.2.3 Synthesis of Model Dipeptide 13

4-Butylaniline-Ala-Fmoc (29)



4-butylaniline (100 μ L, 0.633 mmol, 1 equiv) was dissolved in THF (3 mL) and then added to a solution of NHS-Ala-Fmoc (**28**, 296 mg, 0.689 mmol, 1.1 equiv) in THF (5 mL) at rt. The reaction was stirred overnight. The reaction solution was then added to an additional solution of NHS-Ala-Fmoc (**28**, 132 mg, 0.307 mmol, 0.5 equiv) in THF (5 mL). The solution was stirred overnight before the reaction was evaporated. The residue was purified three times by flash chromatography on silica gel (5-100% EtOAc in PE; 20-100% EtOAc in PE; 0-100% EtOAc in CH_2Cl_2) to give **29** (235 mg, 0.531 mmol, 84%) as a white solid. R_f (5% EtOAc in CH_2Cl_2) 0.51. ^1H NMR (500 MHz, CDCl_3) δ 8.41 (br s, 1H, NH), 7.72 (d, $J = 7.3$ Hz, 2H, Fmoc), 7.55 – 7.51 (m, 2H, Fmoc), 7.38 – 7.36 (m, 4H, Fmoc and H-7), 7.25 (t, $J = 7.3$ Hz, 2H, Fmoc), 7.04 (d, $J = 8.0$ Hz 2H, H-6), 5.73 (br s, 1H, NH), 4.46 (br s, 1H, H-10) 4.39 (d, $J = 7.2$ Hz, 2H, Fmoc), 4.17 (t, $J = 7.1$ Hz, 1H, Fmoc), 2.54 (t, $J = 7.7$ Hz, 2H, H-4), 1.57 – 1.51 (m, 2H, H-3), 1.46 (d, $J = 7.0$ Hz, 3H, H-12), 1.34 (h, $J = 7.4$ Hz, 2H, H-2), 0.91 (t, $J = 7.4$ Hz, 3H, H-1). ^{13}C NMR (125 MHz, CDCl_3) δ 170.6 (C-9), 156.5 (C=O Fmoc) 143.8 (Fmoc), 141.4 (Fmoc), 139.3 (C-5), 135.4 (C-8), 128.9 (C-6), 127.9 (Fmoc), 127.2 (Fmoc), 125.1 (Fmoc), 120.2 (C-7), 120.1 (Fmoc), 67.5 (Fmoc), 51.4 (C-10), 47.2 (Fmoc), 35.2 (C-4), 33.7 (C-3), 22.4 (C-2), 18.8 (C-12), 14.1 (C-1). HRMS–ESI (m/z): $[\text{M} + \text{Na}]^+$ calcd for $\text{C}_{28}\text{H}_{30}\text{N}_2\text{O}_3\text{Na}$, 465.2149; found, 465.2159.

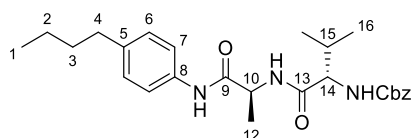
4-Butylaniline-Ala-NH₂ (30)



Piperidine (0.23 mL) was added to a solution of 4-butylaniline-Ala-Fmoc (**29**, 110 mg, 0.247 mmol) in DMF (2 mL). The solution was stirred at rt for 30 min. The solution was concentrated then taken up into CH_3OH three times. The residue was purified by flash

chromatography on silica gel (1-5% CH₃OH (1%Et₃N) in CHCl₃) to give **30** (49 mg, 0.22 mmol, 89%) as a colourless oil. *R*_f (Et₃N:CH₃OH:CHCl₃ 5:25:95) 0.14. ¹H NMR (500 MHz, CDCl₃) δ 9.36 (br s, 1H, NH PABA), 7.48 (d, *J* = 8.4 Hz, 2H, H-7), 7.12 (d, *J* = 8.4 Hz, 2H, H-6), 3.58 (q, *J* = 7.0 Hz, 1H, H-10), 2.56 (t, *J* = 7.8 Hz, 2H, H-4), 1.66 (br s, 2H, NH Ala), 1.60 – 1.54 (m, 2H, H-3), 1.40 (d, *J* = 7.0 Hz, 3H, H-12), 1.33 (dq, *J* = 14.6, 7.4 Hz, 2H, H-2), 0.91 (t, *J* = 7.4 Hz, 3H, H-1). ¹³C NMR (125 MHz, CDCl₃) δ 173.8 (C-9), 138.8 (C-5), 135.6 (C-8), 128.9 (C-6), 119.5 (C-7), 51.3 (C-10), 35.1 (C-4), 33.7 (C-3), 22.3 (C-2), 21.7 (C-12), 14.0 (C-1). HRMS–ESI (*m/z*): [M + H]⁺ calcd for C₁₃H₂₁N₂O, 221.1654; found, 221.1651.

4-Butylaniline-Ala-Val-Cbz (**13**)

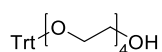


A solution of 4-butylaniline Ala-NH₂ (**30**, 35 mg, 0.16 mmol) in THF (1.4 mL) was added to a solution of NHS-Val-Cbz (**31**, 56 mg, 0.16 mmol) in THF (1.5 mL). The reaction was stirred at rt for 5 h. The reaction was concentrated. The residue was purified by flash chromatography on silica gel (0-100% EtOAc in PE; 0-100% EtOAc in CH₂Cl₂) to give **13** (49 mg, 0.11 mmol, 68%) as a white solid. *R*_f (40% EtOAc in CH₂Cl₂) 0.63. ¹H NMR (500 MHz, CDCl₃) δ 8.45 (br s, 1H, NH PABA), 7.42 (d, *J* = 8.0 Hz, 2H, H-7), 7.32 (br s, 5H, Cbz) 7.07 (d, *J* = 8.5 Hz, 2H, H-6), 6.92 (br s, 1H, NH Ala), 5.51 (br s, 1H, NH Val), 5.14 – 5.07 (m, 2H, Cbz), 4.67 (p, *J* = 7.1 Hz, 1H, H-10), 4.12 – 4.09 (m, 1H, H-14), 2.55 (t, *J* = 7.7 Hz, 2H, H-4), 2.12 (h, *J* = 6.7 Hz, 1H, H-15), 1.59 – 1.54 (m, 2H, H-3), 1.43 (d, *J* = 7.0 Hz, 3H, H-12), 1.33 (h, *J* = 7.3 Hz, 2H, H-2), 0.95 – 0.90 (m, 9H, H-1 and H-16). ¹³C NMR (125 MHz, CDCl₃) δ 171.8 (C-13), 170.0 (C-9), 156.8 (C=O Cbz), 139.3 (C-5), 136.2 (Cbz), 135.5 (C-8), 129.0 (C-7), 128.7 (Cbz), 128.4 (Cbz), 128.2 (Cbz), 120.2 (C-6), 67.4 (Cbz), 60.7 (C-14), 49.8 (C-10), 35.2 (C-4), 33.8 (C-2), 31.2 (C-15), 22.4 (C-2), 19.4 (C-16), 18.0 (C-16), 17.8 (C-12), 14.1 (C-1). HRMS–ESI (*m/z*): [M + H]⁺ calcd for C₂₆H₃₅N₃O₄Na, 476.2525; found, 476.2521.

6.2.4 Iterative Synthesis of Discrete PEGs

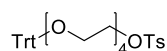
These synthetic procedures are based on that reported by Wawro et al.¹⁶²

TrtO-PEG₄-OH



Water was removed from tetraethylene glycol (5.11 g, 26.3 mmol, 6.8 equiv) by repeated azeotropic evaporation with toluene. The flask was flushed with argon and triethylamine (0.71 mL, 5.1 mmol, 1.3 equiv) was added. Trityl chloride (1.12 g, 3.9 mmol, 1.0 equiv) was then added portionwise over 5 min. The reaction was stirred at rt for 3 h. The mixture was diluted with EtOAc and stirred for a further 10 min. The solid was removed by filtration and rinsed with EtOAc. The filtrate was washed with water, saturated NH₄Cl and brine. The organic layer was dried over MgSO₄ and concentrated to give crude **TrtO-PEG₄-OH** (1.7 g) as a pale-yellow oil, which was used without further purification. Data were collected on the crude material. R_f (EtOAc) 0.5. ¹H NMR (500 MHz, CDCl₃) δ 7.47 – 7.45 (m, 6H, Trt), 7.30 – 7.27 (m, 6H, Trt), 7.24 – 7.20 (m, 3H, Trt), 3.70 – 3.67 (m, 12H, -CH₂-), 3.60 – 3.59 (m, 2H, TrtO-CH₂-CH₂-), 3.25 (t, 2H, *J* = 5.4 Hz, TrtO-CH₂-), 2.36 (t, 2H, *J* = 6.3 Hz, -OH). ¹³C NMR (125 MHz, CDCl₃) δ 144.3 (Trt), 128.9 (Trt), 127.9 (Trt), 127.1 (Trt), 86.7 (Trt), 72.6 (TrtO-CH₂-CH₂), 71.0 (-CH₂-), 70.9 (-CH₂-), 70.6 (-CH₂-), 63.5 (TrtO-CH₂-), 62.0 (-CH₂-). HRMS–ESI (*m/z*): [M + NH₄]⁺ calcd for C₂₇H₃₆NO₅, 454.2593; found, 454.2597.

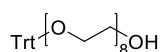
TrtO-PEG₄-OTs



A solution of **TrtO-PEG₄-OH** (used crude, 3.4 g, ~7.8 mmol, 1 equiv) in THF (10 mL) was stirred at 0 °C for 30 min. A solution of NaOH (1.3 g, 32 mmol, 4.1 equiv) in water (4 mL) was added. The resulting heterogenous mixture was stirred at 0 °C for a further 30 min. A solution of *para*-toluenesulfonyl chloride (1.7 g, 8.9 mmol, 1.1 equiv) in THF (4 mL) was added dropwise. The reaction was stirred vigorously at 0 °C for 6.5 h. The reaction was allowed to warm to rt and stirred for 16 h. The reaction was diluted with water and methyl *tert*-butyl ether. The organic layer was washed with water and brine, dried over MgSO₄ and concentrated in

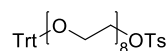
vacuo to give **TrtO-PEG₄-OTs** (4.4 g) as a crude yellow oil which was used without further purification. Data were collected on the crude material. R_f (30% EtOAc in PE) 0.2. ^1H NMR (500 MHz, CDCl_3) δ 7.78 (d, 2H, $J = 8.3$ Hz, Ts), 7.46 – 7.44 (m, 7H, Trt), 7.32 – 7.26 (m, 9H, Trt and Ts), 7.23 – 7.20 (m, 4H, Trt), 4.14 – 4.12 (m, 2H, $-\text{CH}_2-$), 3.68 – 3.56 (m, 13H, $-\text{CH}_2-$), 3.23 (t, 2H, $J = 5.2$ Hz, $-\text{CH}_2-$), 2.42 (s, 3H, $-\text{CH}_3$). ^{13}C NMR (125 MHz, CDCl_3) δ 145.0 (Ts), 144.3 (Trt), 133.3 (Ts), 129.9 (Ts), 128.9 (Trt), 128.1 (Ts), 127.9 (Trt), 127.1 (Trt), 86.7 (Trt), 70.9 ($-\text{CH}_2-$), 70.8 ($-\text{CH}_2-$), 69.4 (TsO- $\underline{\text{CH}_2-}$), 68.9 ($-\text{CH}_2-$), 63.5 (TrtO- $\underline{\text{CH}_2-}$), 21.8 ($-\text{CH}_3$). HRMS–ESI (m/z): $[\text{M} + \text{NH}_4]^+$ calcd for $\text{C}_{34}\text{H}_{42}\text{NO}_7\text{S}$, 608.2682; found, 608.2685.

TrtO-PEG₈-OH



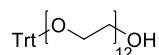
Sodium hydride (60% dispersion in oil, 0.492 g, 12.3 mmol, 1.5 equiv) was washed with PE under Ar twice. Anhydrous THF (4 mL) was added and the mixture was cooled to 0 °C before the dropwise addition of tetraethylene glycol (11 g, 56 mmol, 7.4 equiv), dried previously by azeotropic evaporation with toluene. As long as the evolution of H_2 gas was observed, tetraethylene glycol was added slowly. Once the mixture became a clear solution, the remaining reactant was added more quickly. A solution of **TrtO-PEG₄-OTs** (used crude, 4.4 g, ~7.8 mmol, 1 equiv) in THF (4 mL) was then added dropwise. The reaction was heated to 75 °C for 5 h. The reaction was cooled to rt and stirred overnight. Brine and water were added. The organic layer was washed with 1:1 water/brine, followed by brine, then dried over MgSO_4 and concentrated to give crude **TrtO-PEG₈-OH** (3.9 g) as a crude brown oil. Data were collected on the crude material. R_f (10% CH_3OH in EtOAc) 0.5. ^1H NMR (500 MHz, CDCl_3) δ 7.47 – 7.45 (m, 6H, Trt), 7.30 – 7.27 (m, 7H, Trt), 7.24 – 7.20 (m, 4H, Trt), 3.73 – 3.59 (m, 28H, $-\text{CH}_2-$), 3.43 (t, 2H, $J = 5.2$ Hz, TrtO- $\underline{\text{CH}_2-}$), 2.54 (t, 1H, $J = 6.3$ Hz, $-\text{OH}$). ^{13}C NMR (125 MHz, CDCl_3) δ 144.3 (Trt), 128.9 (Trt), 127.9 (Trt), 127.1 (Trt), 86.7 (Trt), 72.6 (TrtO- CH_2 - $\underline{\text{CH}_2-}$), 71.0 ($-\text{CH}_2-$), 70.9 ($-\text{CH}_2-$), 70.5 ($-\text{CH}_2-$), 63.5 (TrtO- $\underline{\text{CH}_2-}$), 61.9 ($-\text{CH}_2-$). HRMS–ESI (m/z): $[\text{M} + \text{NH}_4]^+$ calcd for $\text{C}_{35}\text{H}_{52}\text{NO}_9$, 630.3642; found, 630.3651.

TrtO-PEG₈-OTs



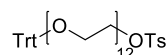
TrtO-PEG₈-OTs was synthesised from **TrtO-PEG₈-OH** following the procedure for **TrtO-PEG₄-OTs**. Data were collected on the crude material. R_f (EtOAc) 0.6. ^1H NMR (500 MHz, CDCl_3) δ 7.79 (d, 2H, $J = 8.4$ Hz, Ts), 7.47 – 7.44 (m, 7H, Trt), 7.33 (d, 2H, $J = 7.6$ Hz, Ts), 7.30 – 7.27 (m, 7H, Trt), 7.23 – 7.20 (m, 3H, Trt), 4.16 – 4.14 (m, 2H, TsO-CH₂-), 3.68 – 3.60 (m, 26H, -CH₂-), 3.57 (s, 4H, -CH₂-), 3.23 (t, 2H, $J = 5.3$ Hz, TrtO-CH₂-), 2.44 (s, 3H, -CH₃). ^{13}C NMR (125 MHz, CDCl_3) δ 144.9 (Ts), 144.3 (Trt), 133.3 (Ts), 130.0 (Ts), 128.9 (Trt), 128.1 (Ts), 127.9 (Trt), 127.1 (Trt), 86.7 (Trt), 70.9 (-CH₂-), 70.8 (-CH₂-), 69.4 (TsO-CH₂-), 68.9 (-CH₂-), 63.5 (TrtO-CH₂-), 21.8 (-CH₃). HRMS-ESI (m/z): $[\text{M} + \text{NH}_4]^+$ calcd for $\text{C}_{42}\text{H}_{58}\text{NO}_{11}\text{S}$, 784.3731; found, 784.3738.

TrtO-PEG₁₂-OH



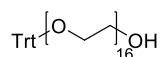
TrtO-PEG₁₂-OH was synthesised from **TrtO-PEG₈-OTs** following the procedure for **TrtO-PEG₈-OH**. Data were collected on the crude material. R_f (EtOAc) 0.29. ^1H NMR (500 MHz, CDCl_3) δ 7.47 – 7.45 (m, 6H, Trt), 7.31 – 7.27 (m, 7H, Trt), 7.24 – 7.20 (m, 4H, Trt), 3.73 – 3.60 (m, 42H, -CH₂-), 3.24 (t, 2H, $J = 5.3$ Hz, TrtO-CH₂-). ^{13}C NMR (125 MHz, CDCl_3) δ 144.3 (Trt), 128.9 (Trt), 127.9 (Trt), 127.1 (Trt), 86.7 (Trt), 72.7 (TrtO-CH₂-CH₂-), 70.9 (-CH₂-), 70.7 (-CH₂-), 70.5 (-CH₂-), 63.5 (TrtO-CH₂-), 61.9 (-CH₂-). HRMS-ESI (m/z): $[\text{M} + \text{NH}_4]^+$ calcd for $\text{C}_{43}\text{H}_{68}\text{NO}_{13}$, 806.4691; found, 806.4689.

TrtO-PEG₁₂-OTs



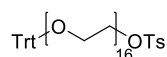
TrtO-PEG₁₂-OTs was synthesised from **TrtO-PEG₁₂-OH** following the procedure for **TrtO-PEG₄-OTs**. The material was reacted onwards before full data could be collected; analysis of the NMR spectra of the partially completed next reaction gave the expected signals; with over integration of the ethylene glycol methylene peaks. R_f (10% CH_3OH in EtOAc) 0.5.

TrtO-PEG₁₆-OH



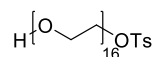
TrtO-PEG₁₆-OH was synthesised from **TrtO-PEG₁₂-OTs** following the procedure for **TrtO-PEG₈-OH**. Data were collected on the crude material. R_f (15% CH₃OH in EtOAc) 0.4. ¹H NMR (500 MHz, CDCl₃) δ 7.47 – 7.45 (m, 6H, Trt), 7.30 – 7.27 (m, 7H, Trt), 7.24 – 7.20 (m, 4H, Trt), 3.73 – 3.60 (m, 53H, -CH₂-), 3.23 (t, 2H, J = 5.2 Hz, TrtO-CH₂-). ¹³C NMR (125 MHz, CDCl₃) δ 144.3 (Trt), 128.9 (Trt), 127.9 (Trt), 127.1 (Trt), 86.7 (Trt), 72.7 (TrtO-CH₂-CH₂-), 70.9 (-CH₂-), 70.7 (-CH₂-), 70.5 (-CH₂-), 63.5 (TrtO-CH₂-), 61.9 (-CH₂-). HRMS-ESI (m/z): $[M + NH_4]^+$ calcd for C₅₁H₈₄NO₁₇, 982.5739; found, 982.5741.

TrtO-PEG₁₆-OTs



TrtO-PEG₁₆-OTs was synthesised from **TrtO-PEG₁₆-OH** following the procedure for **TrtO-PEG₄-OTs**. Data were collected on the crude material. R_f (25% CH₃OH in EtOAc) 0.6. ¹H NMR (500 MHz, CDCl₃) δ 7.80 (d, 2H, J = 8.3 Hz, Ts), 7.47 – 7.44 (m, 8H, Trt), 7.35 – 7.33 (m, 2H, Ts), 7.30 – 7.27 (m, 9H, Trt), 7.24 – 7.20 (m, 3H, Trt), 4.17 – 4.15 (m, 2H, TsO-CH₂-), 3.69 – 3.62 (m, 63H, -CH₂-), 3.62 (s, 4H, -CH₂-), 3.24 (t, 2H, J = 5.2 Hz, TrtO-CH₂-), 2.45 (s, 3H, -CH₃). ¹³C NMR (125 MHz, CDCl₃) δ 144.9 (Ts), 144.3 (Trt), 133.3 (Ts), 130.0 (Ts), 128.9 (Trt), 128.1 (Ts), 127.9 (Trt), 127.1 (Trt), 86.7 (Trt), 70.9 (-CH₂-), 70.8 (-CH₂-), 69.4 (TsO-CH₂-), 68.9 (-CH₂-), 63.5 (TrtO-CH₂-), 21.8 (-CH₃). HRMS-ESI (m/z): $[M + NH_4]^+$ calcd for C₅₈H₉₀NO₁₉S, 1136.5828; found, 1136.5844.

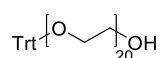
HO-PEG₁₆-OTs



*p*TsOH (60 mg, 0.32 mmol, 0.2 equiv) was added to a suspension of **TrtO-PEG₁₆-OTs** (1.65 g, 1.47 mmol) in CH₃OH (8 mL). The reaction was stirred at rt overnight. Some white precipitate formed, and further precipitation was triggered by the slow addition of crushed ice. Water (8 mL) was added and the mixture was cooled to 0 °C before filtration to remove the precipitate.

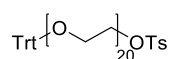
The solid was rinsed with cold water and the filtrate was concentrated. Brine and EtOAc were added, and the aqueous layer was extracted with EtOAc eight times. The combined organic layers were concentrated before redissolution in EtOAc. The organic layer was washed with 1:1 brine/water, saturated NaHCO₃ and brine and dried over MgSO₄ before concentration. The combined aqueous layers and washes were each back extracted with EtOAc. The combined organic layers were dried over MgSO₄ and concentrated to give **HO-PEG₁₆-OTs** (531 mg, 0.61 mmol, 16% over 9 steps) as a colourless oil that solidified upon cooling. *R_f* (25% CH₃OH in EtOAc) 0.2. ¹H NMR (500 MHz, CDCl₃) δ 7.80 (d, 2H, *J* = 8.3 Hz, Ts), 7.34 (d, 2H, *J* = 7.8 Hz, Ts), 4.16 (t, 2H, *J* = 4.8 Hz, TsO-CH₂-), 3.74 – 3.60 (m, 61H, -CH₂-), 3.58 (s, 4H, -CH₂-) 2.65 (t, 1H, *J* = 6.1 Hz, OH), 2.45 (s, 3H, -CH₃). ¹³C NMR (125 MHz, CDCl₃) δ 129.8 (Ts), 128.0 (Ts), 72.6 (-CH₂-CH₂-OH), 70.6 (-CH₂-), 69.2 (TsO-CH₂-CH₂-), 68.7 (TsO-CH₂-), 61.8 (-CH₂-OH), 21.6 (-CH₃). HRMS-ESI (*m/z*): [M + NH₄]⁺ calcd for C₃₉H₇₆NO₁₉S, 894.4732; found, 894.4744.

TrtO-PEG₂₀-OH



TrtO-PEG₂₀-OH was synthesised from **TrtO-PEG₁₆-OTs** following the procedure for **TrtO-PEG₈-OH**. Data were collected on the crude material. *R_f* (25% CH₃OH in EtOAc) 0.5. ¹H NMR (500 MHz, CDCl₃) δ 7.47 – 7.45 (m, 6H, Trt), 7.30 – 7.27 (m, 8H, Trt), 7.24 – 7.20 (m, 3H, Trt), 3.68 – 3.60 (m, 63H, -CH₂-), 3.23 (t, 2H, *J* = 5.3 Hz, TrtO-CH₂-), 2.74 (t, 1H, *J* = 6.1 Hz, -OH). ¹³C NMR (125 MHz, CDCl₃) δ 144.3 (Trt), 128.9 (Trt), 127.9 (Trt), 127.1 (Trt), 72.7 (TrtO-CH₂-CH₂-), 70.8 (-CH₂-), 70.7 (-CH₂-), 70.5 (-CH₂-), 63.5 (TrtO-CH₂-), 61.9 (-CH₂-). HRMS-ESI (*m/z*): [M + NH₄]⁺ calcd for C₅₉H₁₀₀NO₂₁, 1158.6788; found, 1158.6799.

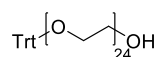
TrtO-PEG₂₀-OTs



TrtO-PEG₂₀-OTs was synthesised from **TrtO-PEG₂₀-OH** following the procedure for **TrtO-PEG₄-OTs**. Data were collected on the crude material. *R_f* (25% CH₃OH in EtOAc) 0.3. ¹H NMR (500 MHz, CDCl₃) δ 7.80 (d, 2H, *J* = 8.3 Hz, Ts), 7.47 – 7.44 (m, 8H, Trt), 7.35 – 7.33 (m, 2H, Ts), 7.30 – 7.27 (m, 9H, Trt), 7.24 – 7.20 (m, 4H, Trt), 4.16 (t, 2H, *J* = 4.8 Hz,

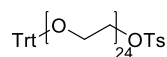
TsO-CH₂-), 3.69 – 3.58 (m, 76H, -CH₂-), 3.58 (s, 4H, -CH₂-), 3.23 (t, 2H, *J* = 5.3 Hz, TrtO-CH₂-), 2.45 (s, 3H, -CH₃). ¹³C NMR (125 MHz, CDCl₃) δ 144.3 (Trt), 130.0 (Ts), 128.9 (Trt), 128.1 (Ts), 127.9 (Trt), 127.1 (Trt), 86.7 (Trt), 70.9 (-CH₂-), 70.7 (-CH₂-), 69.4 (TsO-CH₂-), 68.9 (-CH₂-), 63.5 (TrtO-CH₂-), 21.8 (-CH₃). HRMS–ESI (*m/z*): [M + NH₄]⁺ calcd for C₆₆H₁₀₆NO₂₃S, 1312.6876; found, 1312.6858.

TrtO-PEG₂₄-OH



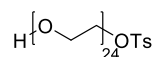
TrtO-PEG₂₄-OH was synthesised from TrtO-PEG₂₀-OTs following the procedure for TrtO-PEG₈-OH. Data were collected on the crude material. R_f (25% CH₃OH in EtOAc) 0.1. ¹H NMR (500 MHz, CDCl₃) δ 7.47 – 7.45 (m, 6H, Trt), 7.30 – 7.27 (m, 7H, Trt), 7.24 – 7.20 (m, 4H, Trt), 3.68 – 3.60 (m, 72H, -CH₂-), 3.24 (t, 2H, *J* = 5.2 Hz, TrtO-CH₂-), 2.72 (t, 1H, *J* = 6.2 Hz, -OH). ¹³C NMR (125 MHz, CDCl₃) δ 144.3 (Trt), 128.9 (Trt), 127.9 (Trt), 127.1 (Trt), 86.7 (Trt), 72.7 (TrtO-CH₂-CH₂-), 71.0 (-CH₂-), 70.7 (-CH₂-), 70.5 (-CH₂-), 63.5 (TrtO-CH₂-), 61.9 (-CH₂-). HRMS–ESI (*m/z*): [M + NH₄]⁺ calcd for C₆₇H₁₁₆NO₂₅, 1334.7836; found, 1334.7850.

TrtO-PEG₂₄-OTs



TrtO-PEG₂₄-OTs was synthesised from TrtO-PEG₂₄-OH following the procedure for TrtO-PEG₄-OTs. Data were collected on the crude material. R_f (20:5:75 CH₃OH:H₂O:EtOAc) 0.4. ¹H NMR (500 MHz, CDCl₃) δ 7.80 (d, 2H, *J* = 8.4 Hz, Ts), 7.47 – 7.44 (m, 9H, Trt), 7.35 – 7.33 (m, 2H, Ts), 7.30 – 7.27 (m, 11H, Trt), 7.24 – 7.20 (m, 4H, Trt), 4.16 (t, 2H, *J* = 5.2 Hz, TsO-CH₂-), 3.69 – 3.61 (m, 92H, -CH₂-), 3.99 (s, 4H, -CH₂-), 3.23 (t, 2H, *J* = 5.2 Hz, TrtO-CH₂-), 2.45 (s, 3H, -CH₃). ¹³C NMR (125 MHz, CDCl₃) δ 144.3 (Trt), 130.0 (Ts), 128.9 (Trt), 128.1 (Ts), 127.9 (Trt), 127.1 (Trt), 70.9 (-CH₂-), 70.8 (-CH₂-), 63.5 (TrtO-CH₂-), 21.2 (-CH₃). HRMS–ESI (*m/z*): [M + 2NH₄]²⁺ calcd for C₇₄H₁₂₆N₂O₂₇S, 753.4129; found, 753.4136.

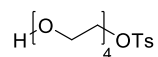
HO-PEG₂₄-OTs



*p*TsOH (11 mg, 0.06 mmol, 0.8 equiv) was added to a suspension of **TrtO-PEG₂₄-OTs** (0.997 g, 0.68 mmol) in CH₃OH (8 mL). The reaction was stirred at rt overnight. Some white precipitate formed, further precipitation was triggered by the slow addition of crushed ice. Water (8 mL) was added and the mixture was cooled to 0 °C before filtration to remove the precipitate. The solid was rinsed with cold water. The filtrate was concentrated. Brine and EtOAc were added. The aqueous layer was extracted with EtOAc. The combined organic layers were dried over MgSO₄ and concentrated to give **HO-PEG₂₄-OTs** (488 mg, 0.40 mmol, 13% over 13 steps) as a white solid. *R_f* (20:5:75 CH₃OH:H₂O:EtOAc) 0.2. ¹H NMR (500 MHz, CDCl₃) δ 7.77 (d, 2H, *J* = 8.3 Hz, Ts), 7.34 (d, 2H, *J* = 8.0 Hz, Ts), 4.16 (t, 2H, *J* = 5.1 Hz, TsO-CH₂-), 3.70 – 3.57 (m, 87H, -CH₂-), 3.55 (s, 4H, -CH₂-), 2.42 (s, 3H, -CH₃). ¹³C NMR (125 MHz, CDCl₃) δ 130.0 (Ts), 128.1 (Ts), 72.7 (-CH₂-CH₂-OH), 70.7 (-CH₂-), 69.4 (TsO-CH₂-CH₂-), 68.8 (TsO-CH₂-), 61.9 (-CH₂-OH), 21.6 (-CH₃). HRMS–ESI (*m/z*): [M + 2NH₄]²⁺ calcd for C₅₅H₁₁₂N₂O₂₇S, 632.3581; found, 632.3580.

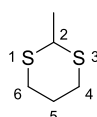
6.2.5 Derivatisation of Discrete PEGs

HO-PEG₄-OTs



A solution of NaOH (0.56 g, 14 mmol) in water (4 mL) was added to a solution of tetraethylene glycol (10.94 g, 56.33 mmol) in THF (4 mL) at 0 °C. A solution of TsCl (1.58 g, 8.29 mmol) in THF (5 mL) was then added dropwise. The reaction was stirred vigorously at 0 °C for 25 min before dilution with ice water. The mixture was extracted with CH₂Cl₂. The combined organic layers were washed with water and brine, dried over MgSO₄ and concentrated to give a colourless oil. The residue was purified by flash chromatography on silica gel (EtOAc) to give **HO-PEG₄-OTs**. (2.08 g, 5.97 mmol, 73%) as a colourless oil. ¹H NMR (500 MHz, CDCl₃) δ 7.80 (d, 2H, *J* = 8.3 Hz, Ts), 7.34 (d, 2H, *J* = 7.9 Hz, Ts), 4.17 (t, 2H, *J* = 4.6 Hz, TsO-CH₂-), 3.72 – 3.68 (m, 4H, -CH₂-), 3.67 – 3.62 (m, 4H, -CH₂-), 3.61 – 3.59 (m, 4H, -CH₂-), 2.45 (s, 3H, -CH₃), 2.38 (t, 1H, *J* = 6.2 Hz, -OH). ¹³C NMR (125 MHz, CDCl₃) δ 144.9 (Ts), 133.2 (Ts), 130.0 (Ts), 128.1 (Ts), 72.6 (-CH₂-CH₂-OH), 70.9 (-CH₂-), 70.8 (-CH₂-), 70.5 (-CH₂-), 69.4 (TsO-CH₂-CH₂-), 69.4 (-CH₂-), 68.9 (TsO-CH₂-), 61.9 (-CH₂-OH), 21.8 (-CH₃).

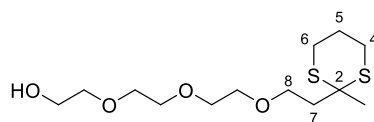
2-Methyl-1,3-dithiane (36)



To a solution of acetaldehyde (2.5 mL, 44 mmol, 1.0 equiv) in anhydrous CH₂Cl₂ (40 mL) was added 1,3-propanedithiol (4.9 mL, 49 mmol, 1.1 equiv) under Ar. The reaction was cooled to 0 °C and stirred for 30 min. BF₃·Et₂O (2.8 mL, 22 mmol, 0.5 equiv) was added dropwise. The reaction was stirred at 0 °C for 1.5 h before being warmed to rt and quenched with saturated aq NH₄Cl. The reaction was extracted into CH₂Cl₂. The combined organic layers were washed with NaOH (0.1 mol L⁻¹) and brine and dried over MgSO₄ before concentration to yield 2-methyl-1,3-dithiane (**36**, 5.5 g, 41 mmol, 92%) as a colourless oil. *R*_f (10% EtOAc in PE) 0.5. ¹H NMR (500 MHz, CDCl₃) δ 4.12 (q, 1H, *J* = 7.1 Hz, H-2), 2.90 (tdd, 2H, *J* = 13.0, 2.5, 1.0 Hz,

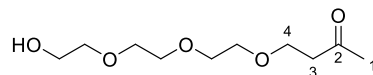
H-4_{ax} and H-6_{ax}), 2.83 – 2.78 (m, 2H, H-4_{eq} and H-6_{eq}), 2.10 (dt, 2H, $J = 14.2, 4.8, 2.6$ Hz, H-5_{eq}), 1.86 – 1.77 (m, 2H, H-5_{ax}), 1.47 (dd, 3H, $J = 7.1, 1.2$ Hz, -CH₃).

HO-PEG₄-dithiane (38)



To a solution of 2-methyl-1,3-dithiane (**36**, 103 mg, 0.767 mmol, 2.5 equiv) in THF (3 mL) in a flame dried flask was added BuLi (2.5 mol L⁻¹ in hexanes, 0.35 mL, 0.85 mmol, 3 equiv) at 0 °C under Ar. After 5 min at 0 °C, a solution of **34** (100 mg, 0.28 mmol, 1 equiv) in THF (1 mL) was added dropwise. The reaction was warmed to rt and stirred for 1.5 h. The reaction was quenched with NH₄Cl and extracted into EtOAc. The combined organic layers were washed with brine and dried over MgSO₄ before concentration. The residue was purified by flash chromatography on silica gel (80-100% EtOAc in PE) to yield **38** (56 mg, 1.8 mmol, 63%) as a colourless oil. R_f (EtOAc) 0.3. ¹H NMR (500 MHz, CDCl₃) δ 3.73 – 3.72 (m, 2H, -CH₂-), 3.69 – 3.63 (m, 8H, -CH₂-), 3.62 – 3.59 (m, 4H, -CH₂-), 2.89 (ddd, 2H, $J = 14.6, 9.4, 3.1$ Hz, H-4_{ax} and H-6_{ax}), 2.79 (ddd, 2H, $J = 14.5, 7.1, 3.3$ Hz, H-4_{eq} and H-6_{eq}), 2.49 (br s, 1H, -OH), 2.27 (t, 2H, $J = 7.2$ Hz, H-7), 2.02 – 1.95 (m, 1H, H-5_{eq}), 1.94 – 1.86 (m, 1H, H-5_{ax}), 1.61 (s, 3H, -CH₃). ¹³C NMR (125 MHz, CDCl₃) δ 72.7 (-CH₂-), 70.8 (-CH₂-), 70.7 (-CH₂-), 70.5 (-CH₂-), 70.4 (-CH₂-), 68.1 (C-8), 61.9 (-CH₂-), 47.6 (C-2), 40.5 (C-7), 28.5 (-CH₃), 26.7 (C-4 and C-6), 25.2 (C-5). HRMS–ESI (m/z): [M + Na]⁺ calcd for C₁₃H₂₆O₄NaS₂, 333.1170; found, 333.1166.

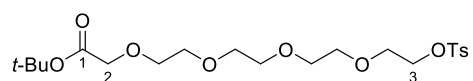
HO-PEG₄-ketone (39)



Calcium carbonate (229 mg, 2.29 mmol, 17 equiv) and iodomethane (0.13 mL, 2.1 mmol, 15 equiv) were added to a solution of **38** (42 mg, 0.14 mmol, 1 equiv) in MeCN (1.8 mL) and H₂O (0.2 mL). The reaction was heated to 50 °C for 5.5 h. The reaction was cooled to rt and quenched with saturated aq NaHCO₃ and extracted with EtOAc. The combined organic layers were washed with brine, dried over MgSO₄ and concentrated. The residue was purified by flash

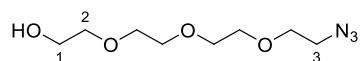
chromatography on silica gel (5% CH₃OH in CHCl₃) to give **39** (0.6 mg, 0.003 mmol, 2%). R_f (5% CH₃OH in CHCl₃) 0.14. ¹H NMR (500 MHz, CDCl₃) δ 3.75 – 3.60 (m, 15H, -CH₂-), 2.71 (t, 2H, *J* = 6.3 Hz, H-3), 2.57 (br s, 1H, -OH), 2.18 (s, 3H, -CH₃). ¹³C NMR (125 MHz, CDCl₃) δ 207.4 (C-2), 72.7 (-CH₂-), 70.8 (-CH₂-), 70.61 (-CH₂-), 70.56 (-CH₂-), 70.5 (-CH₂-), 66.3 (C-4), 61.9 (-CH₂-), 43.8 (C-3), 30.6 (C-1). HRMS–ESI (*m/z*): [M + Na]⁺ calcd for C₁₀H₂₀O₅Na, 243.1208; found, 243.1211.

***t*-BuOOC-CH₂-PEG₄-OTs (**40**)**



To a solution of **34** (51 mg, 0.15 mmol) in THF (3 mL) under Ar was added NaH (60% in oil, 69 mg, 1.7 mmol, 11.6 equiv) at 0 °C. The reaction was stirred at 0 °C for 30 min before the addition of *tert*-butyl bromoacetate (53 μL, 0.36 mmol, 2.5 equiv). The reaction was stirred at 0 °C for a further 60 min then allowed to warm to rt and stirred overnight. The reaction was quenched with water at 0 °C before extraction into EtOAc. The combined organic layers were washed with brine then dried over MgSO₄ before concentration to give a crude yellow oil. The residue was purified by flash chromatography on silica gel (0-100% EtOAc in PE) to yield impure **40** (15 mg). Data were collected on the mixture. R_f(EtOAc) 0.71. ¹H NMR (500 MHz, CDCl₃) δ 7.79 (d, 2H, *J* = 8.3 Hz, Ts), 7.33 (d, 2H, *J* = 7.9 Hz, Ts), 4.17 (m, 2H, *J* = 4.6 Hz, H-3), 4.00 (s, 2H, H-2), 3.71 – 3.60 (m, 12H, -CH₂-), 3.58 (s, 4H, -CH₂-), 2.44 (s, 3H, Ts), 1.47 (s, 10H, *t*-Bu). ¹³C NMR (125 MHz, CDCl₃) δ 169.9 (C-1), 144.9 (Ts), 133.3 (Ts), 129.9 (Ts), 128.1 (Ts), 81.7 (*t*-Bu), 70.90, 70.88, 70.74, 70.67, 69.4, 69.2 (C-2), 68.8, 28.3 (*t*-Bu), 21.8 (Ts). HRMS–ESI (*m/z*): [M + Na]⁺ calcd for C₂₁H₃₄O₉NaS, 485.1821; found, 485.1829.

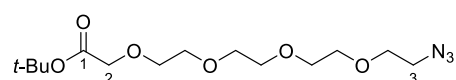
HO-PEG₄-N₃ (43**)**



To a solution of **34** (614 mg, 1.76 mmol) in anhydrous DMF (5 mL) under Ar was added sodium azide (445 mg, 6.78 mmol, 4 equiv). The reaction was heated to 70 °C for 1.5 h. The solvent was removed in vacuo and water was added. The aqueous phase was extracted with CH₂Cl₂ and the combined organic layers were washed with brine. The brine layer was back extracted with

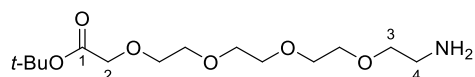
CH₂Cl₂. The combined organic layers were dried over MgSO₄ and concentrated in vacuo to give **43** (364 mg, 1.66 mmol, 94%) as a colourless oil. *R*_f (5% CH₃OH in CHCl₃) 0.42. ¹H NMR (500 MHz, CDCl₃) δ 3.72 (q, 2H, *J* = 4.9 Hz, H-1), 3.69 – 3.65 (m, 10H, -CH₂-), 3.62 – 3.60 (m, H, H-2), 3.39 (t, 2H, *J* = 5.1 Hz, H-3), 2.44 (t, 1H, *J* = 6.0 Hz, -OH). ¹³C NMR (126 MHz, CDCl₃) δ 72.6 (C-2), 70.9 (-CH₂-), 70.83 (-CH₂-), 70.75 (-CH₂-), 70.5 (-CH₂-), 70.2 (-CH₂-), 61.9 (C-1), 50.6 (C-3). HRMS–ESI (*m/z*): [*M* + Na]⁺ calcd for C₁₄H₂₇N₃O₆Na, 356.1798; found, 356.1802.

***t*-BuOOC-CH₂-PEG₄-N₃ (**44**)**



A solution of **43** (77 mg, 0.35 mmol) in THF (6 mL) was added to a suspension of NaH (25 mg, 60% in oil, 0.63 mmol, 1.8 equiv) in THF (4 mL) under Ar at 0 °C. The reaction was stirred at 0 °C for 25 min then cooled to -78 °C. *tert*-Butyl bromo acetate (200 μL, 1.35 mmol, 3.9 equiv) was then added dropwise at -78 °C. The reaction was allowed to warm to rt over 3.5 h. The reaction was quenched with NH₄Cl and the aqueous layer was extracted with EtOAc. The combined organic layers were washed with brine and dried over MgSO₄ before concentration in vacuo yielded **44** (104 mg, 0.312 mmol, 89%) as a colourless oil. *R*_f (EtOAc) 0.27. ¹H NMR (500 MHz, CDCl₃) δ 4.02 (s, 2H, H-2), 3.73 – 3.67 (m, 14H, -CH₂-), 3.39 (t, 2H, *J* = 5.1 Hz, H-3), 1.48 (s, 9H, *t*-Bu). ¹³C NMR (126 MHz, CDCl₃) δ 169.8 (C-1), 81.7 (*t*-Bu), 70.91 (-CH₂-), 70.87 (-CH₂-), 70.83 (-CH₂-), 70.80 (-CH₂-), 70.77 (-CH₂-), 70.2 (-CH₂-), 69.2 (C-2), 50.9 (C-3), 28.3 (*t*-Bu). HRMS–ESI (*m/z*): [*M* + Na]⁺ calcd for C₁₄H₂₇N₃O₆Na, 356.1798; found, 356.1802.

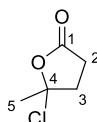
***t*-BuOOC-PEG₄-NH₂ (**45**)**



Staudinger Reduction: PPh₃ (122 mg, 0.465 mmol, 1.4 equiv) was added to a solution of **44** (108 mg, 0.324 mmol) in THF (3 mL) at rt under Ar. The reaction was stirred at rt for 23 h. Water (50 μL) was added and the reaction was stirred exposed to air for a further 5.5 h. Water (12 mL) was then added and the aqueous layer was washed with toluene before concentration

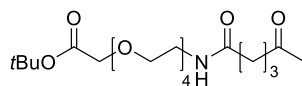
yielded **45** (45 mg, 0.15 mmol, 45%) as a colourless oil. Or Hydrogenolysis: Pd/C (10% mass, 11 mg, 0.010 mmol, 4 mol%) was added to a solution of **44** (82 mg, 0.25 mmol) in EtOH (2 mL). The reaction mixture was evacuated and replaced with an H₂ atmosphere (3x). The reaction was stirred at rt for 2 h. Filtration through Celite and concentration yielded impure **45** (65 mg) as a colourless oil. R_f (65:30:4:0.5 CHCl₃, CH₃OH, water, aq NH₃) 0.82. ¹H NMR (500 MHz, CDCl₃) δ 4.01 (s, 2H, H-2), 3.72 – 3.51 (m, 13H, -CH₂-), 3.52 (t, 2H, J = 5.2 Hz, H-3), 2.87 (t, 2H, J = 5.2 Hz, H-2), 1.98 (br s, 3H, -NH₂), 1.47 (s, 9H, *t*-Bu). ¹³C NMR (126 MHz, CDCl₃) δ 169.8 (C-1), 81.7 (*t*-Bu), 73.3 (C-3), 70.88 (-CH₂-), 70.76 (-CH₂-), 70.74 (-CH₂-), 70.71 (-CH₂-), 70.4 (-CH₂-), 69.2 (C-2), 41.9 (C-4), 28.3 (*t*-Bu). HRMS–ESI (m/z): [M + H]⁺ calcd for C₁₄H₃₀NO₆, 308.2073; found, 308.2074.

γ-Chloro-γ-valerolactone (**53**)



Oxalyl chloride (0.2 mL, 1.7 mmol, 2 equiv) and DMF (2 drops) were added sequentially to a solution of levulinic acid (90 μL, 0.88 mmol) in CH₂Cl₂ (10 mL) under Ar at rt. The reaction was stirred at rt for 3 h before the volatiles were removed under reduced pressure to yield **53** (81 mg, 0.60 mmol, 69%) as a dark red oil. ¹H NMR (500 MHz, CDCl₃) δ 3.00 – 2.92 (m, 1H, H-2_{ax}), 2.76 – 2.71 (m, 1H, H-3_{eq}), 2.64 – 2.59 (m, 1H, H-2_{eq}), 2.45 – 2.38 (m, 1H, H-3_{ax}), 2.06 (t, 3H, H-5). ¹³C NMR (126 MHz, CDCl₃) δ 174.5 (C-1), 104.2 (C-4), 40.1 (C-2), 31.3 (C-5), 28.4 (C-3).

t-Bu ester PEG₄ levulinic amide (**48**)



To a solution of **45** (44 mg, 0.14 mmol) in anhydrous CH₂Cl₂ (2 mL) under Ar at rt was added Et₃N (50 μL, 0.4 mmol). The solution was cooled to 0 °C before a solution of crude γ-chloro-γ-valerolactone (**53**, 0.15 mmol) in CH₂Cl₂ (1.7 mL) was added. After 10 min the reaction was warmed to rt and stirred overnight. The reaction was concentrated in vacuo. THF was added and the suspension filtered (1 μm then 0.2 μm PTFE) to remove excess Et₃NHCl. The filtered

material was purified by flash chromatography on silica gel (0-40% CH₃OH in CH₂Cl₂) to give impure **48** (34 mg) as a yellow oil. R_f (10% CH₃OH in CH₂Cl₂) 0.49. ¹H NMR (500 MHz, CDCl₃) δ *inter alia* 6.52 (br s, 1H), 3.99 (m, 3H), 3.71 – 3.59 (m, 18H), 3.53 (t, *J* = 5.3 Hz, 2H), 3.41 (q, *J* = 5.3 Hz, 2H), 2.76 (t, *J* = 6.7 Hz, 2H), 2.43 (t *J* = 6.7 Hz, 2H), 2.16 (s, 5H), 1.45 (br s, 13H). ¹³C NMR (125 MHz, CDCl₃) δ 207.7, 172.0, 169.7, 132.2, 132.2, 128.7, 128.6, 89.0, 81.7, 70.8, 70.7, 70.6, 70.4, 70.2, 70.0, 69.7, 69.1, 39.5, 39.1, 38.6, 34.7, 30.0, 29.9, 29.6, 28.2, 26.5. HRMS–ESI (*m/z*): [M + Na]⁺ calcd for C₁₉H₃₅NO₈Na, 428.2260; found, 428.2260.

References

1. World Health Organisation *Global vaccine action plan 2011 - 2020*; 2013.
2. Plotkin, S. A., Vaccines: The fourth century. *Clin. Vaccine Immunol.* **2009**, *16* (12), 1709.
3. Plotkin, S. A.; Plotkin, S. L., The development of vaccines: How the past led to the future. *Nat. Rev. Microbiol.* **2011**, *9* (12), 889-893.
4. Minor, P. D., Live attenuated vaccines: Historical successes and current challenges. *Virology* **2015**, *479-480*, 379-392.
5. Reynolds, M. G.; Damon, I. K., Smallpox. In *International Encyclopedia of Public Health (Second Edition)*, Quah, S. R., Ed. Academic Press: Oxford, 2017; pp 524-533.
6. Liu, Z.; Guo, J., NKT-cell glycolipid agonist as adjuvant in synthetic vaccine. *Carbohydr. Res.* **2017**, *452*, 78-90.
7. Plotkin, S., History of vaccination. *Proc. Natl. Acad. Sci. U. S. A.* **2014**, *111* (34), 12283-12287.
8. Ochmann, S.; Roser, M. Smallpox. <https://ourworldindata.org/smallpox> (accessed 26/02/20).
9. Jenner, E., *An inquiry into the causes and effects of the variolae vaccinae*. Low, London, 1798.
10. Hilleman, M. R., Vaccines in historic evolution and perspective: a narrative of vaccine discoveries. *Vaccine* **2000**, *18* (15), 1436-1447.
11. Dunlop, L. R.; Oehlberg, K. A.; Reid, J. J.; Avci, D.; Rosengard, A. M., Variola virus immune evasion proteins. *Microbes and Infection* **2003**, *5* (11), 1049-1056.
12. Riedel, S., Edward Jenner and the history of smallpox and vaccination. *Proc (Bayl Univ Med Cent)* **2005**, *18* (1), 21-25.
13. Army Medical Research Institute for Infectious Diseases (U.S.); Dembek, Z. F., *Medical management of biological casualties handbook*. United States Department of Defense: 2012.
14. Needham, J., Science and civilisation in China. Vol.6. Pt.6, Biology and biological technology. Medicine. Lu, G.-D.; Sivin, N.; ProQuest, Eds. Cambridge : Cambridge University Press: Cambridge, 2000.
15. Boylston, A., The origins of inoculation. *J. R. Soc. Med.* **2012**, *105* (7), 309-313.

16. Kennedy, R. B.; Lane, J. M.; Henderson, D. A.; Poland, G. A., 54 - Smallpox and vaccinia. In *Plotkin's Vaccines (Seventh Edition)*, Plotkin, S. A.; Orenstein, W. A.; Offit, P. A.; Edwards, K. M., Eds. Elsevier: 2018; pp 1001-1030.e12.
17. Gross, C. P.; Sepkowitz, K. A., The myth of the medical breakthrough: Smallpox, vaccination, and Jenner reconsidered. *Int. J. Infect. Dis.* **1998**, 3 (1), 54-60.
18. Ross, D. L., Leicester and the anti-vaccination movement, 1853-1889. **1967**.
19. Fenner, F.; Henderson, D. A.; Arita, I.; Jezek, Z.; Ladnyi, I. D.; World Health, O., Smallpox and its eradication. World Health Organization: Geneva, 1988.
20. Lauring, A. S.; Jones, J. O.; Andino, R., Rationalizing the development of live attenuated virus vaccines. *Nat. Biotechnol.* **2010**, 28 (6), 573-579.
21. Shi, S.; Zhu, H.; Xia, X.; Liang, Z.; Ma, X.; Sun, B., Vaccine adjuvants: Understanding the structure and mechanism of adjuvanticity. *Vaccine* **2019**, 37 (24), 3167-3178.
22. Hajj Hussein, I.; Chams, N.; Chams, S.; El Sayegh, S.; Badran, R.; Raad, M.; Gerges-Geagea, A.; Leone, A.; Jurjus, A., Vaccines through centuries: Major cornerstones of global health. *Front. Public Health* **2015**, 3 (269).
23. Victoria, J. G.; Wang, C.; Jones, M. S.; Jaing, C.; McLoughlin, K.; Gardner, S.; Delwart, E. L., Viral nucleic acids in live-attenuated vaccines: Detection of minority variants and an adventitious virus. *J. Virol.* **2010**, 84 (12), 6033-6040.
24. Badgett, M. R.; Auer, A.; Carmichael, L. E.; Parrish, C. R.; Bull, J. J., Evolutionary dynamics of viral attenuation. *J. Virol.* **2002**, 76 (20), 10524-10529.
25. Lemaire, D.; Barbosa, T.; Rihet, P., Coping with genetic diversity: the contribution of pathogen and human genomics to modern vaccinology. *Braz. J. Med. Biol. Res.* **2012**, 45 (5), 376-385.
26. Moyle, P. M.; Toth, I., Modern subunit vaccines: development, components, and research opportunities. *ChemMedChem* **2013**, 8 (3), 360-376.
27. Ministry of Health New Zealand Immunisation Schedule. <https://www.health.govt.nz/our-work/preventative-health-wellness/immunisation/new-zealand-immunisation-schedule> (accessed 26/02/20).
28. World Health Organisation Vaccine safety basics, e-learning course. <https://vaccine-safety-training.org>.
29. Li, W.; Joshi, M. D.; Singhanian, S.; Ramsey, K. H.; Murthy, A. K., Peptide vaccine: Progress and challenges. *Vaccines (Basel)* **2014**, 2 (3), 515-536.

30. Sasaki, S.; Okuda, K., The use of conventional immunologic adjuvants in DNA vaccine preparations. In *DNA Vaccines: Methods and Protocols*, Lowrie, D. B.; Whalen, R. G., Eds. Humana Press: Totowa, NJ, 2000; pp 241-249.
31. Vogel, F. R., Immunologic adjuvants for modern vaccine formulations. *Ann. N.Y. Acad. Sci.* **1995**, 754 (1), 153-160.
32. Petrovsky, N.; Aguilar, J. C., Vaccine adjuvants: Current state and future trends. *Immunol. Cell Biol.* **2004**, 82 (5), 488-496.
33. Di Pasquale, A.; Preiss, S.; Tavares Da Silva, F.; Garçon, N., Vaccine adjuvants: From 1920 to 2015 and beyond. *Vaccines (Basel)* **2015**, 3 (2), 320-343.
34. Glenny, A. T.; Pope, C. G.; Waddington, H.; Wallace, U., Immunological notes. XVII–XXIV. *J. Pathol. Bacteriol.* **1926**, 29 (1), 31-40.
35. Apostólico, J. d. S.; Lunardelli, V. A. S.; Coirada, F. C.; Boscardin, S. B.; Rosa, D. S., Adjuvants: Classification, modus operandi, and licensing. *J. Immunol. Res.* **2016**, 2016, 1459394-1459394.
36. Coico, R.; Sunshine, G., *Immunology: A Short Course*. Seventh edition ed.; United Kingdom: Wiley-Blackwell: 2015.
37. Lambrecht, B. N.; Kool, M.; Willart, M. A. M.; Hammad, H., Mechanism of action of clinically approved adjuvants. *Curr. Opin. Immunol.* **2009**, 21 (1), 23-29.
38. Ghimire, T. R.; Benson, R. A.; Garside, P.; Brewer, J. M., Alum increases antigen uptake, reduces antigen degradation and sustains antigen presentation by DCs in vitro. *Immunol. Lett.* **2012**, 147 (1), 55-62.
39. Opie, E. L.; Freund, J., An experimental study of protective inoculation with heat killed tubercle bacilli. *J. Exp. Med.* **1937**, 66 (6), 761-788.
40. Billiau, A.; Matthys, P., Modes of action of Freund's adjuvants in experimental models of autoimmune diseases. *J. Leukocyte Biol.* **2001**, 70 (6), 849-860.
41. Chang, J. C. C.; Diveley, J. P.; Savary, J. R.; Jensen, F. C., Adjuvant activity of incomplete Freund's adjuvant. *Adv. Drug Delivery Rev.* **1998**, 32 (3), 173-186.
42. Sarkar, I.; Garg, R.; van Drunen Littel-van den Hurk, S., Selection of adjuvants for vaccines targeting specific pathogens. *Expert Rev. Vaccines* **2019**, 18 (5), 505-521.
43. Hayman, C. M.; Hermans, I. F.; Painter, G. F., Increased efficacy of NKT cell-adjuvanted peptide vaccines through chemical conjugation. In *Coupling and Decoupling of Diverse Molecular Units in Glycosciences*, Witczak, Z. J.; Bielski, R., Eds. Springer International Publishing: Cham, 2018; pp 309-335.

44. Ishikawa, E.; Ishikawa, T.; Morita, Y. S.; Toyonaga, K.; Yamada, H.; Takeuchi, O.; Kinoshita, T.; Akira, S.; Yoshikai, Y.; Yamasaki, S., Direct recognition of the mycobacterial glycolipid, trehalose dimycolate, by C-type lectin Mincle. *J. Exp. Med.* **2009**, *206* (13), 2879.
45. Brandenburg, K.; Garidel, P.; Gutschmann, T., Chapter 38 - Physicochemical properties of microbial glycopolymers. In *Microb. Glycobiol.*, Holst, O.; Brennan, P. J.; Itzstein, M. v.; Moran, A. P., Eds. Academic Press: San Diego, 2010; pp 759-779.
46. Scott, B. A.; Yarchoan, M.; Jaffee, E. M., Prophylactic vaccines for nonviral cancers. *Annu. Rev. of Cancer Biol.* **2018**, *2* (1), 195-211.
47. Tomai, M. A.; Miller, R. L.; Lipson, K. E.; Kieper, W. C.; Zarraga, I. E.; Vasilakos, J. P., Resiquimod and other immune response modifiers as vaccine adjuvants. *Expert Rev. Vaccines* **2007**, *6* (5), 835-847.
48. Hermans, I. F.; Silk, J. D.; Gileadi, U.; Masri, S. H.; Shepherd, D.; Farrand, K. J.; Salio, M.; Cerundolo, V., Dendritic cell function can be modulated through cooperative actions of TLR ligands and invariant NKT cells. *J. Immunol.* **2007**, *178* (5), 2721.
49. Fujii, S.-I.; Shimizu, K.; Smith, C.; Bonifaz, L.; Steinman, R. M., Activation of natural killer T cells by α -galactosylceramide rapidly induces the full maturation of dendritic cells in vivo and thereby acts as an adjuvant for combined CD4 and CD8 T cell immunity to a coadministered protein. *J. Exp. Med.* **2003**, *198* (2), 267-279.
50. Cerundolo, V.; Silk, J. D.; Masri, S. H.; Salio, M., Harnessing invariant NKT cells in vaccination strategies. *Nat. Rev. Immunol.* **2009**, *9* (1), 28-38.
51. Morita, M.; Motoki, K.; Akimoto, K.; Natori, T.; Sakai, T.; Sawa, E.; Yamaji, K.; Koezuka, Y.; Kobayashi, E.; Fukushima, H., Structure-activity relationship of α -galactosylceramides against B16-bearing mice. *J. Med. Chem.* **1995**, *38* (12), 2176-2187.
52. Koch, M.; Stronge, V. S.; Shepherd, D.; Gadola, S. D.; Mathew, B.; Ritter, G.; Fersht, A. R.; Besra, G. S.; Schmidt, R. R.; Jones, E. Y.; Cerundolo, V., The crystal structure of human CD1d with and without α -galactosylceramide. *Nat. Immunol.* **2005**, *6* (8), 819-826.
53. Gonzalez-Aseguinolaza, G.; Van Kaer, L.; Bergmann, C. C.; Wilson, J. M.; Schmieg, J.; Kronenberg, M.; Nakayama, T.; Taniguchi, M.; Koezuka, Y.; Tsuji, M., Natural killer T cell ligand α -galactosylceramide enhances protective immunity induced by malaria vaccines. *J. Exp. Med.* **2002**, *195* (5), 617-624.
54. Huang, Y.; Chen, A.; Li, X.; Chen, Z.; Zhang, W.; Song, Y.; Gurner, D.; Gardiner, D.; Basu, S.; Ho, D. D.; Tsuji, M., Enhancement of HIV DNA vaccine immunogenicity by the NKT cell ligand, α -galactosylceramide. *Vaccine* **2008**, *26* (15), 1807-1816.

55. Galli, G.; Pittoni, P.; Tonti, E.; Malzone, C.; Uematsu, Y.; Tortoli, M.; Maione, D.; Volpini, G.; Finco, O.; Nuti, S.; Tavarini, S.; Dellabona, P.; Rappuoli, R.; Casorati, G.; Abrignani, S., Invariant NKT cells sustain specific B cell responses and memory. *Proc. Natl. Acad. Sci. U. S. A.* **2007**, *104* (10), 3984-3989.
56. Kobayashi, E.; Motoki, K.; Uchida, T.; Fukushima, H.; Koezuka, Y., KRN7000, a novel immunomodulator, and its antitumor activities. *Oncol. Res.* **1995**, *7* (10/11), 529.
57. Zhang, Y.; Springfield, R.; Chen, S.; Li, X.; Feng, X.; Moshirian, R.; Yang, R.; Yuan, W., α -GalCer and iNKT cell-based cancer immunotherapy: Realizing the therapeutic potentials. *Front. Immunol.* **2019**, *10* (1126).
58. Bennett, S. R. M.; Carbone, F. R.; Karamalis, F.; Flavell, R. A.; Miller, J. F. A. P.; Heath, W. R., Help for cytotoxic-T-cell responses is mediated by CD40 signalling. *Nature* **1998**, *393* (6684), 478-480.
59. Schoenberger, S. P.; Toes, R. E. M.; van der Voort, E. I. H.; Offringa, R.; Melief, C. J. M., T-cell help for cytotoxic T lymphocytes is mediated by CD40–CD40L interactions. *Nature* **1998**, *393* (6684), 480-483.
60. Ridge, J. P.; Di Rosa, F.; Matzinger, P., A conditioned dendritic cell can be a temporal bridge between a CD4⁺ T-helper and a T-killer cell. *Nature* **1998**, *393* (6684), 474-478.
61. Liu, H.; Irvine, D. J., Guiding principles in the design of molecular bioconjugates for vaccine applications. *Bioconjugate Chem.* **2015**, *26* (5), 791-801.
62. Moyle, P. M., Biotechnology approaches to produce potent, self-adjuvanting antigen-adjuvant fusion protein subunit vaccines. *Biotechnol. Adv.* **2017**, *35* (3), 375-389.
63. Goldblatt, D., Conjugate vaccines. *Clin. Exp. Immunol.* **2000**, *119* (1), 1-3.
64. Zom, G. G.; Khan, S.; Britten, C. M.; Sommandas, V.; Camps, M. G. M.; Loof, N. M.; Budden, C. F.; Meeuwenoord, N. J.; Filippov, D. V.; van der Marel, G. A.; Overkleeft, H. S.; Melief, C. J. M.; Ossendorp, F., Efficient induction of antitumor immunity by synthetic Toll-like receptor ligand–peptide conjugates. *Cancer Immunology Research* **2014**, *2* (8), 756.
65. Ingale, S.; Wolfert, M. A.; Gaekwad, J.; Buskas, T.; Boons, G.-J., Robust immune responses elicited by a fully synthetic three-component vaccine. *Nat. Chem. Biol.* **2007**, *3* (10), 663-667.
66. Vecchi, S.; Bufali, S.; Uno, T.; Wu, T.; Arcidiacono, L.; Filippini, S.; Rigat, F.; O'Hagan, D., Conjugation of a TLR7 agonist and antigen enhances protection in the *S. pneumoniae* murine infection model. *Eur. J. Pharm. Biopharm.* **2014**, *87* (2), 310-317.

67. Avery, O. T.; Goebel, W. F., Chemo-immunological studies on conjugated carbohydrate-proteins. *J. Exp. Med.* **1929**, 50 (4), 533.
68. Zarei, A. E.; Almeshdar, H. A.; Redwan, E. M., Hib vaccines: Past, present, and future perspectives. *J. Immunol. Res.* **2016**, 2016, 7203587-7203587.
69. Institute of Medicine, *Adverse events associated with childhood vaccines: evidence bearing on causality*. The National Academies Press: Washington, DC, 1994.
70. van der Burg, S. H.; Arens, R.; Ossendorp, F.; van Hall, T.; Melief, C. J. M., Vaccines for established cancer: overcoming the challenges posed by immune evasion. *Nat. Rev. Cancer* **2016**, 16, 219.
71. van der Burg, S. H.; Bijker, M. S.; Welters, M. J. P.; Offringa, R.; Melief, C. J. M., Improved peptide vaccine strategies, creating synthetic artificial infections to maximize immune efficacy. *Adv. Drug Delivery Rev.* **2006**, 58 (8), 916-930.
72. Zom, G. G. P.; Khan, S.; Filippov, D. V.; Ossendorp, F., Chapter 7 - TLR Ligand–peptide conjugate vaccines: Toward clinical application. In *Adv. Immunol.*, Melief, C. J. M., Ed. Academic Press: 2012; Vol. 114, pp 177-201.
73. Kolb, H. C.; Finn, M. G.; Sharpless, K. B., Click chemistry: diverse chemical function from a few good reactions. *Angew. Chem. Int. Ed.* **2001**, 40 (11), 2004-2021.
74. Adamo, R.; Hu, Q.-Y.; Torosantucci, A.; Crotti, S.; Brogioni, G.; Allan, M.; Chiani, P.; Bromuro, C.; Quinn, D.; Tontini, M.; Berti, F., Deciphering the structure–immunogenicity relationship of anti-Candida glycoconjugate vaccines. *Chem. Sci.* **2014**, 5 (11), 4302-4311.
75. Hu, Q.-Y.; Allan, M.; Adamo, R.; Quinn, D.; Zhai, H.; Wu, G.; Clark, K.; Zhou, J.; Ortiz, S.; Wang, B.; Danieli, E.; Crotti, S.; Tontini, M.; Brogioni, G.; Berti, F., Synthesis of a well-defined glycoconjugate vaccine by a tyrosine-selective conjugation strategy. *Chem. Sci.* **2013**, 4 (10), 3827-3832.
76. Stefanetti, G.; Hu, Q.-Y.; Usera, A.; Robinson, Z.; Allan, M.; Singh, A.; Imase, H.; Cobb, J.; Zhai, H.; Quinn, D.; Lei, M.; Saul, A.; Adamo, R.; MacLennan, C. A.; Micoli, F., Sugar–protein connectivity impacts on the immunogenicity of site-selective salmonella O-antigen glycoconjugate vaccines. *Angew. Chem. Int. Ed.* **2015**, 54 (45), 13198-13203.
77. Stefanetti, G.; Saul, A.; MacLennan, C. A.; Micoli, F., Click chemistry applied to the synthesis of Salmonella typhimurium O-antigen glycoconjugate vaccine on solid phase with sugar recycling. *Bioconjugate Chem.* **2015**, 26 (12), 2507-2513.
78. Anderson, R. J.; Li, J.; Kedzierski, L.; Compton, B. J.; Hayman, C. M.; Osmond, T. L.; Tang, C.-w.; Farrand, K. J.; Koay, H.-F.; Almeida, C. F. D. S. S. E.; Holz, L. R.;

Williams, G. M.; Brimble, M. A.; Wang, Z.; Koutsakos, M.; Kedzierska, K.; Godfrey, D. I.; Hermans, I. F.; Turner, S. J.; Painter, G. F., Augmenting Influenza-Specific T Cell Memory Generation with a Natural Killer T Cell-Dependent Glycolipid–Peptide Vaccine. *ACS Chemical Biology* **2017**, *12* (11), 2898-2905.

79. Anderson, R. J.; Compton, B. J.; Tang, C.-w.; Authier-Hall, A.; Hayman, C. M.; Swinerd, G. W.; Kowalczyk, R.; Harris, P.; Brimble, M. A.; Larsen, D. S.; Gasser, O.; Weinkove, R.; Hermans, I. F.; Painter, G. F., NKT cell-dependent glycolipid–peptide vaccines with potent anti-tumour activity. *Chem. Sci.* **2015**, *6* (9), 5120-5127.

80. Anderson, R. J.; Tang, C.-w.; Daniels, N. J.; Compton, B. J.; Hayman, C. M.; Johnston, K. A.; Knight, D. A.; Gasser, O.; Poyntz, H. C.; Ferguson, P. M.; Larsen, D. S.; Ronchese, F.; Painter, G. F.; Hermans, I. F., A self-adjuvanting vaccine induces cytotoxic T lymphocytes that suppress allergy. *Nat. Chem. Biol.* **2014**, *10* (11), 943-949.

81. Compton, B. J.; Farrand, K. J.; Tang, C.-w.; Osmond, T. L.; Speir, M.; Authier-Hall, A.; Wang, J.; Ferguson, P. M.; Chan, S. T. S.; Anderson, R. J.; Cooney, T. R.; Hayman, C. M.; Williams, G. M.; Brimble, M. A.; Brooks, C. R.; Yong, L.-K.; Metelitsa, L. S.; Zajonc, D. M.; Godfrey, D. I.; Gasser, O.; Weinkove, R.; Painter, G. F.; Hermans, I. F., Enhancing T cell responses and tumour immunity by vaccination with peptides conjugated to a weak NKT cell agonist. *Org. Biomol. Chem.* **2019**, *17* (5), 1225-1237.

82. Compton, B. J.; Tang, C.-w.; Johnston, K. A.; Osmond, T. L.; Hayman, C. M.; Larsen, D. S.; Hermans, I. F.; Painter, G. F., Synthesis and activity of 6"-deoxy-6"-thio- α -GalCer and peptide conjugates. *Org. Lett.* **2015**, *17* (24), 5954-5957.

83. Tsuchikama, K.; An, Z., *Antibody-drug conjugates: recent advances in conjugation and linker chemistries*. 2016; Vol. 9.

84. Lu, J.; Jiang, F.; Lu, A.; Zhang, G., Linkers having a crucial role in antibody-drug conjugates. *Int. J. Mol. Sci.* **2016**, *17* (4), 561-561.

85. McCombs, J. R.; Owen, S. C., Antibody drug conjugates: design and selection of linker, payload and conjugation chemistry. *AAPS J.* **2015**, *17* (2), 339-351.

86. Liang, L.; Astruc, D., The copper(I)-catalyzed alkyne-azide cycloaddition (CuAAC) "click" reaction and its applications. An overview. *Coord. Chem. Rev.* **2011**, *255* (23), 2933-2945.

87. Rostovtsev, V. V.; Green, L. G.; Fokin, V. V.; Sharpless, K. B., A stepwise Huisgen cycloaddition process: Copper(I)-catalyzed regioselective "ligation" of azides and terminal alkynes. *Angew. Chem. Int. Ed.* **2002**, *41* (14), 2596-2599.

88. Tornøe, C. W.; Christensen, C.; Meldal, M., Peptidotriazoles on solid phase: [1,2,3]-Triazoles by regiospecific copper(I)-catalyzed 1,3-dipolar cycloadditions of terminal alkynes to azides. *J. Org. Chem.* **2002**, *67* (9), 3057-3064.
89. Li, S.; Cai, H.; He, J.; Chen, H.; Lam, S.; Cai, T.; Zhu, Z.; Bark, S. J.; Cai, C., Extent of the oxidative side reactions to peptides and proteins during the CuAAC reaction. *Bioconjugate Chem.* **2016**, *27* (10), 2315-2322.
90. Agard, N. J.; Prescher, J. A.; Bertozzi, C. R., A strain-promoted [3 + 2] azide–alkyne cycloaddition for covalent modification of biomolecules in living systems. *J. Am. Chem. Soc.* **2004**, *126* (46), 15046-15047.
91. Mbua, N. E.; Guo, J.; Wolfert, M. A.; Steet, R.; Boons, G.-J., Strain-promoted alkyne-azide cycloadditions (SPAAC) reveal new features of glycoconjugate biosynthesis. *Chembiochem* **2011**, *12* (12), 1912-1921.
92. Gang, L.; Eric, A. W.; Jia, Z., Applications of bioorthogonal chemistry in tumor-targeted drug discovery. *Curr. Top. Med. Chem.* **2019**, *19* (11), 892-897.
93. Pickens, C. J.; Johnson, S. N.; Pressnall, M. M.; Leon, M. A.; Berkland, C. J., Practical considerations, challenges, and limitations of bioconjugation via azide–alkyne cycloaddition. *Bioconjugate Chem.* **2018**, *29* (3), 686-701.
94. Ulrich, S.; Boturyn, D.; Marra, A.; Renaudet, O.; Dumy, P., Oxime ligation: A chemoselective click-type reaction for accessing multifunctional biomolecular constructs. *Chem.: Eur. J.* **2014**, *20* (1), 34-41.
95. Buré, C.; Lelièvre, D.; Delmas, A., Identification of by-products from an orthogonal peptide ligation by oxime bonds using mass spectrometry and tandem mass spectrometry. *Rapid Commun. Mass Spectrom.* **2000**, *14* (23), 2158-2164.
96. Girardi, E.; Zajonc, D. M., Molecular basis of lipid antigen presentation by CD1d and recognition by natural killer T cells. *Immunol. Rev.* **2012**, *250* (1), 167-179.
97. Li, X.; Fujio, M.; Imamura, M.; Wu, D.; Vasan, S.; Wong, C.-H.; Ho, D. D.; Tsuji, M., Design of a potent CD1d-binding NKT cell ligand as a vaccine adjuvant. *Proc. Natl. Acad. Sci. U. S. A.* **2010**, *107* (29), 13010-13015.
98. Kamada, N.; Iijima, H.; Kimura, K.; Harada, M.; Shimizu, E.; Motohashi, S.-i.; Kawano, T.; Shinkai, H.; Nakayama, T.; Sakai, T.; Brossay, L.; Kronenberg, M.; Taniguchi, M., Crucial amino acid residues of mouse CD1d for glycolipid ligand presentation to V α 14 NKT cells. *Int. Immunol.* **2001**, *13* (7), 853-861.

99. Prigozy, T. I.; Naidenko, O.; Qasba, P.; Elewaut, D.; Brossay, L.; Khurana, A.; Natori, T.; Koezuka, Y.; Kulkarni, A.; Kronenberg, M., Glycolipid antigen processing for presentation by CD1d molecules. *Science* **2001**, *291* (5504), 664.
100. Borg, N. A.; Wun, K. S.; Kjer-Nielsen, L.; Wilce, M. C. J.; Pellicci, D. G.; Koh, R.; Besra, G. S.; Bharadwaj, M.; Godfrey, D. I.; McCluskey, J.; Rossjohn, J., CD1d-lipid-antigen recognition by the semi-invariant NKT T-cell receptor. *Nature (London, U. K.)* **2007**, *448* (7149), 44-49.
101. Pauwels, N.; Aspeslagh, S.; Vanhoenacker, G.; Sandra, K.; Yu, E. D.; Zajonc, D. M.; Elewaut, D.; Linclau, B.; Van Calenbergh, S., Divergent synthetic approach to 6''-modified α -GalCer analogues. *Org. Biomol. Chem.* **2011**, *9* (24), 8413-8421.
102. Bargh, J. D.; Isidro-Llobet, A.; Parker, J. S.; Spring, D. R., Cleavable linkers in antibody–drug conjugates. *Chem. Soc. Rev.* **2019**, *48* (16), 4361-4374.
103. Sutherland, M. S. K.; Sanderson, R. J.; Gordon, K. A.; Andreyka, J.; Cervený, C. G.; Yu, C.; Lewis, T. S.; Meyer, D. L.; Zabinski, R. F.; Doronina, S. O.; Senter, P. D.; Law, C.-L.; Wahl, A. F., Lysosomal trafficking and cysteine protease metabolism confer target-specific cytotoxicity by peptide-linked anti-CD30-auristatin conjugates. *J. Biol. Chem.* **2006**, *281* (15), 10540-10547.
104. Dubowchik, G. M.; Firestone, R. A.; Padilla, L.; Willner, D.; Hofstead, S. J.; Mosure, K.; Knipe, J. O.; Lasch, S. J.; Trail, P. A., Cathepsin B-labile dipeptide linkers for lysosomal release of doxorubicin from internalizing immunoconjugates: Model studies of enzymatic drug release and antigen-specific in vitro anticancer activity. *Bioconjugate Chem.* **2002**, *13* (4), 855-869.
105. Doronina, S. O.; Mendelsohn, B. A.; Bovee, T. D.; Cervený, C. G.; Alley, S. C.; Meyer, D. L.; Oflazoglu, E.; Toki, B. E.; Sanderson, R. J.; Zabinski, R. F.; Wahl, A. F.; Senter, P. D., Enhanced activity of monomethylauristatin F through monoclonal antibody delivery: effects of linker technology on efficacy and toxicity. *Bioconjugate Chem.* **2006**, *17* (1), 114-124.
106. Dubowchik, G. M.; Firestone, R. A., Cathepsin B-sensitive dipeptide prodrugs. 1. A model study of structural requirements for efficient release of doxorubicin. *Bioorg. Med. Chem. Lett.* **1998**, *8* (23), 3341-3346.
107. Guha, S.; Rajani, M.; Padh, H., Identification and characterization of lipids from endosomes purified by electromagnetic chromatography. *Indian J. Biochem. Biophys.* **2007**, *44* (6), 443-449.

108. Warnecke, A., Site-specific prodrug activation and the concept of self-immolation. *Drug Delivery Oncol.* **2011**.
109. Acar, H.; Samaeekia, R.; Schnorenberg, M. R.; Sasmal, D. K.; Huang, J.; Tirrell, M. V.; LaBelle, J. L., Cathepsin-mediated cleavage of peptides from peptide amphiphiles leads to enhanced intracellular peptide accumulation. *Bioconjugate Chem.* **2017**, 28 (9), 2316-2326.
110. Toki, B. E.; Cervený, C. G.; Wahl, A. F.; Senter, P. D., Protease-mediated fragmentation of *p*-amidobenzyl ethers: A new strategy for the activation of anticancer prodrugs. *J. Org. Chem.* **2002**, 67 (6), 1866-1872.
111. Walther, R.; Rautio, J.; Zelikin, A. N., Prodrugs in medicinal chemistry and enzyme prodrug therapies. *Adv. Drug Delivery Rev.* **2017**, 118, 65-77.
112. Alouane, A.; Labruère, R.; Le Saux, T.; Schmidt, F.; Jullien, L., Self-immolative spacers: kinetic aspects, structure–property relationships, and applications. *Angew. Chem. Int. Ed.* **2015**, 54 (26), 7492-7509.
113. Carl, P. L.; Chakravarty, P. K.; Katzenellenbogen, J. A., A novel connector linkage applicable in prodrug design. *J. Med. Chem.* **1981**, 24 (5), 479-480.
114. Arumugam, S.; Popik, V. V., Dual reactivity of hydroxy- and methoxy- substituted *o*-quinone methides in aqueous solutions: hydration versus tautomerization. *J. Org. Chem.* **2010**, 75 (21), 7338-7346.
115. Alley, S. C.; Okeley, N. M.; Senter, P. D., Antibody–drug conjugates: targeted drug delivery for cancer. *Curr. Opin. Chem. Biol.* **2010**, 14 (4), 529-537.
116. Younes, A.; Bartlett, N. L.; Leonard, J. P.; Kennedy, D. A.; Lynch, C. M.; Sievers, E. L.; Forero-Torres, A., Brentuximab vedotin (SGN-35) for relapsed CD30-positive lymphomas. *N. Engl. J. Med.* **2010**, 363 (19), 1812-1821.
117. Meyer, Y.; Richard, J.-A.; Delest, B.; Noack, P.; Renard, P.-Y.; Romieu, A., A comparative study of the self-immolation of para-aminobenzylalcohol and hemithioaminal-based linkers in the context of protease-sensitive fluorogenic probes. *Org. Biomol. Chem.* **2010**, 8 (8), 1777-1780.
118. Nolting, B., Linker technologies for antibody–drug conjugates. In *Antibody-Drug Conjugates*, Ducry, L., Ed. Humana Press: Totowa, NJ, 2013; pp 71-100.
119. Labruere, R.; Alouane, A.; Le Saux, T.; Aujard, I.; Pelupessy, P.; Gautier, A.; Dubruille, S.; Schmidt, F.; Jullien, L., "Self-immolative" spacer for uncaging with fluorescence reporting. *Angew. Chem., Int. Ed.* **2012**, 51 (37), 9344-9347, S9344/1-S9344/29.

120. Avital-Shmilovici, M.; Shabat, D., Self-immolative dendrimers: A distinctive approach to molecular amplification. *Soft Matter* **2010**, *6* (6), 1073-1080.
121. Binauld, S.; Stenzel, M. H., Acid-degradable polymers for drug delivery: a decade of innovation. *Chem. Commun.* **2013**, *49* (21), 2082-2102.
122. Blencowe, C. A.; Russell, A. T.; Greco, F.; Hayes, W.; Thornthwaite, D. W., Self-immolative linkers in polymeric delivery systems. *Polym. Chem.* **2011**, *2* (4), 773-790.
123. Chen, E. K. Y.; McBride, R. A.; Gillies, E. R., Self-immolative polymers containing rapidly cyclizing spacers: Toward rapid depolymerization rates. *Macromolecules (Washington, DC, U. S.)* **2012**, *45* (18), 7364-7374.
124. de, G. F. M.; Loos, W. J.; Koekkoek, R.; van, B. L. W.; Busscher, G. F.; Seelen, A. E.; Albrecht, C.; de, B. P.; Scheeren, H. W., Elongated multiple electronic cascade and cyclization spacer systems in activatable anticancer prodrugs for enhanced drug release. *J. Org. Chem.* **2001**, *66* (26), 8815-30.
125. Elgersma, R. C.; Huijbregts, T.; Coumans, R. G. E. Non-linear self-immolative linkers for reducing hydrophobicity of antibody-drug conjugates for cancer therapy. WO2018069375, 2018.
126. Krüger, H. R.; Nagel, G.; Wedepohl, S.; Calderón, M., Dendritic polymer imaging systems for the evaluation of conjugate uptake and cleavage. *Nanoscale* **2015**, *7* (9), 3838-3844.
127. Lee, H. Y.; Jiang, X.; Lee, D., Kinetics of self-immolation: Faster signal relay over a longer linear distance? *Org. Lett.* **2009**, *11* (10), 2065-2068.
128. McBride, R. A.; Gillies, E. R., Kinetics of self-immolative degradation in a linear polymeric system: Demonstrating the effect of chain length. *Macromolecules (Washington, DC, U. S.)* **2013**, *46* (13), 5157-5166.
129. Roth, M. E.; Green, O.; Gnaim, S.; Shabat, D., Dendritic, oligomeric, and polymeric self-immolative molecular amplification. *Chem. Rev.* **2016**, *116* (3), 1309-1352.
130. Whang, C.-H.; Kim, K. S.; Bae, J.; Chen, J.; Jun, H.-W.; Jo, S., Novel biodegradable polymer with redox-triggered backbone cleavage through sequential 1,6-elimination and 1,5-cyclization reactions. *Macromol. Rapid Commun.* **2017**, *38* (19), 1700395.
131. Fernandez-Ruiz, D.; Ng, Wei Y.; Holz, L. E.; Ma, Joel Z.; Zaid, A.; Wong, Yik C.; Lau, Lei S.; Mollard, V.; Cozijnsen, A.; Collins, N.; Li, J.; Davey, Gayle M.; Kato, Y.; Devi, S.; Skandari, R.; Pauley, M.; Manton, Jonathan H.; Godfrey, Dale I.; Braun, A.; Tay, Szun S.; Tan, Peck S.; Bowen, David G.; Koch-Nolte, F.; Rissiek, B.; Carbone, Francis R.; Crabb, Brendan S.; Lahoud, M.; Cockburn, Ian A.; Mueller, Scott N.; Bertolino, P.;

- McFadden, Geoffrey I.; Caminschi, I.; Heath, William R., Liver-resident memory CD8⁺ T cells form a front-line defense against malaria liver-stage infection. *Immunity* **2016**, *45* (4), 889-902.
132. Dirksen, A.; Dawson, P. E., Rapid oxime and hydrazone ligations with aromatic aldehydes for biomolecular labeling. *Bioconjugate Chem.* **2008**, *19* (12), 2543-2548.
133. Dirksen, A.; Dirksen, S.; Hackeng, T. M.; Dawson, P. E., Nucleophilic catalysis of hydrazone formation and transimination: Implications for dynamic covalent chemistry. *J. Am. Chem. Soc.* **2006**, *128* (49), 15602-15603.
134. Dirksen, A.; Hackeng, T. M.; Dawson, P. E., Nucleophilic catalysis of oxime ligation. *Angew. Chem. Int. Ed.* **2006**, *45* (45), 7581-7584.
135. Lange, J.; Anderson, R. J.; Marshall, A. J.; Chan, S. T. S.; Bilbrough, T. S.; Gasser, O.; Gonzalez-Lopez, C.; Salio, M.; Cerundolo, V.; Hermans, I. F.; Painter, G. F., The chemical synthesis, stability, and activity of MAIT cell prodrug agonists that access MR1 in recycling endosomes. *ACS Chemical Biology* **2020**.
136. Bryden, F.; Martin, C.; Letast, S.; Lles, E.; Viéitez-Villemin, I.; Rousseau, A.; Colas, C.; Brachet-Botineau, M.; Allard-Vannier, E.; Larbouret, C.; Viaud-Massuard, M.-C.; Joubert, N., Impact of cathepsin B-sensitive triggers and hydrophilic linkers on in vitro efficacy of novel site-specific antibody–drug conjugates. *Org. Biomol. Chem.* **2018**, *16* (11), 1882-1889.
137. Dal Corso, A.; Cazzamalli, S.; Gébleux, R.; Mattarella, M.; Neri, D., Protease-cleavable linkers modulate the anticancer activity of noninternalizing antibody–drug conjugates. *Bioconjugate Chem.* **2017**, *28* (7), 1826-1833.
138. Komarnitsky, P. B.; Lee, H.-J.; Shah, M.; Wong, S.; Gauthier, S.; Dziubinski, J.; Osbaugh, S.; Zhang, F., A phase III study of rovalpituzumab tesirine maintenance therapy following first-line platinum-based chemotherapy in patients with extensive disease small cell lung cancer (ED SCLC). *J. Clin. Oncol.* **2017**, *35* (15_suppl), TPS8583-TPS8583.
139. Cazzamalli, S.; Corso, A. D.; Neri, D., Linker stability influences the anti-tumor activity of acetazolamide-drug conjugates for the therapy of renal cell carcinoma. *J. Control Release* **2017**, *246*, 39-45.
140. Mondal, D.; Ford, J.; Pinney, K. G., Improved methodology for the synthesis of a cathepsin B cleavable dipeptide linker, widely used in antibody-drug conjugate research. *Tetrahedron Lett.* **2018**, *59* (40), 3594-3599.
141. Yang, F.; Zhang, Q.; Snyder, L. B.; Gangwar, S.; Boger, D. L. Preparation of seco-cyclopropapyrroloindole compounds, their conjugates with anti-mesothelin antibodies, and their use as anti-cancer agents. WO2018035391, 2018.

142. Benatuil, L.; Bruncko, M.; Doherty, G.; Frey, R. R.; Judd, A. S.; Li, Y.; McCluskey, A.; Phillips, A. C.; Phillips, D. C.; Song, X.; Seagal, J.; Souers, A. J.; Sullivan, G. M.; Tao, Z.-F. Anti-CD98 antibodies and antibody drug conjugates. WO2017214456, 2017.
143. Cremin, D. J.; Hegarty, A. F.; Begley, M. J., Mechanism of reaction of 2-ethoxy-1-ethoxycarbonyl-1,2-dihydroquinoline (EEDQ) with nucleophiles and its crystal structure. *J. Chem. Soc., Perkin Trans. 2* **1980**, (2), 412-420.
144. Lee, A.; Farrand, K. J.; Dickgreber, N.; Hayman, C. M.; Jürs, S.; Hermans, I. F.; Painter, G. F., Novel synthesis of α -galactosyl-ceramides and confirmation of their powerful NKT cell agonist activity. *Carbohydr. Res.* **2006**, *341* (17), 2785-2798.
145. Ben-Ishai, D.; Berger, A., Cleavage of N-carbobenzoxy groups by dry hydrogen bromide and hydrogen chloride. *J. Org. Chem.* **1952**, *17* (12), 1564-1570.
146. Armstrong, V. C.; Farlow, D. W.; Moodie, R. B., Hydrolysis of amides, esters, and related compounds in acid solution. I. Amides, carbamates, and ureas. *J. Chem. Soc., B* **1968**, (10), 1099.
147. Adams, P.; Baron, F. A., Esters of carbamic acid. *Chem. Rev.* **1965**, *65* (5), 567-602.
148. Jadhav, S. V.; Bandyopadhyay, A.; Benke, S. N.; Mali, S. M.; Gopi, H. N., A facile synthesis and crystallographic analysis of N-protected β -amino alcohols and short peptaibols. *Org. Biomol. Chem.* **2011**, *9* (11), 4182-4187.
149. Widdison, W. C.; Ponte, J. F.; Coccia, J. A.; Lanieri, L.; Setiady, Y.; Dong, L.; Skaletskaya, A.; Hong, E. E.; Wu, R.; Qiu, Q.; Singh, R.; Salomon, P.; Fishkin, N.; Harris, L.; Maloney, E. K.; Kovtun, Y.; Veale, K.; Wilhelm, S. D.; Audette, C. A.; Costopolus, J. A.; Chari, R. V. J., Development of anilino-maytansinoid ADCs that efficiently release cytotoxic metabolites in cancer cells and induce high levels of bystander killing. *Bioconjugate Chem.* **2015**, *26* (11), 2261-2278.
150. Dearden, J. C.; Bresnen, G. M., The measurement of partition coefficients. *Quant. Struct.-Act. Relat.* **1988**, *7* (3), 133-144.
151. Taka'cs-Nova'k, K.; Avdeel, A., Interlaboratory study of logP determination by shake-flask and potentiometric methods. *J. Pharm. Biomed. Anal.* **1996**, *14* (11), 1405-1413.
152. Donovan, S. F.; Pescatore, M. C., Method for measuring the logarithm of the octanol–water partition coefficient by using short octadecyl–poly(vinyl alcohol) high-performance liquid chromatography columns. *J. Chromatogr. A* **2002**, *952* (1), 47-61.

153. Liang, C.; Qiao, J.-q.; Lian, H.-z., Determination of reversed-phase high performance liquid chromatography based octanol-water partition coefficients for neutral and ionizable compounds: Methodology evaluation. *J. Chromatogr. A* **2017**, *1528*, 25-34.
154. Nishimura, I.; Hirano, A.; Yamashita, T.; Fukami, T., Improvement of the high-speed logD assay using an injection marker for the water plug aspiration/injection method. *J. Chromatogr. A* **2009**, *1216* (15), 2984-2988.
155. Székely, G.; Schaepertoens, M.; Gaffney, P. R. J.; Livingston, A. G., Iterative synthesis of monodisperse PEG homostars and linear heterobifunctional PEG. *Polym. Chem.* **2014**, *5* (3), 694-697.
156. Loiseau, F. A.; Hii, K. K.; Hill, A. M., Multigram synthesis of well-defined extended bifunctional polyethylene glycol (PEG) chains. *J. Org. Chem.* **2004**, *69* (3), 639-647.
157. Székely, G.; Schaepertoens, M.; Gaffney, P. R. J.; Livingston, A. G., Beyond PEG2000: Synthesis and functionalisation of monodisperse PEGylated homostars and clickable bivalent polyethyleneglycols. *Chem.: Eur. J.* **2014**, *20* (32), 10038-10051.
158. French, A. C.; Thompson, A. L.; Davis, B. G., High-purity discrete PEG-oligomer crystals allow structural insight. *Angew. Chem. Int. Ed.* **2009**, *48* (7), 1248-1252.
159. Yu, P.; Li, X.; Li, X.; Lu, X.; Ma, G.; Su, Z., Preparative purification of polyethylene glycol derivatives with polystyrene-divinylbenzene beads as chromatographic packing. *Bioorg. Med. Chem. Lett.* **2007**, *17* (20), 5605-5609.
160. Rissler, K., Improved separation of polyethylene glycols widely differing in molecular weight range by reversed-phase high performance liquid chromatography and evaporative light scattering detection. *Chromatographia* **1999**, *49* (11), 615-620.
161. Kinbara, K., Monodisperse engineered PEGs for bio-related applications. *Polym. J.* **2018**, *50* (8), 689-697.
162. Wawro, A. M.; Muraoka, T.; Kato, M.; Kinbara, K., Multigram chromatography-free synthesis of octa(ethylene glycol) *p*-toluenesulfonate. *Org. Chem. Front.* **2016**, *3* (11), 1524-1534.
163. Wawro, A. M.; Muraoka, T.; Kinbara, K., Chromatography-free synthesis of monodisperse oligo(ethylene glycol) mono-*p*-toluenesulfonates and quantitative analysis of oligomer purity. *Polym. Chem.* **2016**, *7* (13), 2389-2394.
164. Dickschat, J. S.; Wickel, S.; Bolten, C. J.; Nawrath, T.; Schulz, S.; Wittmann, C., Pyrazine biosynthesis in *Corynebacterium glutamicum*. *Eur. J. Org. Chem.* **2010**, *2010* (14), 2687-2695.

165. Seebach, D.; Jones, N. R.; Corey, E. J., New synthetic route to cyclic mono- and diketone derivatives via bisthiocarbanions. *J. Org. Chem.* **1968**, *33* (1), 300-305.
166. Seebach, D., Methods and possibilities of nucleophilic acylation. *Angew. Chem., Int. Ed. Engl.* **1969**, *8* (9), 639-649.
167. O'Driscoll, L. J.; Welsh, D. J.; Bailey, S. W. D.; Visontai, D.; Frampton, H.; Bryce, M. R.; Lambert, C. J., Reversible thermal switching of aqueous dispersibility of multiwalled carbon nanotubes. *Chem.: Eur. J.* **2015**, *21* (10), 3891-3894.
168. Watanabe, H.; Watanabe, H.; Bando, M.; Kido, M.; Kitahara, T., An efficient synthesis of pironetins employing a useful chiral building block, (1S,5S,6R)-5-hydroxybicyclo[4.1.0]heptan-2-one. *Tetrahedron* **1999**, *55* (32), 9755-9776.
169. Ribeiro, D. S.; Rittner, R., The conformational energies of 2-methyl- and 4-methyl-1,3-dithiane. The breakdown of 1,3-syn diaxial repulsion hypothesis. *J. Mol. Struct.* **2003**, *657* (1), 85-92.
170. Burghardt, T. E., Developments in the deprotection of thioacetals. *J. Sulfur Chem.* **2005**, *26* (4-5), 411-427.
171. Greene, T. W., *Protective groups in organic synthesis*. 3rd ed. / Theodora W. Greene and Peter G.M. Wuts. ed.; Wiley: New York, 1999.
172. Banerjee, A. K.; Laya, M. S., Reagents for the preparation and cleavage of 1,3-dithiolanes. *Russ. Chem. Rev.* **2000**, *69* (11), 947-955.
173. Keller, V. A.; Martinelli, J. R.; Strieter, E. R.; Burke, S. D., Dioxolane-to-bridged acetal-to-spiroketal via ring-closing metathesis and rearrangement: A novel route to 1,7-dioxaspiro[5.5]undecanes. *Org. Lett.* **2002**, *4* (3), 467-470.
174. Stork, G.; Zhao, K., A simple method of dethioacetalization. *Tetrahedron Lett.* **1989**, *30* (3), 287-290.
175. Ganguly, N. C.; Barik, S. K., A facile mild deprotection protocol for 1,3-dithianes and 1,3-dithiolanes with 30% hydrogen peroxide and iodine catalyst in aqueous micellar system. *Synthesis* **2009**, (8), 1393-1399.
176. Hurski, A.; Zhabinskii, V.; Khripach, V., A short convergent synthesis of the side chains of brassinolide, cathasterone, and cryptolide. *Tetrahedron Lett.* **2013**, *54* (6), 584-586.
177. Hartmann, O.; Kalesse, M., The total synthesis of (-)-aurafuron A. *Org. Lett.* **2012**, *14* (12), 3064-3067.
178. Smith, A. B., 3rd; Foley, M. A.; Dong, S.; Orbin, A., (+)-Rimocidin synthetic studies: construction of the C(1-27) aglycone skeleton. *J. Org. Chem.* **2009**, *74* (16), 5987-6001.

179. Shi, X.-X.; Wu, Q.-Q., Deblocking of dithianes with diacetoxyiodobenzene. *Synth. Commun.* **2000**, *30* (22), 4081-4086.
180. Henrot, M.; Jean, A.; Peixoto, P. A.; Maddaluno, J.; De Paolis, M., Flexible total synthesis of (±)-aureothin, a potent antiproliferative agent. *J. Org. Chem.* **2016**, *81* (12), 5190-5201.
181. Nicolaou, K. C.; Li, Y.; Sugita, K.; Monenschein, H.; Guntupalli, P.; Mitchell, H. J.; Fylaktakidou, K. C.; Vourloumis, D.; Giannakakou, P.; O'Brate, A., Total synthesis of apoptolidin: Completion of the synthesis and analogue synthesis and evaluation. *J. Am. Chem. Soc.* **2003**, *125* (50), 15443-15454.
182. Viktor, V. Z., Benziiodoxole-based hypervalent iodine reagents in organic synthesis. *Curr. Org. Synth.* **2005**, *2* (1), 121-145.
183. Tohma, H.; Kita, Y., Hypervalent iodine reagents for the oxidation of alcohols and their application to complex molecule synthesis. *Adv. Synth. Catal.* **2004**, *346* (2-3), 111-124.
184. Langille, N. F.; Dakin, L. A.; Panek, J. S., A mild, chemoselective protocol for the removal of thioketals and thioacetals mediated by Dess–Martin periodinane. *Org. Lett.* **2003**, *5* (4), 575-578.
185. Fetizon, M.; Jurion, M., Aldehydes and ketones from thioacetals. *J. Chem. Soc., Chem. Commun.* **1972**, (7), 382-383.
186. Chang, H.-L. W., Novel cleavage of ethylene thioketals to carbonyl compounds with methyl iodide. *Tetrahedron Lett.* **1972**, (19), 1989.
187. Le Sann, C.; Muñoz, D. M.; Saunders, N.; Simpson, T. J.; Smith, D. I.; Soulas, F.; Watts, P.; Willis, C. L., Assembly intermediates in polyketide biosynthesis: enantioselective syntheses of β-hydroxycarbonyl compounds. *Org. Biomol. Chem.* **2005**, *3* (9), 1719-1728.
188. Trost, B. M.; Preckel, M.; Leichter, L. M., New synthetic reactions. Geminal alkylation via α-trimethylenedithiocyclobutanones. *J. Am. Chem. Soc.* **1975**, *97* (8), 2224-2232.
189. Cheung, K.-M.; Coles, S. J.; Hursthouse, M. B.; Johnson, N. I.; Shoolingin – Jordan, P. M., The determination of the absolute configurations of diastereomers of (S)-camphanoyl 3-hydroxy-5-oxohexanoic acid derivatives by X-ray crystallography. *Angew. Chem. Int. Ed.* **2002**, *41* (7), 1198-1202.
190. Acosta, J. A. M.; Muddala, R.; Barbosa, L. C. A.; Boukouvalas, J., Total synthesis of the antitumor antibiotic basidalin. *J. Org. Chem.* **2016**, *81* (15), 6883-6886.
191. Brunner, K.; Harder, J.; Halbach, T.; Willibald, J.; Spada, F.; Gnerlich, F.; Sparrer, K.; Beil, A.; Möckl, L.; Bräuchle, C.; Conzelmann, K.-K.; Carell, T., Cell-penetrating and

- neurotargeting dendritic siRNA nanostructures. *Angew. Chem. Int. Ed.* **2014**, *54* (6), 1946-1949.
192. Wan, Z.; Li, Y.; Bo, S.; Gao, M.; Wang, X.; Zeng, K.; Tao, X.; Li, X.; Yang, Z.; Jiang, Z.-X., Amide bond-containing monodisperse polyethylene glycols beyond 10 000 Da. *Org. Biomol. Chem.* **2016**, *14* (33), 7912-7919.
193. Lu, G.; Lam, S.; Burgess, K., An iterative route to “decorated” ethylene glycol-based linkers. *Chem. Commun.* **2006**, (15), 1652-1654.
194. Zhu, Z.; Wang, J.; Lopez, A. I.; Yu, F.; Huang, Y.; Kumar, A.; Li, S.; Zhang, L.; Cai, C., Surfaces presenting α -phenyl mannoside derivatives enable formation of stable, high coverage, non-pathogenic *Escherichia coli* biofilms against pathogen colonization. *Biomater. Sci.* **2015**, *3* (6), 842-851.
195. Sato, R.; Kozuka, J.; Ueda, M.; Mishima, R.; Kumagai, Y.; Yoshimura, A.; Minoshima, M.; Mizukami, S.; Kikuchi, K., Intracellular protein-labeling probes for multicolor single-molecule imaging of immune receptor-adaptor molecular dynamics. *J. Am. Chem. Soc.* **2017**, *139* (48), 17397-17404.
196. Abronina, P. I.; Zinin, A. I.; Orlova, A. V.; Sedinkin, S. L.; Kononov, L. O., An easy access to asymmetrically substituted oligoethylene glycols from 18-crown-6. *Tetrahedron Lett.* **2013**, *54* (34), 4533-4535.
197. Paul, S.; Schmidt, R. R., A new base mediated method for the cleavage of tert-butyl esters. *Synlett* **2002**, *2002* (07), 1107-1108.
198. Filali, E.; Lloyd-Jones, G. C.; Sale, D. A., Cleavage of tert-butyl benzoates with NaH in DMF: Comments on the -mechanism and a simple and safe alternative procedure. *Synlett* **2009**, *2009* (02), 205-208.
199. Van, B. C. A. A.; Buijsman, R. C.; De, K. M.; Meuleman, D. G. Preparation of oligosaccharide uronates as antithrombotic agents. EP1574516, 2005.
200. Sengupta, S.; Roy, M.; Gupta, N.; Hossain, S. S. Preparation of targeted drug delivery conjugates through affinity based linkers. WO2015148126, 2015.
201. Amantini, D.; Fringuelli, F.; Pizzo, F.; Vaccaro, L., Selected methods for the reduction of the azido group. *Org. Prep. Proced. Int.* **2002**, *34* (2), 109, 111.
202. Mattarei, A.; Biasutto, L.; Zoratti, M.; Paradisi, C.; Marotta, E.; Garbisa, S.; Azzolini, M.; Bradaschia, A.; Carraro, M.; Sassi, N. Preparation of new carbamate derivatives of resveratrol. EP2774915, 2014.

203. Yue, X.; Feng, Y.; Yu, Y. B., Synthesis and characterization of fluorinated conjugates of albumin. *J. Fluorine Chem.* **2013**, *152*, 173-181.
204. Svedhem, S.; Hollander, C.-Å.; Shi, J.; Konradsson, P.; Liedberg, B.; Svensson, S. C. T., Synthesis of a series of oligo(ethylene glycol)-terminated alkanethiol amides designed to address structure and stability of biosensing interfaces. *J. Org. Chem.* **2001**, *66* (13), 4494-4503.
205. Bhosale, S.; Bhosale, S.; Wang, T.; Kopaczynska, M.; Fuhrhop, J.-H., Hydrophobic and hydrophilic yocrowells as receptors in water. *J. Am. Chem. Soc.* **2006**, *128* (7), 2156-2157.
206. Parker, M. H.; Yap, M. C. H.; Eckelbarger, J. D.; Buysse, A. M.; Babcock, J. M.; Hunter, R.; Adelfinskaya, Y.; Samaritoni, J. G.; Garizi, N.; Trullinger, T. K. Preparation of 1,3,4-thiadiazole derivatives as pesticides. US20120053146, 2012.
207. Choi, M. G.; Hwang, J.; Moon, J. O.; Sung, J.; Chang, S.-K., Hydrazine-selective chromogenic and fluorogenic probe based on levulinated coumarin. *Org. Lett.* **2011**, *13* (19), 5260-5263.
208. Stensrud, K.; Smith, B. Methods for production of sugar-derived ester, glycol and polymers. WO2017065980, 2017.
209. Candu, N.; Paul, D.; Marcu, I.-C.; Tudorache, M.; Parvulescu, V. I.; Coman, S. M., New organic-inorganic LDH composites: Synthesis, characterization and catalytic behavior in the green epoxidation of α , β -unsaturated esters. *Inorg. Chim. Acta* **2018**, *475*, 127-132.
210. Thomasco, L. M.; Gadwood, R. C.; Anderson, D. J. Preparation of thiadiazolyl and oxadiazolyl phenyl oxazolidinones as antibacterial agents. WO9902525, 1999.
211. Rips, R.; Derappe, C.; Buu-Hoï, N. P., 1,2,5-Trisubstituted pyrroles of pharmacologic interest. *J. Org. Chem.* **1960**, *25* (3), 390-392.
212. Arora, S. K.; Sinha, N.; Jain, S.; Upadhyaya, R. S.; Tyagi, O. D.; Nalam, V.; Chauhan, Y. K. Process for preparation of N-[2-methyl-5-phenyl-3-(piperazin-1-ylmethyl)]pyrroles starting from levulinic acid. WO2006109323, 2006.
213. Sansonetti, P.; Phalipon, A.; Guerreiro, C.; Nato, F.; Boutet, J.; Mulard, L. Preparation of glycoconjugates and their use as vaccine against *Shigella flexneri* serotype 3a and X. CA2631453, 2008.
214. Cason, J.; Reist, E. J., Structure of succinyl dichloride and of certain other potentially cyclic difunctional compounds. *J. Org. Chem.* **1958**, *23* (10), 1492-1496.

215. Elliott, W. J.; Fried, J., A simple carbon-13 nuclear magnetic resonance spectroscopic method for distinguishing between open-chain and pseudoacid chlorides. *J. Org. Chem.* **1978**, *43* (13), 2708-2710.
216. McManus, S. P.; Kozłowski, A.; Shen, X.; Cook, D. C. Polymeric reagents comprising a ketone or a related functional group. WO2004060406, 2004.
217. Clark, M.; Kiser, P., In situ crosslinked hydrogels formed using Cu(I)-free Huisgen cycloaddition reaction. *Polym. Int.* **2009**, *58* (10), 1190-1195.
218. Foot, J. S.; Lui, F. E.; Kluger, R., Hemoglobin bis-tetramers via cooperative azide-alkyne coupling. *Chem. Commun. (Cambridge, U. K.)* **2009**, (47), 7315-7317.
219. Agten, S. M.; Suylen, D.; Ippel, H.; Kokozidou, M.; Tans, G.; van de Vijver, P.; Koenen, R. R.; Hackeng, T. M., Chemoselective oxime reactions in proteins and peptides by using an optimized oxime strategy: the demise of levulinic acid. *ChemBioChem* **2013**, *14* (18), 2431-2434.